

学位論文

Theory of Quantum Thermoelectricity with
High Efficiency and High Power
(高効率高パワーの量子熱電効果の理論)

平成29年12月博士(理学)申請

東京大学大学院理学系研究科
物理学専攻

山本 薫

Abstract

Thermoelectric material is a device that converts heat into electric power. Although many researchers have been working on it, its efficiency has been still low. Thanks to the recent development of nanotechnology, thermoelectricity in quantum systems named quantum thermoelectricity attracts increasing interest. Since quantum thermoelectricity is a vast unexplored field, there is still plenty room to find a highly efficient thermoelectricity. Moreover, not only on the maximum efficiency but also on the efficiency at the maximum power attracts increasing interest because the power as well as the efficiency is important for practical applications.

In the present thesis, we seek quantum thermoelectricity in the linear-response regime with a high maximum efficiency and a high efficiency at the maximum power. We consider the following two cases: For a symmetric linear-response matrix, we investigate (1) thermoelectricity near Anderson localization transitions, while for an asymmetric linear-response matrix, we investigate (2) thermoelectricity with an electron-phonon interaction under a magnetic field.

(1) Thermoelectricity near Anderson localization transitions

For a symmetric linear-response matrix, one of the main parameters that characterize the efficiency is the Seebeck coefficient. Since a rapid change of the density of states may give a high Seebeck coefficient, the Anderson localization transition is one of the candidates to have a high Seebeck coefficient. After we correct and extend the previous researches, we consider the following three points: For a single mobility edge, (1-i) corrections to the leading power-law singularity in the zero-temperature conductivity; (1-ii) finite size effects; (1-iii) the pair of two mobility edges. In particular on the last point, we find that increasing randomness increases the efficiency.

(2) Thermoelectricity with an electron-phonon interaction under a magnetic field

The main problem for an asymmetric linear-response matrix that we tackle for quantum thermoelectricity in the present thesis is whether or not we can achieve the Carnot efficiency with *nonvanishing* power, which is claimed by Benenti *et al.* [G. Benenti, K. Saito, and G. Casati, Phys. Rev. Lett. **106**, 230602 (2011).]. In the realm of the Landauer-Büttiker formula, the unitarity of the scattering matrix prohibits the Carnot efficiency with nonvanishing power. However, little is known for the case to which we cannot apply the Landauer-Büttiker formula. We consider the model of quantum thermoelectricity with an weak electron-phonon interaction under a magnetic field, to which we cannot apply the Landauer-Büttiker formula. We find the following two results for energy-independent space-symmetric resonant widths within the approximations that the vertex corrections are neglected and the electron-phonon coupling is taken into account only up to the second order: (2-i) We prove that we cannot obtain the Carnot efficiency with nonvanishing power. (2-ii) We find that the maximum efficiency and the efficiency at the maximum power for delivering electric power using heat supply from a phonon bath can be high. We finally consider a general 3×3 asymmetric linear-response matrix and clarify the conditions for the Carnot efficiency with nonvanishing power.

Acknowledgements

It is a pleasure to express my gratitudes here. I first thank Prof. Naomichi Hatano. His positive attitude and wide interest in physics always influenced me. Without his continuous encouragement, I would not have finished this thesis. I also thank my Israeli collaborators, Prof. Ora Entin-Wohlman and Prof. Amnon Aharony. Their deep insight in physics and hard work influenced me a lot.

I would like to thank the former and previous members of the Hatano group for their valuable suggestions and comments: Prof. Emiko Arahata, Prof. Masaaki Nakamura, Prof. Savannah Garmon, Prof. Jaeha Lee, Dr. Mariagiovanna Gianfreda, Dr. Tatsuro Kawamoto, Dr. Masayuki Tashima, Dr. Hiroyasu Tajima, Dr. Tomotaka Kuwahara, Dr. Yoshihito Hotta, Yohei Morikuni, Rikugen Takagi, Takashi Ishii, Yuji Shirai, Kentaro Sugimoto, Takaaki Aoki, Kanae Mukai, and Yusuke Tanaka.

I am also grateful to the former and present members of the Miyashita group because I often visited there during my Ph.D. course for discussions: Prof. Seiji Miyashita, Prof. Takashi Mori, Dr. Tatsuhiko Shirai, Dr. Takafumi J. Suzuki, Dr. Eriko Kaminishi, Prof. Sergio Andraus, Dr. Sasmita Mohakud, Dr. Taichi Hinokihara, Adrien Bolens, Takuya Hatomura, Hiroki Ikeuchi, Yuta Goto, and Hayate Nakano. In particular, I learned a lot about the Keldysh Green's function from Dr. Takafumi J. Suzuki. He was my teacher on it.

In my Ph.D. course, I stayed in Israel for a few months, during which I was helped by a lot of people. I would also like to thank them here; Prof. Doron Cohen, Prof. Eytan Grosfeld, Prof. Moshe Schechter, Dr. Debashree Chowdhury, Dr. Shlomi Matityahu, Daniel Ariad, Geva Arwas, Daniel Dahan, Moamen Jbara, Yaakov Kleeorin, Dekel Shapira, to name a few.

My research was supported by the Advanced Leading Graduate Course for Photon Science (ALPS), the University of Tokyo as well as by a Grant-in-Aid for Japan Society for the Promotion of Science (JSPS) Fellows (Grant No.16J11542).

Finally, I would like to thank the secretaries of the Hatano and Miyashita groups: Keiko Mitsui, Noriko Jimbo, and Keiko Yashima.

Contents

Acknowledgements	3
Publications	9
1 Introduction	11
1.1 Introduction	11
1.1.1 Introduction of quantum thermoelectricity	11
1.1.2 From the viewpoint of stochastic thermodynamics	12
1.1.3 From the viewpoint of information thermodynamics	12
1.1.4 From the viewpoint of quantum thermodynamics	13
1.1.5 From the viewpoint of nonequilibrium thermodynamics and statistical physics	13
1.1.6 Motivation and structure of the present thesis	13
1.2 Thermoelectricity as a steady-state heat engine	15
1.2.1 Thermoelectric heat engine in mesoscopic transport systems	15
1.2.2 Thermoelectric heat engine in bulk systems	20
2 Linear irreversible thermodynamics for thermoelectricity	21
2.1 Construction of the linear-response formalism	22
2.2 Linear irreversible thermodynamics for a symmetric linear-response matrix	24
2.2.1 Constraints from the second law of thermodynamics	24
2.2.2 Maximum efficiency and the power at the maximum efficiency	24
2.2.3 The efficiency at the maximum power	25
2.3 Linear irreversible thermodynamics for an asymmetric linear-response matrix with a magnetic field	26
2.3.1 Constraints from the second law of thermodynamics	27
2.3.2 Maximum efficiency	28
2.3.3 Upper bound of the maximum efficiency from the second law of thermodynamics	30
2.3.4 Nonvanishing power at the Carnot efficiency	32
2.3.5 The efficiency at the maximum power	34
2.3.6 Upper bound of the efficiency at the maximum power from the second law of thermodynamics	35
2.4 Example of the Landauer-Büttiker formula with two reservoirs	35
2.4.1 Setup	35

2.4.2	Derivation of the Landauer-Büttiker formula for many reservoirs	37
2.4.3	The Landauer-Büttiker formula for two reservoirs	38
2.4.4	The linear-response coefficients	39
2.5	Summary and conclusion	40
3	Thermoelectricity near Anderson localization transitions	41
3.1	Introduction and preparation	42
3.1.1	Thermoelectric transport coefficients	42
3.1.2	Expression of the linear-response coefficients	43
3.1.3	Transmission for the Carnot efficiency	44
3.1.4	Transmission near the Anderson localization transitions	45
3.2	The infinite system	48
3.2.1	General considerations	48
3.2.2	Approximations	50
3.3	Finite-size effects	55
3.4	A band with two mobility edges	62
3.5	Summary and discussions	64
4	Efficiency bounds on thermoelectric transport in magnetic fields: The role of inelastic processes	67
4.1	Exploring the possibility of the Carnot efficiency with nonvanishing power under a magnetic field	68
4.2	Analysis of mesoscopic transport systems under a magnetic field using the Landauer-Büttiker formula	69
4.2.1	The case of three reservoirs	69
4.2.2	The case of many reservoirs	76
4.3	Efficiency bounds on thermoelectric transport in magnetic fields with electron-phonon interaction	76
4.3.1	Model and the Hamiltonian	77
4.3.2	Brief introduction of the Keldysh Green's function	78
4.3.3	Expressions of the Green's functions and the currents	80
4.3.4	Construction of the linear-response matrix in the case of three reservoirs	83
4.3.5	A constraint from the nonnegativity of the three-terminal entropy production	85
4.3.6	From the 3×3 to the effective 2×2 matrix with a probe condition	86
4.3.7	A constraint from the nonnegativity of the entropy production of the effective two-terminal setup	87
4.3.8	The efficiency at the maximum power	88
4.3.9	The maximum efficiency	90
4.3.10	Asymmetry of the efficiency with respect to $a = t_0 \sin \Phi$	91
4.3.11	Calculation with experimental values	92
4.4	Further considerations	94
4.4.1	For an asymmetric resonant widths $\Gamma_L \neq \Gamma_R$	94
4.4.2	The probe condition $J_Q^P = 0$ for general cases	96

4.5	Restriction for the effective 2×2 matrix from the nonnegativity from the general 3×3 matrix	97
4.6	Summary and Conclusion	100
5	Summary and future work	103
5.1	Summary	103
5.2	Future work	104
A	Approximations in Chapter 3	107
A.1	Low temperatures and $\mu - E_c \gg k_B T$	107
A.2	At the mobility edge: $ z = 0$	108
A.3	High temperatures: $ z \ll 1$	108
A.4	Low temperatures and $\mu - E_c \ll -k_B T$	110
B	Calculation of the currents with phonon with the Keldysh Green's function	113
B.1	The expression of the current with Green's functions	113
B.2	The Dyson equations of various (contour-ordered) Green's functions	114
B.2.1	The Dyson equations of $G_{k_L d}$, $G_{k_R k_L}$, $G_{k_R d}$, and so on	114
B.2.2	The Dyson equation of the Green's function of the dot G_{dd}	117
B.3	Langreth theorem	118
B.4	Calculation of the retarded, advanced and the lesser components of the Green's functions	119
B.4.1	The expression of the integrand of the current	124
B.4.2	The heat current from the Bosonic reservoir from the conservation of energy	125
B.4.3	Dividing the current into an elastic and inelastic parts	127

Publications

The present thesis is based on the following publications:

- Kaoru Yamamoto, Amnon Aharony, Ora Entin-Wohlman, Naomichi Hatano, Thermoelectricity near Anderson localization transitions, *Phys. Rev. B* **96**, 155201 (2017).
- Kaoru Yamamoto, Ora Entin-Wohlman, Amnon Aharony, Naomichi Hatano, Efficiency bounds on thermoelectric transport in magnetic fields: The role of inelastic processes, *Phys. Rev. B* **94**, 121402(R) (2016).
- Kaoru Yamamoto, Naomichi Hatano, Thermodynamics of the mesoscopic thermoelectric heat engine beyond the linear-response regime, *Phys. Rev. E* **92**, 042165 (2015).

Chapter 1

Introduction

1.1 Introduction

1.1.1 Introduction of quantum thermoelectricity

Heat engine was invented in the nineteenth century and led the industrial revolution. The first heat engine was a steam engine, which converts heat to mechanical work. In contrast, the modern society is interested in heat engines that create electricity, such as a solar power plant. The heat engine that directly converts heat to electricity is called a thermoelectric material. Efficient thermoelectric materials may solve the energy problem, which is crucial in the modern society, because they utilize wasted heat to generate electric power.

Research on thermoelectricity has a long history. The first thermoelectric effect may have been found by Seebeck in 1821, who found that heating one side of a piece of metal produces electric current. The thermoelectric efficiency of metals, however, is very low. There may be two main breakthroughs in the history on research of the efficiency. First, Ioffe found in the middle of the twentieth century that instead of metals, semiconductors can attain a high efficiency [1, 2]. The second breakthrough was the argument made by Dresselhaus *et al.* [3–5] that materials in low dimensions can have a high efficiency. The latter breakthrough directed our attention to materials in mesoscopic scales, in which quantum effects are stronger.

Despite its long history and breakthroughs, the efficiency of thermoelectric devices is still low for practical use. Because of its advantage, however, it is used in specific cases. For example, a thermoelectric device needs little maintenance because it has no moving part. It was therefore used in an unmanned spacecraft named Voyager. Because of the same reason, it is not noisy and does not vibrate, hence it is used for a refrigerator in a hotel or for a wine cooler. More efficient thermoelectric devices will be more used with these advantages.

As nanotechnology has developed, the theory of quantum thermoelectricity, particularly thermoelectricity in mesoscopic transport systems, has attracted more attention [6–46]. A quantum thermoelectric device has been realized experimentally on chip [47–50] and in cold atom systems [51]. While conventional works seek for efficient thermoelectric materials, theory of quantum thermoelectricity searches for structures that produce a highly efficient thermoelectricity. The aim of the theory of quantum thermoelectricity is not only to enhance the efficiency but also to understand the nature of quantum properties. Quantum thermoelectric-

ity is therefore related to many fields of applications as well as of basic science. We show below the relation to the following fields of basic science: stochastic thermodynamics, information thermodynamics, quantum thermodynamics, and nonequilibrium physics.

1.1.2 From the viewpoint of stochastic thermodynamics

Classical thermodynamics usually treats the system in the thermodynamic limit, which means that the system is macroscopic. However, since the twentieth century, people have become interested in small systems, such as Brownian particles, to which we cannot apply conventional classical thermodynamics.

Fluctuation is crucial in small systems, which we treat with stochastic thermodynamics. One of the celebrated results from stochastic thermodynamics is the fluctuation theorem [52–57], $\langle e^{-\Delta S} \rangle = 1$, where ΔS is the change of the entropy of the system of interest. It implies that the change of the entropy also fluctuates; it can decrease in a single trial. Of course, the expectation value of the entropy should be nonnegative, which we can derive from Jensen’s inequality, $e^{-\langle \Delta S \rangle} \leq \langle e^{-\Delta S} \rangle = 1$: this is actually the second law of thermodynamics. The fluctuation theorem has been proved for many kinds of systems including mesoscopic transport systems [58]. The fluctuation theorem in mesoscopic transport systems yields the relations among nonlinear transport coefficients beyond the linear-response regime [58], which have been observed experimentally [59, 60]. The fluctuation theorem has also been proved for thermoelectricity in mesoscopic transport systems [61, 62], which yields the relations among nonlinear transport coefficients of the electric and the heat currents [62].

The efficiency of a heat engine in small systems behaves stochastically, hence fluctuates, which is called the stochastic efficiency [34, 35, 43, 63–68]. The fluctuation theorem tells us that the probability that the stochastic efficiency attains the Carnot efficiency is most unlikely in the long-time limit [63]. The stochastic efficiency of quantum thermoelectricity is proved to satisfy this property [34, 35, 43] in the framework of the Landauer-Büttiker formula [69].

1.1.3 From the viewpoint of information thermodynamics

Information thermodynamics was developed to solve the paradox of Maxwell’s demon [70], which breaks the second law of thermodynamics at first sight. The demon may have been first suggested by Maxwell, who did the thought experiment as follows. He considered a box filled with particles. The box is divided in two parts by a wall, at which there is a door. Maxwell imagined a demon, who measures the velocity of the particles and opens the door only for fast ones. Finally slow particles are on one side of the box and fast particles are on the other side. The demon thus increases the temperature of one side and decreases that of the other without any work, which seems to violate the second law: In other words, the demon decreases the entropy of the box without any work. Szilard used this idea to consider an engine called the Szilard engine, which produces work only from isothermal process [70]. The engine looked like a perpetual motion machine. This paradox was solved by considering that the information from the measurement should be included in the entropy production [70, 71]. Work extraction with the feedback control was realized in experiment using the Brownian particle [72].

Maxwell’s demon is also realized in quantum thermoelectric devices. Autonomous Maxwell’s

demon, which is called the on-chip Maxwell's demon, was suggested theoretically [73] and then realized experimentally [48, 49]. Very recently, nonautonomous Maxwell's demon in mesoscopic transport systems was studied theoretically [74] and experimentally [50]; they observed electrons and applied the feedback control depending on the result of the measurement.

1.1.4 From the viewpoint of quantum thermodynamics

The development of nanotechnology has stimulated much interest in thermodynamics in quantum systems [75, 76], which is called quantum thermodynamics. The main difficulty in quantum thermodynamics is that we do not know how to define heat and work in quantum systems. We can define them and prove the laws of thermodynamics for systems with a weak coupling and under the Markov approximation [75], that is, in the regime to which we can apply the quantum master equation [77]. It is difficult, however, to show the laws of thermodynamics in other cases; for example, it is much difficult to define work and heat for strong coupling because we do not know if the energy used for switching the interaction on and off is work or heat.

Quantum thermoelectricity is one of the fields in quantum thermodynamics. The advantage of considering quantum thermoelectric system is that we can define work and heat even in the case of strong coupling [15, 78], which we will explain later in the present chapter. With the work and heat, we can construct thermodynamics for quantum systems as we can for standard classical heat engines [78].

1.1.5 From the viewpoint of nonequilibrium thermodynamics and statistical physics

Thermoelectricity occurs in nonequilibrium steady states, which requires the theory of nonequilibrium thermodynamics and statistical physics for its analysis. Conventional thermoelectricity can be usually described by linear irreversible thermodynamics in the linear-response regime, which we explain in Chapter 2. The familiar transport coefficients, such as the Seebeck coefficient, is described in terms of the linear-response coefficients. It is much more difficult, however, to construct a theory beyond the linear-response regime, which is highly nonequilibrium. We do not even know how to express the currents generally in nonlinear regimes.

In the theory of mesoscopic transport systems, we can treat the regime beyond the linear-response regime. We often use the Landauer-Büttiker formula [69], the quantum master equation [77], and the Keldysh Green's function [79] to calculate the expressions of currents, which may be valid beyond the linear-response regime. In experiments, we can also observe nonlinear phenomena [59, 60, 80]. Quantum thermoelectricity in mesoscopic transport systems can also treat the regime beyond the linear-response one. For example, nonlinear effects of the heat current have been studied [17, 18, 40, 81–83]. There have been also several works on the rectification of heat to propose a good heat diode theoretically [82, 84–88].

1.1.6 Motivation and structure of the present thesis

In the present thesis, we investigate quantum thermoelectricity with a high efficiency and a high power in the linear-response regime both for a symmetric and an asymmetric linear-response

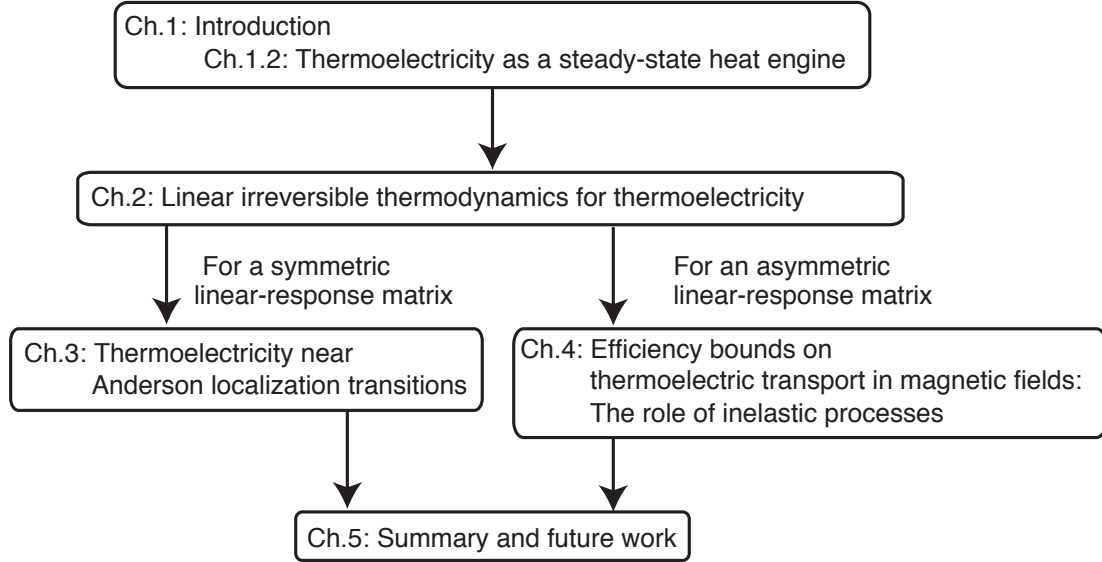


Figure 1.1: Structure of the present thesis.

matrices. The structure of the present thesis is as follows; see also Fig. 1.1. In Section 1.2 below, we introduce how to see quantum thermoelectric device as a heat engine, the perspective of which is used throughout the present thesis.

In Chapter 2, we review the linear irreversible thermodynamics, which describes thermoelectric transport in the linear-response regime. Based only on Onsager's reciprocal theorem and the second law of thermodynamics, we prove that the upper limit of the maximum efficiency is the Carnot efficiency. For a symmetric linear-response matrix, we show that we obtain zero power at the Carnot efficiency. We also show that the efficiency at the maximum power is bounded above by a universal value, a half of the Carnot efficiency, which is called the Curzon-Ahlborn bound [89]. For an asymmetric matrix, we show that we can attain the Carnot efficiency with nonvanishing power when the linear-response coefficients satisfy specific conditions [90], which are not attained in several cases in Chapter 4. We also give an example in the framework of the Landauer-Büttiker formula, which is a famous formula for mesoscopic transport systems.

In Chapter 3, we consider how to enhance the maximum efficiency and the efficiency at the maximum power for a symmetric linear-response matrix, which are both described by a single parameter called the figure of merit. After representing the familiar transport coefficients, such as the electric conductivity, the Seebeck coefficient, and the thermal conductivity, in terms of the linear-response coefficients, we focus on the Seebeck coefficient to enhance the figure of merit, whose high value requires breaking the electron-hole symmetry. We consider one of the candidates for a high Seebeck coefficient, namely thermoelectricity near Anderson localization transitions. For a single mobility edge, after we correct and extend previous studies, we consider corrections to the leading power-law singularity in the zero-temperature conductivity. Next, we investigate a finite-size effect on the thermoelectric coefficients. Although the Seebeck coefficient decreases with decreasing size, the figure of merit, first decreases but then increases as the size

decreases. We finally study thermoelectricity in systems with a pair of localization edges, the ubiquitous situation in random systems near the centers of electronic energy bands. As the two thresholds approach each other, the Seebeck coefficient and the figure of merit increase significantly.

In Chapter 4, we investigate the argument that there is a possibility to achieve the Carnot efficiency with nonvanishing power for quantum thermoelectricity with an asymmetric linear-response matrix in the linear-response regime. We first review Brandner *et al.*'s work [10] for quantum thermoelectricity in the framework of the Landauer-Büttiker formula. They found a bound from the unitarity of the scattering matrix, which prohibits the Carnot efficiency with nonvanishing power. However, little is known for the case to which we cannot apply the Landauer-Büttiker formula. We consider the model of quantum thermoelectricity with an weak electron-phonon interaction under a magnetic field, to which we cannot apply the formula. We obtain the following two results for energy-independent space-symmetric resonant widths within the approximations that the vertex corrections are neglected and the electron-phonon couplings are taken into account only up to the second order: We first find that we cannot attain the Carnot efficiency with nonvanishing power. We next find that the maximum efficiency and the efficiency at the maximum power for delivering electric power by heat supply from a phonon bath can be high within our framework. We finally consider a general 3×3 asymmetric linear-response matrix and clarify the conditions for the Carnot efficiency with nonvanishing power.

Finally, we summarize the thesis and give possible future works in Chapter 5.

1.2 Thermoelectricity as a steady-state heat engine

Throughout this thesis, we often consider a thermoelectric system as a steady-state heat engine, which we will call a thermoelectric heat engine hereafter. Here we explain how to define the efficiency and the power of the engine.

We first explain a thermoelectric heat engine in mesoscopic transport systems [78] in Subsection 1.2.1, in which there is a structure, such as a quantum dot and an Aharonov-Bohm ring, in a scale smaller than the relaxation length of electrons. We will use the thermoelectric heat engine in mesoscopic transport systems in Chapter 4.

We next explain a thermoelectric heat engine in bulk systems in Subsection 1.2.2, which is often used for the analysis of conventional thermoelectric materials. In bulk systems, there is no structure (except for the unit cell) in a scale smaller than the relaxation length of the electrons. We therefore assume the local equilibrium with a coarse-grained picture and smooth change of the chemical potential and temperature, hence we can see the system as a set of reservoirs. We can construct the thermodynamics similar to that in Subsection 1.2.1 by taking our notice of the adjacent pair of reservoirs.

1.2.1 Thermoelectric heat engine in mesoscopic transport systems

Setup

Consider a central system, for example quantum dots or quantum wires, attached to two reservoirs on both sides; see Fig. 1.2. We then make the following three assumptions:

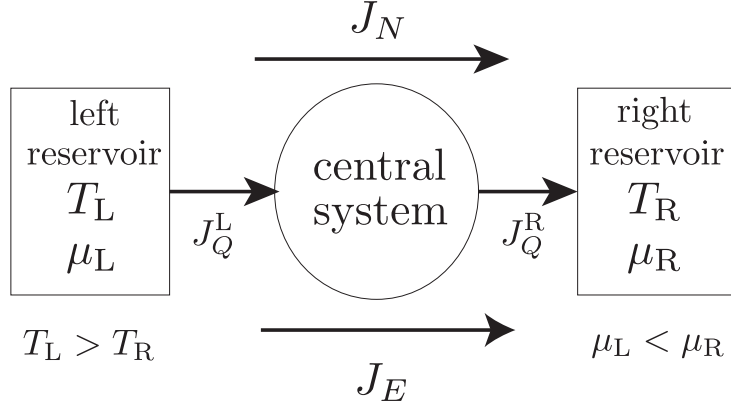


Figure 1.2: Schematic picture of a mesoscopic heat engine. We set the chemical potential of the right reservoir higher than the left, while the temperature of the left reservoir higher than the right so that electrons may go from left to right against the difference of the chemical potential.

1. The reservoirs are so much larger than the central system that it is always at equilibrium even if they interact with the central system, and hence we can define thermodynamic quantities of each reservoir, such as the temperature and the chemical potential;
2. The central system has reached a non-equilibrium steady state in which there are constant flows;
3. There is no entropy production in the central system because electrons undergo only elastic scatterings there.

We can regard this system as a heat engine in the following situation. We set the chemical potential of the right reservoir higher than that of the left, while the temperature of the left reservoir higher than that of the right. We particularly set the reservoirs as well as the central system so that a particle current of electrons may go from left to right against the difference of the chemical potential. What happens per unit time is the following. Electrons gain heat J_Q^L from the hot left reservoir, flow to the right against the potential difference, during which electrons perform the work of amount

$$\dot{W} = -J_e V, \quad (1.1)$$

where

$$J_e = e J_N \quad (1.2)$$

is the electric current with denoting J_N a particle current and

$$V = \frac{\mu_L - \mu_R}{e} \quad (1.3)$$

is the voltage difference with denoting μ_L and μ_R the chemical potentials of the left and the right reservoirs, respectively, and then dump heat J_Q^R to the cold right reservoir. We will derive the expressions of the heat currents J_Q^L and J_Q^R below. We can thus consider this system as a

heat engine. This is an explanation specific to the case of electrons, which we can generalize as follows; the central system gains heat from the left reservoir, does work, and then dumps heat to the right reservoir. In this perspective, we can regard the central system as a working system of cyclic heat engines. Because there is no entropy production in the central system, as we assumed above, we must have

$$J_Q^L - J_Q^R = \dot{W}. \quad (1.4)$$

Its efficiency η is thereby given by

$$\eta = \frac{\dot{W}}{J_Q^L} = 1 - \frac{J_Q^R}{J_Q^L}, \quad (1.5)$$

which is the same as the standard cyclic heat engine.

Note that we can regard the system as a heat engine only when J_N and J_Q^L are positive. The electrons do not necessarily flow from the hot reservoir to the cold one; the current which goes from the right to the left is considered to be negative. The direction of the flow depends on μ_L , μ_R , T_L , and T_R as well as the details of the system. For example, we can regard the system as a refrigerator when electrons go from right to left against the temperature difference. In this case, the efficiency, which is called the coefficient of performance, is given by $\eta_{\text{cop}} = J_Q^L/(J_e V)$, not as in Eq. (1.5).

Derivation of the heat currents going into and from a reservoir

We here derive the heat currents J_Q^L and J_Q^R in a thermodynamically consistent manner [62, 78]. Although many researchers have used them, the derivation is often skipped or described too briefly.

Our starting point is to identify the heat currents coming into or going out of the central system as those coming from or going into the reservoirs. We will give an important remark on this point later. We now derive the latter using general thermodynamics. The first law of thermodynamics gives the relation

$$dU_i = dQ_i + dW_i, \quad (1.6)$$

where $i = L, R$, and dU_i , dQ_i denote the energy and heat flowing into the left or right reservoir, as well as $dW_i = \mu_i dN_i$ with denoting dN_i the particle flowing into the left or right reservoirs is the work *done to* the reservoir. Using (1.6), we can express dQ_i in the form

$$dQ_i = dU_i - \mu_i dN_i. \quad (1.7)$$

Since we treat the nonequilibrium steady state, we can define the changes of the particle number and the energy in a reservoir as a steady current, which enables us to define the particle and energy currents as

$$J_N = -\frac{dN_L}{dt} = \frac{dN_R}{dt}, \quad J_E = -\frac{dU_L}{dt} = \frac{dU_R}{dt}, \quad (1.8)$$

where we used the conservation of particle number and energy, $dN_L + dN_R = 0$ and $dU_L + dU_R =$

0, because there is no dissipation in the central system. The negative signs appeared because we defined the positive direction so that the currents going to the right may be positive. We then define the heat currents using (1.7) and (1.8) in the form

$$\begin{aligned} J_Q^L &= -\frac{dQ_L}{dt} = J_E - \mu_L J_N, \\ J_Q^R &= \frac{dQ_R}{dt} = J_E - \mu_R J_N, \end{aligned} \quad (1.9)$$

where J_Q^L is the heat current flowing from the left reservoir into the system and J_Q^R is that flowing from the system into the right reservoir.

Note that these expressions of the heat currents may be valid even in the presence of many-body interactions if our assumptions 1–3 hold. We can therefore apply them to systems for which we cannot use the Landauer-Büttiker formula.

Let us come back to our starting point above. It is crucial to note that the working system of the engine is now the central system in Fig. 1.2, for which we cannot define the temperature and the chemical potential because it is highly nonequilibrium. In the textbook [69], Datta argued that we could define an “effective” chemical potential in quantum wires, but it is in fact not a thermodynamic observable. We should therefore be aware that it is not trivial at all to define the heat and the work for the central system. We here identify the heat current coming into the central system as that coming from a reservoir under the assumption below, which corresponds to the one that there is no entropy production in the central system.

According to the first law of thermodynamics, in order to calculate the heat current coming into or from the central system, we need to specify the energy current coming into or from it and the work done to or by it. The former is easy to specify as J_E because the energy current is a conserved quantity. The problem arises when we try to specify the work done to or by the central system, in which we cannot define thermodynamic intensive variables.

We here make the following assumption to specify it: the work done to or by the central system is respectively equal to that done by or to the reservoir. This assumption enables us to conclude that the work done to the system on the left side is equal to that done by the left reservoir, $\mu_L J_N$, and the work done by the system on the right side is equal to that done to the right reservoir, $\mu_R J_N$. We can thus find that the expression of the heat current coming into or from the central system is equal to those that we derived in Eq. (1.9). Although the expression of the heat currents corresponds to that used in previous researches, we believe that our derivation is more accurate than the previous ones. The crucial point is that we derived the heat current coming into or from the central system, not a reservoir; we need to make the assumption above to specify it.

Second law of thermodynamics and the upper bound of the efficiency

Let us show that we can construct the same formalism as that of the cyclic engine using the heat currents (1.9). We first easily find that they indeed satisfy (1.4). This is the first check of the consistency of the expression (1.9).

We then show that the upper limit of the efficiency (1.5) is the Carnot efficiency as is

expected from the theory of the standard cyclic heat engine. Let

$$\dot{S}_L dt = \frac{dQ_L}{T_L} \quad (1.10)$$

and

$$\dot{S}_R dt = \frac{dQ_R}{T_R} \quad (1.11)$$

denote the entropy productions in the left and right reservoirs, respectively, where T_L and T_R are the temperatures of the left and right reservoirs, respectively. Using (1.9), we can relate these entropy productions to the heat currents as

$$J_Q^L = -T_L \dot{S}_L, \quad J_Q^R = T_R \dot{S}_R. \quad (1.12)$$

According to the second law of thermodynamics, an entropy production of an isolated system increases. Our whole system, which consists of the two reservoirs and the central system is indeed isolated. The net entropy production of the whole system

$$\dot{S} = \dot{S}_L + \dot{S}_R \quad (1.13)$$

is thus non-negative, that is, $-\dot{S}_R \leq \dot{S}_L$; we assumed that there is no entropy production in the central system because electrons undergo only elastic scatterings there. We thus have from (1.4), (1.5), and (1.12),

$$\eta = \frac{-T_L \dot{S}_L - T_R \dot{S}_R}{-T_L \dot{S}_L} \leq 1 - \frac{T_R}{T_L} = \eta_c, \quad (1.14)$$

where η_c is the Carnot efficiency. We can achieve the equality if and only if $\dot{S}_L = -\dot{S}_R$, that is, $\dot{S} = 0$. We conclude that with the heat currents (1.9), we can produce Eqs. (1.4) and (1.14), which are the same formulas as those of the cyclic engine.

For the case of many reservoirs

We can easily generalize the expressions of the heat current (1.9) and the entropy production (1.13) for the case of many reservoirs. For N reservoirs, the heat flowing into the i th reservoir \dot{Q}_i per time in the i th reservoir is given by

$$\dot{Q}_i = \frac{dQ_i}{dt} = \frac{dU_i}{dt} - \mu_i \frac{dN_i}{dt} = \dot{U}_i - \mu_i \dot{N}_i, \quad (1.15)$$

where μ_i is the chemical potential of the i th reservoir and dN_i , dU_i and dQ_i denote the particle, energy and heat flowing into the i th reservoir. The entropy production of the whole system is the sum of the entropy production in each reservoir as in i th reservoir is given by

$$\dot{S} = \sum_{i=1}^N \dot{S}_i = \sum_{i=1}^N \frac{\dot{Q}_i}{T_i}, \quad (1.16)$$

where \dot{S}_i is the entropy production in i th reservoir and T_i is the temperature of the i th reservoir.

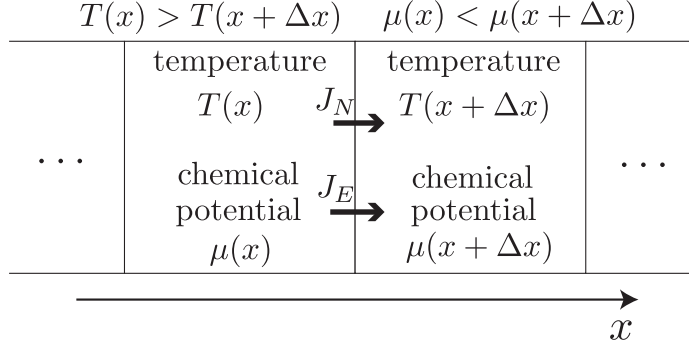


Figure 1.3: A schematic picture of a thermoelectric heat engine in a bulk system. We consider the two points, x and $x + \Delta x$. We assume that the current flows in a direction, which we call x -axis. We set the chemical potential of the right reservoir higher than the left, while the temperature of the left reservoir higher than the right so that an electric current (density) may go from left to right against the difference of the chemical potential.

1.2.2 Thermoelectric heat engine in bulk systems

For bulk systems, there is no structure on the scale smaller than the relaxation length of the electrons. We therefore assume that the system is local equilibrium in each point with a coarse-grained picture, hence we define the chemical potential and the temperature everywhere. In order to describe a thermoelectric heat engine in bulk systems, we take two adjacent local equilibrium points and regard them as reservoirs as in Fig. 1.3. We find that the structure of the whole system in Fig. 1.3 is similar to that of the thermoelectric heat engine in mesoscopic transport systems in Fig. 1.2 without the central system; both have two reservoirs. Therefore, for bulk systems, we can define the heat current (density), the efficiency, the entropy production (density) and so on as we did above for mesoscopic transport systems. We will consider the thermoelectric heat engine in bulk systems near Anderson localization transitions in Chapter 3.

Chapter 2

Linear irreversible thermodynamics for thermoelectricity

Thermoelectricity is usually characterized in the linear-response regime. In the present chapter, we review the linear irreversible thermodynamics, which describes non-equilibrium thermodynamics in the linear-response regime.

In Section 2.1, we explain how to construct the consistent linear-response formalism, that is, how to find the conjugate affinities for the currents that we choose. This may appear to be trivial in the case of two reservoirs. In the case of many reservoirs, however, it can be a confusing task to choose the correct affinities; if we do not choose them correctly, Onsager's reciprocal theorem [91] may not hold.

In Section 2.2, we consider the case of a symmetric linear-response matrix. We first show that the second law of thermodynamics, that is, the nonnegativity of the entropy production, gives a constraint for the linear-response coefficients. We next calculate the maximum efficiency and the efficiency at the maximum power, both of which are described by a single parameter called the figure of merit. We find that when the figure of merit goes to infinity, the maximum efficiency goes to the Carnot efficiency and the efficiency at the maximum power goes to a half of the Carnot efficiency, which is called the Curzon-Ahlborn bound [89]. We also find that we can only achieve the Carnot efficiency with vanishing power. We will investigate how to obtain a high figure of merit with a symmetric linear-response matrix in Chapter 3 in the present thesis.

In Section 2.3, we carry out an analysis similar to Section 2.2 but for an asymmetric linear-response matrix, which may come from the presence of a magnetic field, for example. In this case, the maximum efficiency and the efficiency at the maximum power are described by two parameters. We show that we can achieve the Carnot efficiency with nonvanishing power under specific conditions for the linear-response coefficients [90], which is the main purpose of the present chapter.

In Section 2.4, we calculate the linear-response coefficients in the framework of the Landauer-Büttiker formula with two reservoirs for example. In this case, we find that we cannot obtain an asymmetric linear-response matrix even though we apply a magnetic field to the system. We will investigate the attempt to obtain an asymmetric linear-response matrix and the possibility to attain the Carnot efficiency with nonvanishing power in Chapter 4 in the present thesis.

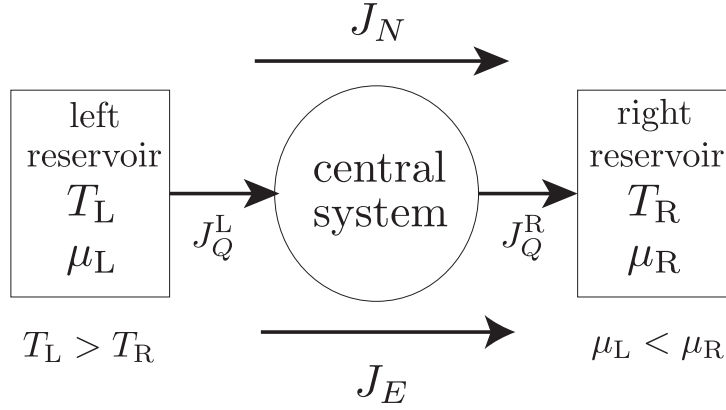


Figure 2.1: Schematic picture of a mesoscopic heat engine (repeat of Fig. 1.2). We set the chemical potential of the right reservoir higher than the left, while the temperature of the left reservoir higher than the right so that an electric current may go from left to right against the difference of the chemical potential.

In Section 2.5, we summarize the present chapter.

2.1 Construction of the linear-response formalism

In the present section, we explain how to construct the linear-response formalism, especially how to find the conjugate affinities. This may appear to be trivial, but it will be important in Chapter 4, where we consider the case of three reservoirs. For simplicity, we consider the thermoelectric heat engine in mesoscopic transport systems with two reservoirs in Fig. 2.1 throughout the present chapter. Note that we can construct almost the same formalism with the thermoelectric heat engine in bulk systems explained in Subsection 1.2.2, which we will remark in Section 3.1

In order to construct the linear-response formalism, we take the following four steps. First, we find how many independent currents there are in the model. In the case of two electronic reservoirs, there are four currents; electric and energy currents from left and right reservoirs. Since there are two relations between these currents, that is, the laws of particle and energy conservation, we know that the number of independent currents is two.

Second, we decide which independent currents we take. There are several ways to choose independent currents; we can take J_Q^L and J_Q^R , for example, but here let us choose J_e and J_Q^L so that we can calculate the efficiency $\eta = -J_e V / J_Q^L$ easily.

Third, we find the affinities conjugate to the currents that we chose. We can decide the affinities conjugate to the currents from the entropy production, whose expression comes from Eqs. (1.12) and (1.13):

$$\dot{S} = -\frac{J_Q^L}{T_L} + \frac{J_Q^R}{T_R} \quad (2.1)$$

$$= J_e \frac{V}{T_R} + J_Q^L \frac{\Delta T}{T_R^2} \quad (2.2)$$

$$= \frac{1}{T_R} \left(J_e V + \frac{\Delta T}{T_R} \right), \quad (2.3)$$

where we used the first law of thermodynamics, $J_Q^L - J_Q^R = -J_e V$. Here $V \equiv (\mu_L - \mu_R)/e$ is the voltage difference and $\Delta T \equiv T_L - T_R$ is the temperature difference.

In general, when the entropy production is written as $\dot{S} \propto \sum_i J_i F_i$ with denoting J_i the i th independent current, we call F_i the conjugate affinity or force to the independent current [62]. One may find that we can choose the coefficient of the affinities arbitrary. The following two choices are mainly used. In statistical physics, the affinities V/T_R and $\Delta T/T_R^2$ from Eq. (2.2) are often used, while in condensed matter physics V and $\Delta T/T_R$ from Eq. (2.3) are often used. Since the latter choice makes the linear-response coefficient L_{11} the electric conductance, we use the latter choice hereafter in the present thesis.

Fourth, we expand these independent currents J_e and J_Q^L with respect to the conjugate affinities V and $\Delta T/T_R$:

$$\begin{pmatrix} J_e \\ J_Q^L \end{pmatrix} = \begin{pmatrix} L_{11}(B) & L_{12}(B) \\ L_{21}(B) & L_{22}(B) \end{pmatrix} \begin{pmatrix} V \\ \Delta T/T_R \end{pmatrix}, \quad (2.4)$$

where we call $L_{ij}(B)$ a linear-response or Onsager coefficient with B denoting a magnetic field. Onsager's reciprocal theorem dictates $L_{11}(B) = L_{11}(-B)$, $L_{12}(B) = L_{21}(-B)$, and $L_{22}(B) = L_{22}(-B)$, which are called the Onsager-Casimir relations [91, 92]. If we expanded them with wrong affinities, these relations would not hold.

Let us make a note on the difference in the choice of affinities. We obtain the linear-response matrix as

$$\begin{pmatrix} J_e \\ J_Q^L \end{pmatrix} = \begin{pmatrix} L'_{11}(B) & L'_{12}(B) \\ L'_{21}(B) & L'_{22}(B) \end{pmatrix} \begin{pmatrix} V/T_R \\ \Delta T/T_R^2 \end{pmatrix} \quad (2.5)$$

for the choice of affinities V/T_R and $\Delta T/T_R^2$, while

$$\begin{pmatrix} J_e \\ J_Q^L \end{pmatrix} = \begin{pmatrix} L_{11}(B) & L_{12}(B) \\ L_{21}(B) & L_{22}(B) \end{pmatrix} \begin{pmatrix} V \\ \Delta T/T_R \end{pmatrix} \quad (2.6)$$

for V and $\Delta T/T_R$. One may easily find that these linear-response matrices have the difference of only the factor of $1/T_R$

$$\frac{1}{T_R} \begin{pmatrix} L'_{11}(B) & L'_{12}(B) \\ L'_{21}(B) & L'_{22}(B) \end{pmatrix} = \begin{pmatrix} L_{11}(B) & L_{12}(B) \\ L_{21}(B) & L_{22}(B) \end{pmatrix}, \quad (2.7)$$

which does not affect the result essentially.

We should further remark that we always maximize the efficiency and the power with respect to not the temperature difference ΔT but the voltage difference V , which is the definition of “maximum efficiency” and “maximum power” in the present thesis; we consider a given temperature difference ΔT . This way is the same as that of standard heat engines, in which we consider the maximum efficiency under a given temperature difference.

2.2 Linear irreversible thermodynamics for a symmetric linear-response matrix

In the present section, we calculate the maximum efficiency and the efficiency at the maximum power in the linear-response regime for a symmetric linear-response matrix. After introducing the constraints (2.11) from the nonnegativity of the entropy production, we show that the efficiency at the maximum power, which is given by a single parameter called the figure of merit, is bounded from above by a universal value, a half of the Carnot efficiency, which is called the Curzon-Ahlborn bound [89]. We also show that we obtain vanishing power at the Carnot efficiency.

In the case without magnetic fields, Eq. (2.5) is reduced to

$$\begin{pmatrix} J_e \\ J_Q^L \end{pmatrix} = \begin{pmatrix} L_{11} & L_{12} \\ L_{12} & L_{22} \end{pmatrix} \begin{pmatrix} V \\ \Delta T/T_R \end{pmatrix}. \quad (2.8)$$

We obtain the efficiency by inserting Eq. (2.8) into Eq. (1.5) as

$$\eta = -\frac{J_e V}{J_Q^L} = -\frac{L_{11}V^2 + L_{12}V\Delta T/T_R}{L_{12}V + L_{22}\Delta T/T_R}, \quad (2.9)$$

whose numerator $-J_e V$ is the electric power as shown in Eq. (1.1).

2.2.1 Constraints from the second law of thermodynamics

We first show that there exist constraints from the second law of thermodynamics, that is, the non-negativity of the entropy production. The entropy production in the linear-response regime (2.3) is written in the form

$$\dot{S} = \frac{1}{T_R} \left(J_e V + J_Q^L \frac{\Delta T}{T_R} \right) = \frac{1}{T_R} \begin{pmatrix} V & \Delta T/T_R \end{pmatrix} \begin{pmatrix} L_{11} & L_{12} \\ L_{12} & L_{22} \end{pmatrix} \begin{pmatrix} V \\ \Delta T/T_R \end{pmatrix}, \quad (2.10)$$

which is a quadratic form. The necessary and sufficient condition for $\dot{S} \geq 0$ is that the linear-response matrix is positive semi-definite. Since the matrix under consideration is symmetric, it is positive semi-definite if and only if all its principal minors are nonnegative:

$$L_{11} \geq 0, \quad L_{22} \geq 0, \quad L_{11}L_{22} - L_{12}^2 \geq 0. \quad (2.11)$$

These constraints, especially the last one, give the bound for the maximum efficiency and the efficiency at the maximum power, which are quite important in the linear irreversible thermodynamics.

2.2.2 Maximum efficiency and the power at the maximum efficiency

In the present subsection, we show that the upper bound of the maximum efficiency is the Carnot efficiency and that the power at the Carnot efficiency is zero.

Let us calculate the maximum efficiency with respect to V . Differentiating $\eta = -J_e V / J_Q^L$ with respect to V and setting it to zero as in

$$\frac{\partial \eta}{\partial V} = 0 \Leftrightarrow L_{11} L_{12} V^2 + 2 L_{11} L_{22} V \frac{\Delta T}{T_R} + L_{12} L_{22} \left(\frac{\Delta T}{T_R} \right)^2 = 0, \quad (2.12)$$

we obtain the voltage that gives the maximum efficiency as

$$V_{\max}^{\pm} = \left[-\frac{L_{22}}{L_{12}} \pm \sqrt{\left(\frac{L_{22}}{L_{12}} \right)^2 - \frac{L_{22}}{L_{11}}} \right] \frac{\Delta T}{T_R}. \quad (2.13)$$

Considering the condition $J_Q^L \geq 0$ for the system to work as a heat engine (see Section 1.2), which gives

$$J_Q^L|_{V=V_{\max}^{\pm}} = L_{12} V_{\max}^{\pm} + L_{22} \frac{\Delta T}{T_R} = \pm \frac{\Delta T}{T_R} \sqrt{\left(\frac{L_{22}}{L_{12}} \right)^2 - \frac{L_{22}}{L_{11}}} \geq 0, \quad (2.14)$$

we choose V_{\max}^+ . We set $V_{\max} \equiv V_{\max}^+$ hereafter. Inserting V_{\max} into the efficiency (2.9), we obtain

$$\eta(V = V_{\max}) = \eta_c \frac{\sqrt{1 + ZT} - 1}{\sqrt{1 + ZT} + 1}, \quad (2.15)$$

where $\eta_c = \Delta T / T_R$ is the Carnot efficiency coming from the calculation

$$\eta_c = 1 - \frac{T_R}{T_L} = 1 - \frac{T_L}{T_R} + \mathcal{O}[(\Delta T)^2] \approx \frac{\Delta T}{T_R}, \quad (2.16)$$

and

$$ZT \equiv \frac{L_{12}^2}{L_{11} L_{22} - L_{12}^2} \geq 0 \quad (2.17)$$

is called the figure of merit, which is nonnegative because of the constraint from the nonnegativity of the entropy production (2.11). Since $\eta(V = V_{\max})$ is monotonically increasing function of ZT , it is bounded from above by $\eta_c = \lim_{ZT \rightarrow \infty} \eta(V = V_{\max})$.

The power at the maximum efficiency is

$$\dot{W}(V = V_{\max}) = -J_e V_{\max} = - \left(L_{11} V_{\max}^2 + L_{12} V_{\max} \frac{\Delta T}{T_R} \right) \quad (2.18)$$

$$= \left(\frac{\Delta T}{T_R} \right)^2 L_{22} \left[\frac{2}{ZT} \left(-1 + \sqrt{\frac{1}{1 + ZT}} \right) + \sqrt{\frac{1}{1 + ZT}} \right], \quad (2.19)$$

which becomes zero in the limit $ZT \rightarrow \infty$. We thus obtain zero power at the Carnot efficiency. It may be consistent with the fact that we obtain zero power from the Carnot cycle with quasi-static processes.

2.2.3 The efficiency at the maximum power

Let us next see the efficiency at the maximum power. In the real world, devices with zero power are useless even if they have a high efficiency; we need a device with a high power. According

to Ref. [93], H. B. Reitlinger for the first time considered the efficiency at the maximum power and found that the upper bound is a universal value, $1 - \sqrt{T_{\text{cold}}/T_{\text{hot}}}$. After several researchers found it independently [93], Curzon and Ahlborn also found the same result [89]. However, works prior to Curzon and Ahlborn's are often overlooked and call the value $1 - \sqrt{T_{\text{cold}}/T_{\text{hot}}}$ the Curzon-Ahlborn (CA) bound. In the present thesis, we also call this bound the CA bound. After Curzon and Ahlborn's work, there had been few studies on the efficiency at the maximum power until Van den Broeck proved [94] that the CA bound gives the upper bound of the efficiency at the maximum power for a general symmetric linear-response matrix. Since his result can be applied to very general cases, it triggered many researches on the efficiency at the maximum power [95–106]. In the present subsection, we review Van den Broeck's work [94].

Let us maximize the power $-J_e V$. In order to do this, we differentiate the power with respect to V and set it to be zero:

$$\frac{\partial(-J_e V)}{\partial V} = 0 \Leftrightarrow 2L_{11}V + L_{12}\frac{\Delta T}{T_R} = 0. \quad (2.20)$$

We thereby obtain the voltage difference that gives the maximum power as

$$V_{\text{maxp}} = -\frac{L_{12}}{2L_{11}}\frac{\Delta T}{T_R}. \quad (2.21)$$

Inserting this voltage into the efficiency (2.9), we obtain the efficiency at the maximum power in the form

$$\eta(V = V_{\text{maxp}}) = \frac{\eta_c}{2} \frac{ZT}{ZT + 2} \leq \frac{\eta_c}{2}. \quad (2.22)$$

The upper bound is given by taking the limit $ZT \rightarrow \infty$ because of the fact that $ZT/(ZT + 2)$ is an monotonically increasing function of ZT . This bound is consistent with the Curzon-Ahlborn bound [89, 94]

$$\eta_{\text{CA}} = 1 - \sqrt{\frac{T_R}{T_L}} = \frac{\eta_c}{2} + \mathcal{O}[(\Delta T)^2]. \quad (2.23)$$

To summarize the present section, we calculated the maximum efficiency and the efficiency at the maximum power, which are characterized only by the figure of merit. Increasing the figure of merit ZT increases the maximum efficiency (2.15) and the efficiency at the maximum power (2.22). We showed that the upper bound of the maximum efficiency is the Carnot efficiency, at which we obtain vanishing power. We also showed that the upper bound of the efficiency at the maximum power is a half of the Carnot efficiency, which is called the CA bound. We will consider a guiding principle to enhance the figure of merit for a symmetric linear-response matrix in Chapter 3.

2.3 Linear irreversible thermodynamics for an asymmetric linear-response matrix with a magnetic field

In the present section, we review Benenti *et al.*'s work [90], in which they argue that the Onsager-Casimir relations and the second law of thermodynamics do not prohibit the Carnot

efficiency with nonvanishing power for an asymmetric linear-response matrix under a magnetic field. We calculate the maximum efficiency, the power at the maximum efficiency, the efficiency at the maximum power and the maximum power.

With a magnetic field, the linear-response formalism is given by Eq. (2.6) as

$$\begin{pmatrix} J_e \\ J_Q^L \end{pmatrix} = \begin{pmatrix} L_{11}(B) & L_{12}(B) \\ L_{21}(B) & L_{22}(B) \end{pmatrix} \begin{pmatrix} V \\ \Delta T/T_R \end{pmatrix}. \quad (2.24)$$

Note that the Onsager-Casimir relations [91, 92] does not state $L_{12}(B) = L_{21}(B)$: they tell us

$$L_{11}(B) = L_{11}(-B), \quad L_{22}(B) = L_{22}(-B), \quad L_{12}(B) = L_{21}(-B). \quad (2.25)$$

We will omit B hereafter whenever there is no risk of confusion.

2.3.1 Constraints from the second law of thermodynamics

Let us consider constraints from the nonnegativity of the entropy production, which give the upper bounds for the maximum efficiency and the efficiency at the maximum power. The nonnegativity yields

$$T_R \dot{S} = J_e V + J_Q^L \frac{\Delta T}{T_R} \quad (2.26)$$

$$= L_{11} V^2 + (L_{12} + L_{21}) V \frac{\Delta T}{T_R} + L_{22} \left(\frac{\Delta T}{T_R} \right)^2 \quad (2.27)$$

$$= L_{11} \left(V - \frac{L_{12} + L_{21}}{2L_{11}} \frac{\Delta T}{T_R} \right)^2 + \left[L_{22} - \frac{(L_{12} + L_{21})^2}{4L_{11}} \right] \left(\frac{\Delta T}{T_R} \right)^2 \quad (2.28)$$

$$= L_{22} \left(\frac{\Delta T}{T_R} - \frac{L_{12} + L_{21}}{2L_{22}} V \right)^2 + \left[L_{11} - \frac{(L_{12} + L_{21})^2}{4L_{22}} \right] V^2 \quad (2.29)$$

$$\geq 0, \quad (2.30)$$

from which we obtain the following constraints for the linear-response coefficients [90]:

$$L_{11}(B) \geq 0, \quad L_{22}(B) \geq 0, \quad (2.31)$$

$$L_{11}(B)L_{22}(B) - \frac{1}{4} [L_{12}(B) + L_{21}(B)]^2 \geq 0. \quad (2.32)$$

Here we introduce the two parameters [90]

$$x \equiv \frac{L_{12}}{L_{21}}, \quad y = \frac{L_{12}L_{21}}{L_{11}L_{22} - L_{12}L_{21}} \quad (2.33)$$

in order to express the condition (2.32) simpler. The parameter x is an asymmetric parameter and y is a parameter similar to ZT . Indeed, when there is no magnetic field, $x = 1$ and y reduces to ZT .

Let us express the condition (2.32) in terms of x and y :

$$L_{11}L_{22} - \frac{1}{4}(L_{12} + L_{21})^2 = \left(\frac{1}{y} + 1\right) L_{12}L_{21} - \frac{1}{4}(L_{12}^2 + L_{21}^2 + 2L_{12}L_{21}) \geq 0. \quad (2.34)$$

Assuming $L_{21} \neq 0$ and dividing the both sides by $L_{21}^2 > 0$, we obtain

$$\left(\frac{1}{y} + 1\right) x - \frac{1}{4}(x^2 + 1 + 2x) \geq 0, \quad (2.35)$$

that is,

$$4\left(\frac{1}{y} + 1\right) x - (x^2 + 1 + 2x) = \frac{4x}{y} - (x - 1)^2 \geq 0. \quad (2.36)$$

Assuming $x \neq 1$, we divide both sides by $(x - 1)^2 > 0$ to obtain

$$\frac{1}{y} \frac{4x}{(x - 1)^2} \geq 1. \quad (2.37)$$

Therefore we find [90]

$$\begin{aligned} 0 \leq y &\leq \frac{4x}{(x - 1)^2} \quad \text{for } y \geq 0, \\ \frac{4x}{(x - 1)^2} &\leq y \leq 0 \quad \text{for } y \leq 0. \end{aligned} \quad (2.38)$$

We can confirm that this inequality is also satisfied at $x = 1$, where y reduces to the figure of merit ZT and produces the same bound as Eq. (2.17):

$$0 \leq y = ZT. \quad (2.39)$$

We can also confirm that this inequality is satisfied at $L_{21} = 0$, where

$$y = \frac{L_{12}L_{21}}{L_{11}L_{22} - L_{12}L_{21}} = 0 \quad (2.40)$$

and $x = L_{12}/L_{21}$ goes to infinity and then

$$\lim_{x \rightarrow \infty} \frac{4x}{(x - 1)^2} = 0. \quad (2.41)$$

2.3.2 Maximum efficiency

Let us calculate the maximum efficiency. Differentiating the efficiency

$$\eta = -\frac{J_e V}{J_Q^L} = -\frac{L_{11}V^2 + L_{12}V\Delta T/T_R}{L_{21}V + L_{22}(\Delta T/T_R)^2}, \quad (2.42)$$

with respect to V and setting it zero, we obtain the following equation:

$$L_{11}L_{21}V^2 + 2L_{11}L_{22}\frac{\Delta T}{T_R}V + L_{12}L_{22}\left(\frac{\Delta T}{T_R}\right)^2 = 0. \quad (2.43)$$

The solutions are as follows:

$$V_{\max}^{\pm} = -\frac{L_{22}}{L_{21}}\frac{\Delta T}{T_R} \pm \sqrt{\frac{L_{22}^2}{L_{21}^2}\left(\frac{\Delta T}{T_R}\right)^2 - \frac{L_{12}L_{22}}{L_{11}L_{21}}\left(\frac{\Delta T}{T_R}\right)^2} \quad (2.44)$$

$$= \frac{L_{22}}{L_{21}}\left(-1 \pm \sqrt{\frac{L_{11}L_{22} - L_{12}L_{21}}{L_{11}L_{22}}}\right)\frac{\Delta T}{T_R}. \quad (2.45)$$

Considering the positivity of J_Q^L as in

$$J_Q^L = L_{21}V_{\max}^{\pm} + L_{22}\frac{\Delta T}{T_R} \quad (2.46)$$

$$= \pm L_{22}\sqrt{\frac{L_{11}L_{22} - L_{12}L_{21}}{L_{11}L_{22}}}\frac{\Delta T}{T_R} \geq 0, \quad (2.47)$$

we choose the solution with a positive sign and call it V_{\max} :

$$V_{\max} \equiv V_{\max}^+ = \frac{L_{22}}{L_{21}}\left(-1 + \sqrt{\frac{L_{11}L_{22} - L_{12}L_{21}}{L_{11}L_{22}}}\right)\frac{\Delta T}{T_R} \quad (2.48)$$

$$= \frac{L_{22}}{L_{21}}\left(-1 + \sqrt{\frac{1}{1+y}}\right)\frac{\Delta T}{T_R}, \quad (2.49)$$

where we used the relations

$$L_{11}L_{22} - L_{12}L_{21} = \frac{L_{12}L_{21}}{y}, \quad L_{11}L_{22} = \frac{L_{12}L_{21}}{y} + L_{12}L_{21}, \quad (2.50)$$

and

$$\frac{L_{11}L_{22} - L_{12}L_{21}}{L_{11}L_{22}} = \frac{\frac{L_{12}L_{21}}{y}}{\frac{L_{12}L_{21}}{y} + L_{12}L_{21}} = \frac{1}{1+y}. \quad (2.51)$$

In order to calculate the maximum efficiency, we first calculate the power (numerator) and the heat current (denominator) at the maximum efficiency. Using the relation from Eq. (2.43),

$$L_{11}V_{\max}^2 = -2\frac{L_{11}L_{22}}{L_{21}}\frac{\Delta T}{T_R}V_{\max} - \frac{L_{12}L_{22}}{L_{21}}\left(\frac{\Delta T}{T_R}\right)^2, \quad (2.52)$$

we obtain the power at the maximum efficiency as in

$$\dot{W}(V = V_{\max}) = -\left(L_{11}V_{\max}^2 + L_{12}V_{\max}\frac{\Delta T}{T_R}\right) \quad (2.53)$$

$$= -\left[-2\frac{L_{11}L_{22}}{L_{21}}\frac{\Delta T}{T_R}V_{\max} - \frac{L_{12}L_{22}}{L_{21}}\left(\frac{\Delta T}{T_R}\right)^2 + L_{12}V_{\max}\frac{\Delta T}{T_R}\right] \quad (2.54)$$

$$= \left(\frac{\Delta T}{T_R} \right)^2 L_{22} x \left[\frac{2}{y} \left(-1 + \sqrt{\frac{1}{1+y}} \right) + \sqrt{\frac{1}{1+y}} \right], \quad (2.55)$$

where we used the relation (2.33). We also obtain the heat current from Eqs. (2.47) and (2.51):

$$J_Q^L(V = V_{\max}) = L_{21} V_{\max} + L_{22} \frac{\Delta T}{T_R} \quad (2.56)$$

$$= L_{22} \sqrt{\frac{1}{1+y}} \frac{\Delta T}{T_R}. \quad (2.57)$$

We thereby obtain the maximum efficiency in the form [90]

$$\eta(V = V_{\max}) = \frac{\dot{W}(V = V_{\max})}{J_Q^L(V = V_{\max})} \quad (2.58)$$

$$= \eta_c x \frac{\frac{2}{y} \left(-1 + \sqrt{\frac{1}{1+y}} \right) + \sqrt{\frac{1}{1+y}}}{\sqrt{\frac{1}{1+y}}} \quad (2.59)$$

$$= \eta_c x \frac{\sqrt{1+y} - 1}{\sqrt{1+y} + 1}. \quad (2.60)$$

2.3.3 Upper bound of the maximum efficiency from the second law of thermodynamics

Let us consider the upper bound of the maximum efficiency from the constraint (2.38) due to the nonnegativity of the entropy production (2.30). We show that the bound is the Carnot efficiency and the power at the Carnot efficiency does not vanish for $|x| > 1$.

Since $\eta(V = V_{\max})$ in Eq. (2.60) monotonically increases with respect to y , it takes the maximum at $y = 4x/(x-1)^2$; see the constraint (2.38). At this point, we find that

$$\sqrt{1+y} = \sqrt{\frac{4x + (x-1)^2}{(x-1)^2}} = \sqrt{\frac{(x+1)^2}{(x-1)^2}} = \left| \frac{x+1}{x-1} \right|, \quad (2.61)$$

from which we have

$$\eta(V = V_{\max}) \leq \eta_c x \frac{\frac{-x+1}{x-1} - 1}{\frac{-x+1}{x-1} + 1} \quad (2.62)$$

$$= \eta_c x^2 \quad (2.63)$$

for $|x| \leq 1$ and

$$\eta(V = V_{\max}) \leq \eta_c x \frac{\frac{x+1}{x-1} - 1}{\frac{x+1}{x-1} + 1} \quad (2.64)$$

$$= \eta_c \quad (2.65)$$

for $|x| < 1$. To summarize, the upper bound of the maximum efficiency is given by [90]

$$\eta(V = V_{\max}) \leq \begin{cases} \eta_c x^2 < \eta_c & (|x| < 1), \\ \eta_c & (|x| \geq 1). \end{cases} \quad (2.66)$$

We find that we can attain the Carnot efficiency only when $|x| \geq 1$ [90].

We can prove that the entropy production is zero only at the Carnot efficiency in the following manner [90]. Let us calculate the entropy production at the upper bound (2.66) of the maximum efficiency. The entropy production (multiplied by T_R) is obtained by inserting $y = 4x/(x-1)^2$ as

$$\begin{aligned} T_R \dot{S} \left(V = V_{\max}, y = \frac{4x}{(x-1)^2} \right) \\ = J_e V_{\max} + J_Q^L \left(\frac{\Delta T}{T_R} \right) \Big|_{y=4x/(x-1)^2} \end{aligned} \quad (2.67)$$

$$= \left(\frac{\Delta T}{T_R} \right)^2 L_{22} \left[\left| \frac{x-1}{x+1} \right| - \frac{(x-1)^2}{2} \left(-1 + \left| \frac{x-1}{x+1} \right| \right) - x \left| \frac{x-1}{x+1} \right| \right]. \quad (2.68)$$

We have for $|x| < 1$

$$T_R \dot{S} \left(V = V_{\max}, y = \frac{4x}{(x-1)^2} \right) = \left(\frac{\Delta T}{T_R} \right)^2 L_{22} \left[-\frac{x-1}{x+1} - \frac{(x-1)^2}{2} \left(-1 - \frac{x-1}{x+1} \right) + x \frac{x-1}{x+1} \right] \quad (2.69)$$

$$= \left(\frac{\Delta T}{T_R} \right)^2 \frac{L_{21}^2}{4L_{11}} (x^2 - 1)^2 \quad (2.70)$$

$$= \left(\frac{\Delta T}{T_R} \right)^2 \frac{(L_{12}^2 - L_{21}^2)^2}{4L_{11}L_{21}^2}, \quad (2.71)$$

where we used Eq. (2.33) and

$$L_{22} = \frac{1}{L_{11}} \left[\frac{L_{12}L_{21}}{y} + L_{12}L_{21} \right] \quad (2.72)$$

$$= \frac{L_{12}L_{21}}{L_{11}} \left[\frac{(x-1)^2}{4x} + 1 \right] \quad (2.73)$$

$$= \frac{L_{21}^2}{4L_{11}} (x+1)^2 \quad (2.74)$$

from Eq. 2.50, while we have for $|x| \geq 1$

$$T_R \dot{S} \left(V = V_{\max}, y = \frac{4x}{(x-1)^2} \right) = \left(\frac{\Delta T}{T_R} \right)^2 L_{22} \left[\frac{x-1}{x+1} - \frac{(x-1)^2}{2} \left(-1 + \frac{x-1}{x+1} \right) - x \frac{x-1}{x+1} \right] \quad (2.75)$$

$$= 0. \quad (2.76)$$

To summarize, we find [90]

$$\dot{S} \left(V = V_{\max}, y = \frac{4x}{(x-1)^2} \right) = \begin{cases} \left(\frac{\Delta T}{T_R} \right)^2 \frac{(L_{12}^2 - L_{21}^2)^2}{4L_{11}L_{21}^2} > 0 & (|x| < 1), \\ 0 & (|x| \geq 1). \end{cases} \quad (2.77)$$

from which we find that we can achieve the Carnot efficiency and zero entropy production only when $|x| \geq 1$.

2.3.4 Nonvanishing power at the Carnot efficiency

Let us also calculate the power at the upper bound of the maximum efficiency to show that we can obtain nonvanishing power at the Carnot efficiency [90]. Substituting $y = 4x/(x-1)^2$ into the power at the maximum efficiency $-J_e V_{\max}$, we obtain

$$\dot{W} \left(V = V_{\max}, y = \frac{4x}{(x-1)^2} \right) = -J_e V_{\max} \Big|_{y=4x/(x-1)^2} \quad (2.78)$$

$$= \left(\frac{\Delta T}{T_R} \right)^2 L_{22} x \left[\frac{(x-1)^2}{2x} \left(-1 + \frac{|x-1|}{x+1} \right) + \frac{|x-1|}{x+1} \right], \quad (2.79)$$

from which we have

$$\dot{W} \left(V = V_{\max}, y = \frac{4x}{(x-1)^2} \right) = \left(\frac{\Delta T}{T_R} \right)^2 L_{22} x \left[\frac{(x-1)^2}{2x} \left(-1 - \frac{x-1}{x+1} \right) - \frac{x-1}{x+1} \right] \quad (2.80)$$

$$= \left(\frac{\Delta T}{T_R} \right)^2 L_{22} x^2 \frac{-(x-1)}{x+1} \quad (2.81)$$

$$= \left(\frac{\Delta T}{T_R} \right)^2 L_{22} x^2 \frac{|x-1|}{x+1} \quad (2.82)$$

$$= \left(\frac{\Delta T}{T_R} \right)^2 \frac{L_{21}^2}{4L_{11}} x^2 |x^2 - 1| \quad (2.83)$$

for $|x| < 1$ and

$$\dot{W} \left(V = V_{\max}, y = \frac{4x}{(x-1)^2} \right) = \left(\frac{\Delta T}{T_R} \right)^2 L_{22} x \left[\frac{(x-1)^2}{2x} \left(-1 + \frac{x-1}{x+1} \right) + \frac{x-1}{x+1} \right] \quad (2.84)$$

$$= \left(\frac{\Delta T}{T_R} \right)^2 L_{22} x \frac{x-1}{x(x+1)} \quad (2.85)$$

$$= \left(\frac{\Delta T}{T_R} \right)^2 L_{22} \frac{|x-1|}{x+1} \quad (2.86)$$

$$= \frac{L_{21}^2}{4L_{11}} |x^2 - 1| \quad (2.87)$$

for $|x| \geq 1$. In the last equality in each of Eqs. (2.83) and (2.87), we used Eq. (2.74). We find from Eqs. (2.66) and (2.87) that we can obtain nonvanishing power at the Carnot efficiency

only for

$$|x| > 1 \quad \text{and} \quad y = 4x/(x-1)^2, \quad (2.88)$$

which is the main results of Benenti *et al.*'s work [90]. However, several works have shown that the conditions $|x| > 1$ and $y = 4x/(x-1)^2$ cannot be satisfied simultaneously for specific models, which we will review in Chapter 4.

The possibility of the Carnot efficiency with nonvanishing power might be explained by the following dissipationless currents [10]. Let us divide the electric current into its symmetric and antisymmetric parts with respect to a magnetic-field reversal $B \leftrightarrow -B$ in the form

$$J_e = L_{11}V + L_{12}\frac{\Delta T}{T_R} \quad (2.89)$$

$$= L_{11}V + \frac{L_{12} + L_{21}}{2}\frac{\Delta T}{T_R} + \frac{L_{12} - L_{21}}{2}\frac{\Delta T}{T_R} \quad (2.90)$$

$$= J_e^{\text{irr}} + J_e^{\text{rev}}, \quad (2.91)$$

where we defined

$$J_e^{\text{irr}} \equiv L_{11}V + \frac{L_{12} + L_{21}}{2}\frac{\Delta T}{T_R}, \quad (2.92)$$

$$J_e^{\text{rev}} \equiv \frac{L_{12} - L_{21}}{2}\frac{\Delta T}{T_R}. \quad (2.93)$$

Note that we find $J_e^{\text{irr}}(B) = J_e^{\text{irr}}(-B)$ while $J_e^{\text{rev}}(B) = -J_e^{\text{rev}}(-B)$ from the Onsager-Casimir relations (2.25). Let us do a similar division for the heat current in the form

$$J_Q^{\text{L}} = L_{21}V + L_{22}\frac{\Delta T}{T_R} \quad (2.94)$$

$$= \frac{L_{21} - L_{12}}{2}V + \frac{L_{21} + L_{12}}{2}\frac{\Delta T}{T_R} + L_{22}\frac{\Delta T}{T_R} \quad (2.95)$$

$$= J_Q^{\text{L,rev}} + J_Q^{\text{L,irr}}, \quad (2.96)$$

where

$$J_Q^{\text{L,rev}} \equiv \frac{L_{21} - L_{12}}{2}V, \quad (2.97)$$

$$J_Q^{\text{L,irr}} \equiv \frac{L_{21} + L_{12}}{2}\frac{\Delta T}{T_R} + L_{22}\frac{\Delta T}{T_R}. \quad (2.98)$$

Let us express the entropy production (multiplied by T_R) in terms of $J_N^{\text{irr}}, J_N^{\text{rev}}, J_Q^{\text{L,irr}}$ and $J_Q^{\text{L,rev}}$ as

$$T_R\dot{S} = J_eV + J_Q^{\text{L}}\frac{\Delta T}{T_R} \quad (2.99)$$

$$= \left(J_e^{\text{irr}}V + J_Q^{\text{L,irr}}\frac{\Delta T}{T_R} \right) + \left(J_e^{\text{rev}}V + J_Q^{\text{L,rev}}\frac{\Delta T}{T_R} \right) \quad (2.100)$$

$$= J_e^{\text{irr}}V + J_Q^{\text{L,irr}}\frac{\Delta T}{T_R}, \quad (2.101)$$

where we used the fact that the ‘reversible’ currents (the antisymmetric part) do not affect the entropy production as in

$$J_e^{\text{rev}}V + J_Q^{\text{L,rev}}\frac{\Delta T}{T_R} = \frac{L_{12} - L_{21}}{2}V\frac{\Delta T}{T_R} + \frac{L_{21} - L_{12}}{2}V\frac{\Delta T}{T_R} \quad (2.102)$$

$$= 0. \quad (2.103)$$

The currents J_e^{rev} and $J_Q^{\text{L,rev}}$ are sometimes called the dissipationless currents [10, 46]. We therefore find that we can produce finite currents J_e^{rev} and $J_Q^{\text{L,rev}}$ with zero entropy production $\dot{S} = 0$, which might produce nonvanishing power at the Carnot efficiency. Note that we will use the fact that the antisymmetric part with respect to a magnetic-field reversal does not affect the entropy production in Section 4.5.

2.3.5 The efficiency at the maximum power

Let us calculate the efficiency at the maximum power [90]. Differentiating the power

$$\dot{W} = -J_e V \quad (2.104)$$

$$= -\left(L_{11}V^2 + L_{12}V\frac{\Delta T}{T_R}\right) \quad (2.105)$$

with respect to V , we obtain

$$V_{\text{maxp}} = -\frac{L_{12}}{2L_{11}}\frac{\Delta T}{T_R}, \quad (2.106)$$

which gives the maximum power as

$$\dot{W}(V = V_{\text{maxp}}) = -\left(L_{11}V_{\text{maxp}} + L_{12}\frac{\Delta T}{T_R}\right) \quad (2.107)$$

$$= \frac{\Delta T}{T_R}\frac{L_{12}^2}{4L_{11}}. \quad (2.108)$$

The heat current at the maximum power is of the form [90]

$$J_Q^{\text{L}}(V = V_{\text{maxp}}) = L_{21}V_{\text{maxp}} + L_{22}\frac{\Delta T}{T_R} \quad (2.109)$$

$$= \frac{2L_{11}L_{22} - L_{12}L_{21}}{2L_{11}}\frac{\Delta T}{T_R}. \quad (2.110)$$

With these currents at the maximum power, we obtain the efficiency at the maximum power as follows:

$$\eta(V = V_{\text{maxp}}) = \frac{\dot{W}(V = V_{\text{maxp}})}{J_Q^{\text{L}}(V = V_{\text{maxp}})} \quad (2.111)$$

$$= \frac{\eta_c}{2}\frac{L_{12}^2}{2L_{11}L_{22} - L_{12}L_{21}}. \quad (2.112)$$

Substituting the relation (2.51) into the efficiency (2.112), we obtain [90]

$$\eta(V = V_{\text{maxp}}) = \frac{\eta_c}{2} \frac{L_{12}^2}{2L_{11}L_{22} - L_{12}L_{21}} \quad (2.113)$$

$$= \frac{\eta_c}{2} \frac{L_{12}^2}{\frac{2L_{12}L_{21}}{y} + L_{12}L_{21}} \quad (2.114)$$

$$= \frac{\eta_c}{2} \frac{xy}{2 + y}. \quad (2.115)$$

2.3.6 Upper bound of the efficiency at the maximum power from the second law of thermodynamics

Let us seek for the upper bound of the efficiency at the maximum power under the condition $\dot{S} \geq 0$. The efficiency at the maximum power was given in Eq. (2.115) in the form

$$\eta(V = V_{\text{maxp}}) = \frac{\eta_c}{2} \frac{xy}{2 + y}, \quad (2.116)$$

which monotonically increases with respect to y . Therefore, for $x > 0$, we find that $\eta(V = V_{\text{maxp}})$ takes the maximum at $y = \frac{4x}{(x-1)^2}$ as well as for $x < 0$. Substituting this into Eq. (2.116), we obtain the upper bound of the efficiency at the maximum power as [90]

$$\eta(V = V_{\text{maxp}}) \leq \frac{\eta_c}{2} \frac{x \frac{4x}{(x-1)^2}}{2 + \frac{4x}{(x-1)^2}} \quad (2.117)$$

$$= \eta_c \frac{x^2}{x^2 + 1}. \quad (2.118)$$

For $|x| = 1$, that is, when the time-reversal symmetry exists, the least upper bound (2.118) becomes $\eta_c/2$, which is consistent with the Curzon-Ahlborn bound. We find that in the limit $|x| \rightarrow \infty$, the upper bound of the efficiency at the maximum power becomes the Carnot efficiency η_c .

2.4 Example of the Landauer-Büttiker formula with two reservoirs

In the present section, we calculate the linear-response coefficients in the framework of the Landauer-Büttiker formula for example. A tutorial textbook for the formula is Datta's [69]. The derivation of the formula is based on Chapter 2 in Ref. [107]. Note that we neglect the spin degree of freedom of electrons throughout the present appendix.

2.4.1 Setup

Although we need the Landauer-Büttiker formula for two reservoirs, we derive the formula for many reservoirs for later use. The Landauer-Büttiker formula can be applied to the system attached to several semi-infinite one-dimensional leads as shown in Fig. 2.2. The electrons are

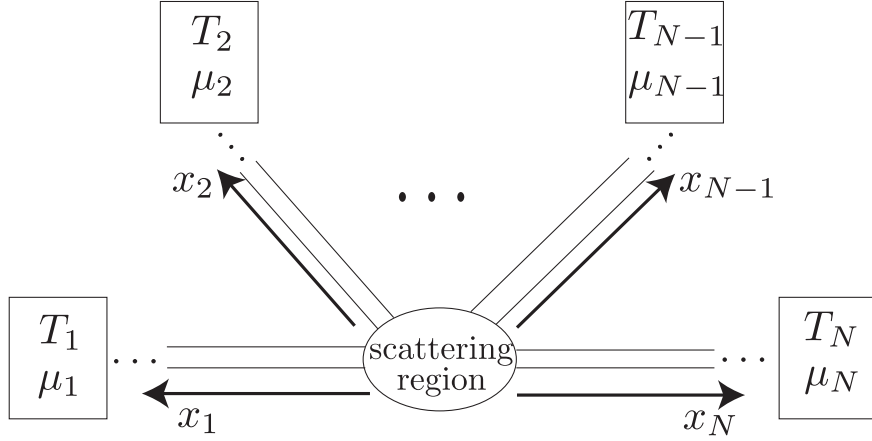


Figure 2.2: The setup of multi-terminal model for the Landauer-Büttiker formula. There are N semi-infinite leads attached to the central scattering region, which is described by the scattering matrix \mathbb{S} . There is an electronic reservoir with its temperature T_i and chemical potential μ_i at the end of a each lead.

assumed to experience only elastic scatterings in the system. In other words, there is only one-body potential in the system. We can also apply a magnetic field to the system. At the end of each lead, there is a reservoir with a Fermi distribution $f_\alpha(E) = [1 + e^{\beta_\alpha(E - \mu_\alpha)}]^{-1}$, where $\beta = (k_B T_\alpha)^{-1}$, T_α , and μ_α are the inverse temperature, the temperature, and the chemical potential of the reservoir, respectively, with k_B being the Boltzmann constant.

We make the following assumptions in order to obtain the Landauer-Büttiker formula:

- The current coming into the lead holds the Fermi distribution of the reservoir in which it originally was and relaxes in the reservoir which it goes into.
- The current which goes from the lead into the reservoir is not reflected back into the lead.
- The electrons in the lead are one-dimensional non-interacting Fermi particles, and therefore the incoming and outgoing currents are independent of each other.

We will derive the Landauer-Büttiker formula for the case with many reservoirs under the above setup in the next subsection.

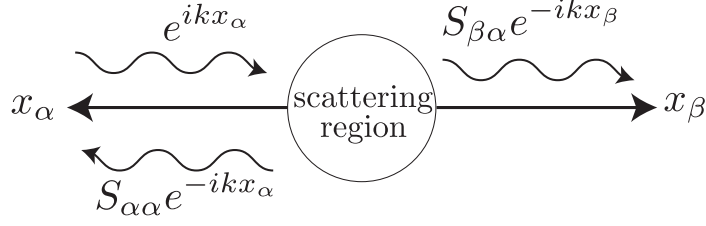


Figure 2.3: A schematic picture of the incoming wave function from the lead α . Electrons coming from the lead α are scattered and then reflected or transmitted.

2.4.2 Derivation of the Landauer-Büttiker formula for many reservoirs

We here consider the case in which the incoming wave function comes from the lead α . The scattering wave function of electrons coming from the α th lead with energy E is written as

$$\psi_\alpha(x_\beta, E, B) = \sqrt{\frac{m}{2\pi k \hbar^2}} [\delta_{\alpha\beta} e^{ikx_\beta} + S_{\beta\alpha}(E, B) e^{-ikx_\beta}], \quad (2.119)$$

where x_β denotes the position in the lead β , $k = \sqrt{2mE}/\hbar$ is the wave number, m is the electron mass, E is a kinetic energy of electrons, \hbar is the Planck constant, $S_{\beta\alpha}$ is the scattering amplitude from the lead α to the lead β , and B denotes a magnetic field; see also Fig. 2.3. The scattering matrix has the following properties: First, it is a unitary matrix,

$$SS^\dagger = S^\dagger S = I, \quad (2.120)$$

where I is the identity matrix, which comes from the conservation of particles [69]. Second, the time-reversal symmetry of the Schrödinger equation gives

$$S_{\alpha\beta}(E, B) = S_{\beta\alpha}(E, -B) \quad (2.121)$$

with B denoting a magnetic field, which guarantees the Onsager-Casimir relations [69]. Third, the matrix $|\mathbb{S}|^2 \equiv \{|S_{\alpha\beta}|^2\}_{\alpha,\beta}$ is doubly stochastic, that is,

$$\sum_\alpha |S_{\alpha\beta}(E, B)|^2 = \sum_\beta |S_{\alpha\beta}(E, B)|^2 = 1, \quad (2.122)$$

which is a consequence of the unitarity of the scattering matrix Eq. (2.120). We decided the normalization factor in Eq. (2.119) so that the wave function can satisfy the following orthogonal condition

$$\int dx \psi_\alpha(x, E_1, B) \psi_\beta^*(x, E_2, B) = \delta_{\alpha\beta} \delta(E_1 - E_2). \quad (2.123)$$

The current with the energy E coming from the lead α is defined as

$$j_\alpha(x, E, B) = \frac{i\hbar}{2m} \left[\psi_\alpha(x, E, B) \frac{\partial \psi_\alpha^*(x, E, B)}{\partial x} - \psi_\alpha^*(x, E, B) \frac{\partial \psi_\alpha(x, E, B)}{\partial x} \right]. \quad (2.124)$$

Inserting Eq. (2.119) to Eq. (2.124) with $x = x_\beta$, we find that the current in the lead β is independent of the position as in

$$j_\alpha(x_\beta, E, B) = \frac{1}{h} [\delta_{\alpha\beta} - |S_{\beta\alpha}(E, B)|^2]. \quad (2.125)$$

Since a reservoir is attached to the semi-infinite lead α , the incoming electrons has a Fermi distribution of the reservoir. Therefore, we obtain the particle current J_N from the reservoir α in the lead α with multiplying the corresponding Fermi distribution and integrating Eq. (2.125) with respect to energy as

$$J_N^\alpha = \sum_\beta \int dE j_\beta(x_\alpha, E, B) f_\beta(E). \quad (2.126)$$

Note that the one-dimensional density of states and the velocity of electrons are implicitly incorporated in the current operator (2.124), so that we only integrated Eq. (2.125) with respect to energy. The energy current is obtained by multiplying E with the current operator and calculating in the same way, which results in

$$J_E^\alpha = \sum_\beta \int dE E j_\beta(x_\alpha, E, B) f_\beta(E). \quad (2.127)$$

This is the kinetic energy that electrons carry. Note that when there are inelastic interactions such as an electron-electron interaction or an electron-phonon interaction, we need more terms for the energy current because such an interaction also carries energy [108]. In the present thesis, however, we always treat noninteracting electrons in the lead (or reservoir). Therefore the energy current operator is defined by the current operator multiplied by the kinetic energy of the electron E .

As explained in Eq. (1.9), the heat current from the reservoir α is calculated as

$$J_Q^\alpha = J_E^\alpha - \mu_\alpha J_N^\alpha = \sum_\beta \int dE (E - \mu_\alpha) j_\beta(x_\alpha, E, B) f_\beta(E). \quad (2.128)$$

2.4.3 The Landauer-Büttiker formula for two reservoirs

Let us consider the case of two reservoirs, in which there is the left reservoir L and the right one R as shown in Fig. 2.4. The particle current from the left reservoir is calculated as

$$J_N^L = \sum_{\beta=L,R} \int dE j_\beta(x_L, E, B) f_\beta(E) \quad (2.129)$$

$$= \frac{1}{h} \int dE \{ [1 - |S_{LL}(E, B)|^2] f_L(E) - |S_{LR}(E, B)|^2 f_R(E) \} \quad (2.130)$$



Figure 2.4: A setup of two reservoirs. In this picture, the reservoirs and the leads are denoted by L and R, respectively.

$$= \frac{1}{h} \int dE |S_{LR}(E, B)|^2 [f_L(E) - f_R(E)], \quad (2.131)$$

where we used the relation $1 - |S_{LL}(E, B)|^2 = |S_{LR}(E, B)|^2$, which we find from the unitarity of the scattering matrix $\sum_{\beta=L,R} |S_{\alpha\beta}(E, B)|^2 = \sum_{\alpha=L,R} |S_{\alpha\beta}(E, B)|^2 = 1$ in Eq. (2.122). Here $|S_{LR}(E, B)|^2$ is the transmission probability of electrons with an energy E under a magnetic field B from the right reservoir to the left one. Note that the relation $\sum_{\beta=L,R} |S_{\alpha\beta}(E, B)|^2 = \sum_{\alpha=L,R} |S_{\alpha\beta}(E, B)|^2 = 1$ also gives $|S_{LR}(E, B)|^2 = |S_{RL}(E, B)|^2$, with which we can easily show that the particle current from the right reservoir satisfies $J_N^R = -J_N^L$, which is the conservation of the particle number. We obtain the expressions of the particle and electric currents as

$$J_N \equiv J_N^L = \frac{1}{h} \int dE |S_{LR}(E, B)|^2 [f_L(E) - f_R(E)], \quad (2.132)$$

$$J_e = eJ_N = \frac{e}{h} \int dE |S_{LR}(E, B)|^2 [f_L(E) - f_R(E)]. \quad (2.133)$$

We also obtain the energy and the heat currents from the left reservoir with Eqs. (2.127) and (2.128) as

$$J_E = \frac{1}{h} \int dE E |S_{LR}(E, B)|^2 [f_L(E) - f_R(E)], \quad (2.134)$$

$$J_Q^L = J_E - \mu_L J_N = \frac{1}{h} \int dE (E - \mu_L) |S_{LR}(E, B)|^2 [f_L(E) - f_R(E)]. \quad (2.135)$$

2.4.4 The linear-response coefficients

Let us expand J_e and J_Q^L with respect to the conjugate affinities V and $\Delta T/T_R$, which gives the linear-response matrix as follows:

$$\mathbb{L} = \frac{e^2}{h} \int dE \frac{|S_{LR}(E, B)|^2}{4k_B T_R \cosh^2 \left(\frac{E - \mu_R}{2k_B T_R} \right)} \begin{pmatrix} 1 & \frac{E - \mu_R}{e} \\ \frac{E - \mu_R}{e} & \left(\frac{E - \mu_R}{e} \right)^2 \end{pmatrix}. \quad (2.136)$$

Here we used the expansion of the Fermi function as in

$$f_L - f_R = \frac{\partial f_R}{\partial \mu_R} \Delta \mu + \frac{\partial f_R}{\partial T_R} \Delta T \quad (2.137)$$

$$\equiv F(E)\Delta\mu + \frac{E - \mu_R}{T_R}F(E)\Delta T, \quad (2.138)$$

where k_B is the Boltzmann constant, $\Delta\mu \equiv \mu_L - \mu_R$, $\Delta T \equiv T_L - T_R$, and

$$F(E) \equiv \frac{1}{4k_B T_R \cosh^2\left(\frac{E - \mu_R}{2k_B T_R}\right)}. \quad (2.139)$$

We find from this result that we cannot obtain an asymmetric linear-response matrix under a magnetic field in the framework of the Landauer-Büttiker formula only with two reservoirs.

Since the linear-response matrix (2.136) is symmetric, the maximum efficiency and the efficiency at the maximum power are both characterized by the figure of merit as in Eqs. (2.15) and (2.22). As proven in Section (3.1.3), we can show that we obtain an infinite figure of merit when the transmission function $|S_{LR}(E, B)|^2$ is a delta function.

2.5 Summary and conclusion

In the present chapter, we have reviewed the linear irreversible thermodynamics, which describes thermoelectricity in the linear-response regime.

In Section 2.1, we have explained how to construct the consistent linear-response formalism, that is, how to find the conjugate affinities for the currents that we choose. We will apply the construction to the case of three reservoirs in Chapter 4.

In Section 2.2, we have considered the case of a symmetric linear-response matrix. We have first shown that the second law of thermodynamics, that is, the nonnegativity of the entropy production gives a constraint for the linear-response coefficients. We have next calculated the maximum efficiency and the efficiency at the maximum power, both of which are described by a single parameter called the figure of merit. We have found that at an infinite figure of merit, the maximum efficiency is bounded from above by the Carnot efficiency and that of the efficiency at the maximum power is a half of the Carnot efficiency, which is called the Curzon-Ahlborn bound [89]. We have also found that we can achieve the Carnot efficiency only with zero power. We will investigate how to obtain a high figure of merit with a symmetric linear-response matrix in Chapter 3 in the present thesis.

In Section 2.3, we have carried out an analysis similar to Section 2.2 but for an asymmetric linear-response matrix, which may come from the presence of a magnetic field, for example. In this case, the maximum efficiency and the efficiency at the maximum power are described by two parameters x and y in Eq. (2.33). We have found that in this case there is a possibility to break the CA bound. Moreover, we have also found that we can achieve the Carnot efficiency with nonvanishing power [90] with the conditions (2.88). However, we do not know whether or not these conditions can be satisfied in a specific model.

In Section 2.4, we have calculated the linear-response coefficients in the framework of the Landauer-Büttiker formula with two reservoirs for example. We have found that we cannot obtain an asymmetric linear-response matrix even in the presence of a magnetic field in the framework. We will investigate specific models for quantum thermoelectricity and check the conditions in Chapter 4 in the present thesis.

Chapter 3

Thermoelectricity near Anderson localization transitions

In the present chapter, we consider how to increase thermoelectric efficiency for a symmetric linear-response matrix, which is usually the case of conventional thermoelectricity. In Section 3.1, we represent familiar transport coefficients, such as the electric conductivity, the Seebeck coefficient and the thermal conductivity, in terms of the linear-response coefficients. We next obtain an expression of the linear-response coefficients from the Chester-Thellung-Kubo-Greenwood (CTKG) formulation, which can be applied only to the case in which electrons scattered elastically. Using this expression, we show that the Carnot efficiency is achieved with the delta-like density of states, which may not be achieved in real materials. We next focus on thermoelectricity near the Anderson localization, which may make a high Seebeck coefficient thanks to broken electron-hole symmetry.

In Section 3.2, we correct and extend previous studies, and introduce universal approximations that allow us to deduce the critical exponent for the zero-temperature conductivity from thermoelectric measurements for a single mobility edge. In particular, we find that at nonzero low temperatures the Seebeck coefficient and the thermoelectric efficiency can be very large on the “insulating” side, that is, for chemical potentials below the (zero-temperature) localization threshold. Corrections to the leading power-law singularity in the zero-temperature conductivity are shown to introduce nonuniversal temperature-dependent corrections to the otherwise universal functions which describe the Seebeck coefficient, the figure of merit and the Wiedemann-Franz ratio.

In Section 3.3, we consider finite-size effects. The thermoelectric coefficients are shown to have interesting dependences on the system size. While the Seebeck coefficient decreases with decreasing size, the figure of merit first decreases but then increases, while the Wiedemann-Franz ratio first increases but then decreases as the size decreases. Small (but finite) samples may thus have larger thermoelectric efficiencies.

In Section 3.4, we study thermoelectricity in systems with a pair of localization edges, the ubiquitous situation in random systems near the centers of electronic energy bands. As the disorder increases, the two thresholds approach each other, and then the Seebeck coefficient and the figure of merit increase significantly, as expected from the general arguments of Mahan and Sofo [109] for a narrow energy range of the zero-temperature metallic behavior.

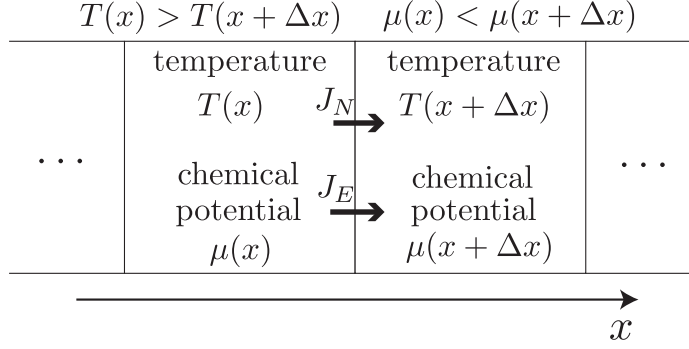


Figure 3.1: (Repeat of Fig. 1.3) Schematic picture of a thermoelectric heat engine in a bulk system. We consider the two points, x and $x + \Delta x$. We assume that the current flows in a direction, which we call x -axis. We set the chemical potential of the right reservoir higher than the left, while the temperature of the left reservoir higher than the right so that an electric current may go from left to right against the difference of the chemical potential.

In Section 3.5, we summarize the present chapter and give a discussion on our results.

3.1 Introduction and preparation

3.1.1 Thermoelectric transport coefficients

Let us consider a thermoelectric heat engine in a bulk systems in Fig. 3.1. We here make a note on the construction of the linear-response formalism in bulk systems. In bulk systems in the linear-response regime, it is conventional to use a current density (current divided by a cross section) instead of current as well as the voltage and the temperature gradients instead of their differences as in

$$\begin{pmatrix} j_e \\ j_Q^L \end{pmatrix} = \begin{pmatrix} L_{11} & L_{12} \\ L_{12} & L_{22} \end{pmatrix} \begin{pmatrix} \nabla_x V \\ \nabla_x T/T \end{pmatrix}, \quad (3.1)$$

where j_e and j_Q^L is electric and heat currents *density*, while $\nabla_x V(x) \equiv \nabla_x \mu(x)/e$ and $\nabla_x T(x)$ are the voltage and the temperature gradients. Note that we take the direction of the current as x -axis. Here $T = T(x)$ is the temperature of the system. Note that L_{11} in Eq. (3.1) has a dimension of the electric conductivity, not the electric conductance. The expression (3.1) in the linear-response regime is a bit different from the expression (2.8) in Section 2.2. However, with changing $J_e \leftrightarrow j_e$, $J_Q^L \leftrightarrow j_Q^L$, $V \leftrightarrow \nabla_x V$, $\Delta T \leftrightarrow \nabla_x T$, and considering an entropy-production density instead of an entropy production, we easily show that we can do the same discussion as in Section 2.2.

The commonly observed transport properties, namely the electrical conductivity σ , the thermopower (or the Seebeck coefficient) S and the electronic heat conductivity κ , are related

to the elements of the linear-response matrix as follows:

$$\begin{aligned}\sigma &= \left. \frac{\partial j_e}{\partial \nabla_x V} \right|_{\nabla_x T=0} = L_{11}, \\ S &= - \left. \frac{\partial \nabla_x V}{\partial \nabla_x T} \right|_{j_e=0} = \frac{L_{12}}{TL_{11}}, \\ \kappa &= \left. \frac{\partial j_Q^L}{\partial \nabla_x T} \right|_{j_e=0} = \frac{L_{11}L_{22} - L_{12}^2}{TL_{11}}.\end{aligned}\tag{3.2}$$

Note that many authors define S with a minus sign for electrons and $S > 0$ for holes, but we here define it with the opposite sign for the simplicity of presentation. For a symmetric linear-response matrix, the Peltier coefficient Π and the Seebeck coefficient S are related via the Onsager relation,

$$\Pi = \left. \frac{\partial j_Q^L}{\partial j_e} \right|_{\nabla_x T=0} = TS = \frac{L_{12}}{L_{11}}.\tag{3.3}$$

With these coefficients, the figure of merit ZT in Eq. (2.17) is written as

$$ZT = \frac{\sigma S^2}{\kappa} T.\tag{3.4}$$

In the definition of ZT , the heat conductivity κ consists of *both* the electronic heat conductivity and the phononic heat conductivity. In the present chapter, we mostly concentrate on the electronic heat conductivity and assume sufficiently low temperatures so that we can ignore the phononic heat conductivity. We briefly discuss what happens in the presence of phonons in Section 3.5. Another quantity of interest is the Wiedemann-Franz ratio,

$$\mathcal{L} = \frac{\kappa}{\sigma T} \equiv \frac{S^2}{ZT}.\tag{3.5}$$

For the electronic charge and heat conductivities in metals, the Sommerfeld expansion yields the universal Lorenz value [110] $\mathcal{L}_0 = (\pi^2/3)k_B^2/e^2$. However, as we discuss below, one encounters smaller values of \mathcal{L} in many cases, which may imply larger values of ZT .

3.1.2 Expression of the linear-response coefficients

Ignoring inelastic phononic effects, the linear-response coefficients L_{ij} are obtained with the Chester-Thellung-Kubo-Greenwood (CTKG) formulation [111–113] as

$$L_{11} = \int_{-\infty}^{\infty} dE \sigma_0(E) F(E),\tag{3.6}$$

$$L_{12} = \frac{1}{|e|} \int_{-\infty}^{\infty} dE (E - \mu) \sigma_0(E) F(E),\tag{3.7}$$

$$L_{22} = \frac{1}{e^2} \int_{-\infty}^{\infty} dE (E - \mu)^2 \sigma_0(E) F(E),\tag{3.8}$$

where

$$F(E) = -\frac{df(E)}{dE} \equiv \frac{e^\epsilon}{k_B T (1 + e^\epsilon)^2} = \frac{1}{4k_B T \cosh^2(\epsilon/2)} \quad (3.9)$$

is the negative derivative of the Fermi function with respect to the energy E , $f(E) = (1 + e^\epsilon)^{-1}$, with $\epsilon = (E - \mu)/k_B T$. Here k_B is the Boltzmann constant. Note that μ depends on the temperature, coinciding with the Fermi energy E_F only at $T = 0$ [114]. Our results are expressed in terms of μ , and thereby this subtle point is circumvented. In Eq. (3.8), $\sigma_0(E)$ is the zero-temperature conductivity of the system, which contains both the electronic density of states and the Landauer transmission through the system.

3.1.3 Transmission for the Carnot efficiency

We already know that we can achieve the Carnot efficiency with an infinite figure of merit ZT , but have not discussed with what specific system we can achieve an infinite figure of merit. The answer was given by Mahan and Sofo [109], which we briefly review here; we can attain the Carnot efficiency with the delta-like transmission.

First, we rewrite Eq. (3.8) by changing the variable $\epsilon \equiv E - \mu/(k_B T)$:

$$L_{11} = \int_{-\infty}^{\infty} dx \frac{e^\epsilon}{(1 + e^\epsilon)^2} \sigma_0(\mu + \epsilon k_B T), \quad (3.10)$$

$$L_{12} = \frac{k_B T}{|e|} \int_{-\infty}^{\infty} dx \frac{e^\epsilon}{(1 + e^\epsilon)^2} \epsilon \sigma_0(\mu + \epsilon k_B T), \quad (3.11)$$

$$L_{22} = \left(\frac{k_B T}{e}\right)^2 \int_{-\infty}^{\infty} dx \frac{e^\epsilon}{(1 + e^\epsilon)^2} \epsilon^2 \sigma_0(\mu + \epsilon k_B T). \quad (3.12)$$

Let us regard these integrals as the expectation values with respect to the distribution

$$P(\epsilon) \equiv \sigma_0(\mu + \epsilon k_B T) \frac{e^\epsilon}{(1 + e^\epsilon)^2} \quad (3.13)$$

and consider the condition for an infinite ZT :

$$L_{11}L_{22} - L_{12}^2 = \left(\frac{k_B T}{e}\right)^2 (\langle \epsilon^2 \rangle - \langle \epsilon \rangle^2) = 0, \quad (3.14)$$

where the bracket $\langle \cdot \rangle$ denotes the expectation value with respect to the distribution $P(\epsilon)$. Equation (3.14) means that the variance of the distribution $P(\epsilon)$ is zero. Such a function is a delta function. Indeed, when we consider the delta-like distribution $P(\epsilon) \equiv a\delta(\epsilon - b)$, where a and b are some constants, we confirm that the figure of merit goes to infinity.

Unfortunately, there are few materials with such a property. We therefore need a guiding principle to seek real materials with a high figure of merit. Many researchers pay attention to a high Seebeck coefficient in order to obtain a high figure of merit. We introduce in the next subsection a guiding principle to enhance the Seebeck coefficient.

3.1.4 Transmission near the Anderson localization transitions

Since $E - \mu$ is antisymmetric and $F(E)$ is symmetric with respect to μ , if $\sigma_0(E)$ is symmetric with respect to μ then the integrand of L_{12} is antisymmetric with respect to μ , which leads to $L_{12} = 0$ in Eq. (3.7), and then the Seebeck coefficient $S = 0$. Therefore, the thermoelectric effect requires breaking the electron-hole symmetry. An extreme case of such breaking arises when μ is close to a mobility threshold E_c , such that $\sigma_0(E) = 0$ for $E < E_c$ and $\sigma_0(E) > 0$ for $E > E_c$. This led to many studies of thermoelectricity in systems which obey the leading power-law behavior of the form

$$\sigma_0(E) = \begin{cases} 0 & (\text{for } E < E_c), \\ A \left| \frac{E - E_c}{E_c} \right|^x & (\text{for } E \geq E_c), \end{cases} \quad (3.15)$$

where A is a system-dependent constant (with the dimension of conductivity) and x is a universal exponent (which depends on the dimension d and on the symmetry of the system). Such behavior arises near band edges of nonrandom systems, where the electronic density of states vanishes in the gap outside the band [115], and near the mobility edge of disordered electronic systems which undergo the Anderson localization transition [116–119]. In the former case, the density of states near the band edge in d dimensions with a quadratic dispersion $(E - E_c) \propto k^2$ yields $x = (d - 2)/2$ [see Fig. 3.1.4(a)]. In the absence of electron-electron interactions, the Anderson localization transition exists only for $d > 2$, and for $d = 3$ numerical estimation [120] yields $x = (d - 2)\nu \approx 1.5$, where ν is the critical exponent for the localization length:

$$\xi = \xi_0 \left| \frac{E - E_c}{E_c} \right|^{-\nu}. \quad (3.16)$$

Theoretical analyses of Eqs. (3.8) with Eq. (3.15) are presented in quite a number of papers [114, 121–130]. Below we comment on these analyses and add several new approximations for the thermoelectric coefficients. In addition, we include three new generalizations. First, we note that Eq. (3.15) contains only the leading singularity in $\sigma_0(E)$, very close to E_c . Irrelevant variables near the localization fixed point introduce corrections to this leading behavior for $E > E_c$ of the form [119]

$$\sigma_0(E) = A \left| \frac{E - E_c}{E_c} \right|^x \left[1 + a \left| \frac{E - E_c}{E_c} \right|^y + \dots \right], \quad (3.17)$$

where a is the amplitude of the leading correction term and the dots represent higher-order corrections. For the three-dimensional Anderson localization, the singular correction exponent y seems to be much larger than unity [119]. Therefore, larger deviations are expected to arise from analytic corrections with $y = 1$, which may result from nonlinear scaling fields [131] and from the energy dependence of the density of states. Section 3.2 presents detailed calculations of the thermoelectric coefficients in various regimes, including these corrections.

Second, the finite-size dependence of the linear-response coefficients is introduced in Section

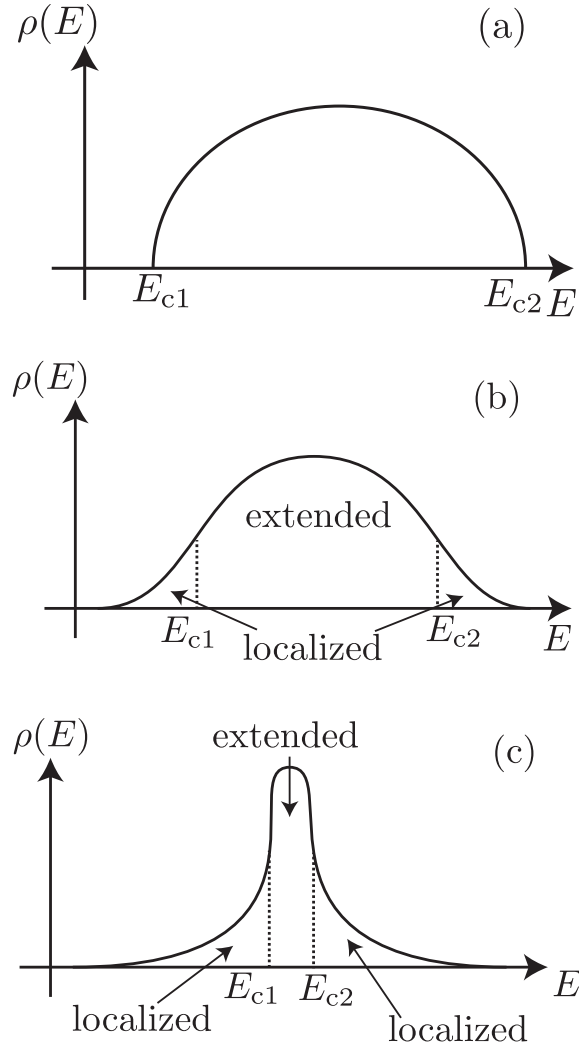


Figure 3.2: Schematic pictures of the density of states, $\rho(E)$, as a function of the energy E in three dimensions for (a) a nonrandom system, (b) with two mobility edges near the band edges, (c) with two mobility edges near the center of the band.

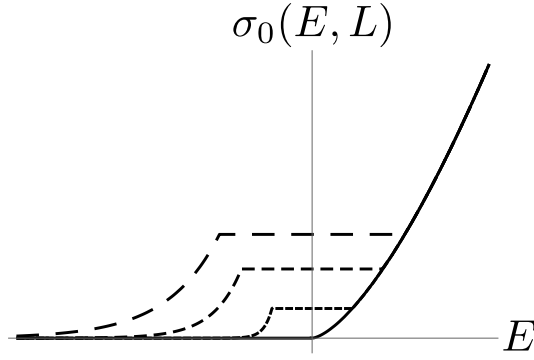


Figure 3.3: A schematic picture of the energy dependence of the zero-temperature conductivity in a finite system. The flat horizontal line is broader and higher for smaller samples.

3.3. For a sample of linear size L , Eq. (3.15) must be replaced by the scaling form [119]

$$\sigma_0(E, L) = A \left| \frac{E - E_c}{E_c} \right|^x \mathcal{F} \left(\frac{L}{\xi} \right), \quad (3.18)$$

where $\mathcal{F}(z)$ is a universal scaling function which obeys

$$\mathcal{F}(u) = \begin{cases} 1 & (\text{for } u \gg 1, E > E_c), \\ u^{-x/\nu} & (\text{for } |u| \ll 1), \\ e^{-u} & (\text{for } u \gg 1, E < E_c). \end{cases} \quad (3.19)$$

In three dimensions, the exponents are related by $x/\nu = d - 2 = 1$ [132].

Fig. 3.3 illustrates the zero-temperature conductivity of a finite system. The plateaus appear in the region $|(E - E_c)/E_c| < (L/\xi_0)^{-1/\nu}$, where $L < \xi$, and therefore the zero-temperature conductivity depends only on L and not on ξ . As the system size L decreases, the width of the plateau increases. Since on this plateau σ_0 does not depend on the energy, electron-hole symmetry is maintained and this region will not contribute to the Seebeck coefficient. In Section 3.3, we present new explicit results for the size dependence of the various thermoelectric coefficients and ratios.

Third, we note that the above discussion assumed a single mobility edge at $E = E_c$, so that $\sigma_0(E)$ is nonzero for all energies $E > E_c$, as in Eq. (3.15). As noted in Refs. [133–135] in a band of a finite width, the Anderson localization arises in the two band tails, and therefore the zero-temperature conductivity is nonzero only over a finite energy range. For the nonrandom case [Fig. 3.1.4(a)], the effects of the finite width of the energy bands were emphasized in Refs. [136, 137]. However, we are not aware of any analysis of thermoelectricity with two mobility edges at E_{c1} and E_{c2} [Figs. 3.1.4(b) and (c)]. For a large splitting between the two mobility edges, $E_{c2} - E_{c1} \gg k_B T$, it is enough to consider a single mobility edge [the function $F(E)$ in Eqs. (3.8) “captures” only one mobility edge]. However, when the width $k_B T$ of $F(E)$ is larger than $E_{c2} - E_{c1}$, both mobility edges should be included. If one assumes a symmetric band around $E = 0$, with fully localized states for $|E| > |E_c|$ [Figs. 3.1.4(b) and 3.1.4(c)], then

Eq. (3.15) must be replaced by

$$\sigma_0(E) = \begin{cases} 0 & (\text{for } |E| > |E_c|), \\ A \left[1 - \left| \frac{E}{E_c} \right| \right]^x & (\text{for } |E| \leq |E_c|) \end{cases} \quad (3.20)$$

(The absolute value of E was missing in Ref. [114]). Note that this function should vary smoothly near $E = 0$, but such a change has only a small effect on the results. In Section 3.4 we extend the analysis to the case of such a narrow band. When $|E_c| \gg k_B T$, the two localization thresholds are far apart, and the results of a single threshold are reproduced.

However, when $|E_c| < k_B T$, the zero-temperature conductivity is nonzero only over a narrow range, and then we find a large thermoelectric efficiency. In the limit of a very narrow energy range, such an increase was originally noted by Mahan and Sofo [78, 109] as shown in Subsection 3.1.3. Since the width $2|E_c|$ decreases with increasing disorder [going from Fig. 3.1.4(b) to 3.1.4(c)], we thus find that *increasing the disorder generates more efficient thermoelectricity*.

3.2 The infinite system

3.2.1 General considerations

Defining

$$\epsilon \equiv \frac{E - \mu}{k_B T}, \quad z \equiv \frac{\mu - E_c}{k_B T}, \quad (3.21)$$

and using Eq. (3.17), we can rewrite Eqs. (3.8) as

$$\begin{aligned} L_{11} &= A t^x [K_0(x, z) + a t^y K_0(x + y, z) + \dots], \\ L_{12} &= A \frac{k_B T}{|e|} t^x [K_1(x, z) + a t^y K_1(x + y, z) + \dots], \\ L_{22} &= A \left(\frac{k_B T}{e} \right)^2 t^x [K_2(x, z) + a t^y K_2(x + y, z) + \dots], \end{aligned} \quad (3.22)$$

where

$$t = \frac{k_B T}{|E_c|}. \quad (3.23)$$

The coefficient A in Eq. (3.22) comes from Eq. (3.15) or from Eq. (3.17); it is canceled in the expressions for S , ZT , and \mathcal{L} , which we analyze below. The coefficient a comes from the leading correction in Eq. (3.17), and the dots denote terms of order $(a t^y)^2$ and higher terms. The functions $K_n(x, z)$ are defined as

$$K_n(x, z) = \int_{-z}^{\infty} d\epsilon \epsilon^n (\epsilon + z)^x \frac{1}{4 \cosh^2(\epsilon/2)}. \quad (3.24)$$

In terms of the integrals (3.24), the Seebeck coefficient S , the figure of merit ZT , and the

Wiedemann-Franz ratio \mathcal{L} , take the forms

$$S = \frac{k_B}{|e|} \frac{K_1(x, z)}{K_0(x, z)} \left[1 + at^y \left(\frac{K_1(x+y, z)}{K_1(x, z)} - \frac{K_0(x+y, z)}{K_0(x, z)} \right) + \dots \right], \quad (3.25)$$

$$ZT = \frac{K_1(x, z)^2}{K_0(x, z)K_2(x, z) - K_1(x, z)^2} \left[1 + at^y \left(2 \frac{K_1(x+y, z)}{K_1(x, z)} - \frac{K_0(x, z)K_2(x+y, z) + K_2(x, z)K_0(x+y, z) - 2K_1(x, z)K_1(x+y, z)}{K_0(x, z)K_2(x, z) - K_1(x, z)^2} \right) + \dots \right], \quad (3.26)$$

and

$$\begin{aligned} \mathcal{L} = & \left(\frac{k_B}{e} \right)^2 \frac{K_0(x, z)K_2(x, z) - K_1(x, z)^2}{K_0(x, z)^2} \left[1 + \right. \\ & at^y \left(\frac{K_0(x, z)K_2(x+y, z) + K_2(x, z)K_0(x+y, z) - 2K_1(x, z)K_1(x+y, z)}{K_0(x, z)K_2(x, z) - K_1(x, z)^2} - 2 \frac{K_0(x+y, z)}{K_0(x, z)} \right) \\ & \left. + \dots \right]. \end{aligned} \quad (3.27)$$

Using only the leading term in the zero-temperature conductivity [Eq. (3.15)], Eqs. (3.25), (3.26), and (3.27) become

$$S = \frac{k_B}{|e|} \frac{K_1(x, z)}{K_0(x, z)}, \quad (3.28)$$

$$ZT = \frac{K_1(x, z)^2}{K_0(x, z)K_2(x, z) - K_1(x, z)^2}, \quad (3.29)$$

and

$$\mathcal{L} = \left(\frac{k_B}{e} \right)^2 \frac{K_0(x, z)K_2(x, z) - K_1(x, z)^2}{K_0(x, z)^2}, \quad (3.30)$$

respectively. For a given value of the exponent x , these are universal functions of $z = (\mu - E_c)/(k_B T)$ [Eq. (3.21)]. These functions are calculated numerically and plotted in Fig. 3.4 for four values of x . Similar numerical plots for S appeared in Refs. [114, 126] for any value of z , and in Refs. [129, 130] for $z \geq 0$. Ones for ZT appeared in Refs. [128, 130] for $z > 0$.

As seen in Fig. 3.4(a), S vanishes at positive infinite z and increases monotonically to infinity as $z \rightarrow -\infty$. Moreover, at each value of z , the Seebeck coefficient increases with x . Therefore, in three dimensions, we expect this coefficient to be larger near the Anderson threshold in the random system ($x = \nu \approx 1.5$), compared to its behavior near the band edge of the normal metal, for which $x = 0.5$.

The figure of merit ZT [Fig. 3.4(b)] also vanishes at infinite z and increases monotonically to infinity as $z \rightarrow -\infty$. Although ZT increases monotonically with x for $z > 0$, the lines cross at negative z and ZT decreases with increasing x for large negative z . Interestingly, ZT crosses the “desired” value of 3 already at $z \approx -0.5$.

As seen in Fig. 3.4(c), \mathcal{L} always approaches the Lorenz value [$\mathcal{L}_0 = (\pi^2/3)k_B^2/e^2$, shown in the figure by the thin horizontal line] for large z , but it decreases with decreasing x , approaching different x -dependent constants for large negative values of z .

3.2.2 Approximations

Appendix A elaborates on the computation of the integrals $K_n(x, z)$ in Eq. (3.24) in three regimes of z , *i.e.* $z \gg 1$, $|z| \ll 1$, and $z \ll -1$, and uses them to obtain analytic approximations for the linear-response coefficients L_{ij} . The behavior of the Seebeck coefficient S , the figure of merit ZT , and the Wiedemann-Franz ratio \mathcal{L} in these regimes is discussed in the following. As can be seen in Fig. 3.5, the three approximations found in Appendix A are accurate over wide ranges of z .

1. $z \gg 1$: For $\mu - E_c \gg k_B T$, *i.e.*, $z \gg 1$, the expansion (A.2) in powers of $1/z$ is equivalent to the Sommerfeld approximation [110]. The leading term in S decays for $(\mu - E_c) \gg k_B T$ as [114, 122, 123, 126, 129, 130]

$$S \approx \frac{k_B}{|e|} \frac{\pi^2}{3} \frac{x}{z} = \frac{k_B}{|e|} \frac{\pi^2}{3} \frac{x k_B T}{\mu - E_c}. \quad (3.31)$$

An accurate measurement of the decay of S for $\mu - E_c \gg k_B T$ can therefore yield the value of the exponent x [129].

Equation (A.4) contains two leading corrections to the leading-order Seebeck coefficient, Eq. (3.31). The first correction

$$\pi^2 \frac{x(x-1)(x-7)}{15z^2} \quad (3.32)$$

is universal. It arises from the expansion of S to the second order in $1/z$ [129] and modifies the linear temperature dependence of S by adding a term of order T^3 . Writing

$$\frac{3|e|}{k_B \pi^2} S = c_1 T + c_3 T^3, \quad (3.33)$$

one finds

$$\frac{c_3}{c_1^2} = \frac{\pi^2}{15} x(x-1)(x-7). \quad (3.34)$$

Interestingly, this ratio becomes negative for $x > 1$. Measuring this ratio can yield another identification of the exponent x . As seen in Fig. 3.5(a), the approximation Eq. (A.4) (at $a = 0$) is excellent for $z > 3$.

The second correction to S in Eq. (A.4), ayt^y , which comes from the leading correction to scaling in Eq. (3.17), introduces a nonuniversal temperature dependence to the universal amplitude $(\pi^2/3)xk_B/|e|$ in Eq. (3.31). At a fixed chemical potential μ , this correction also implies that S is not linear in the temperature:

$$S \propto T \left[x + ay \left(\frac{k_B T}{|E_c|} \right)^y \right]. \quad (3.35)$$

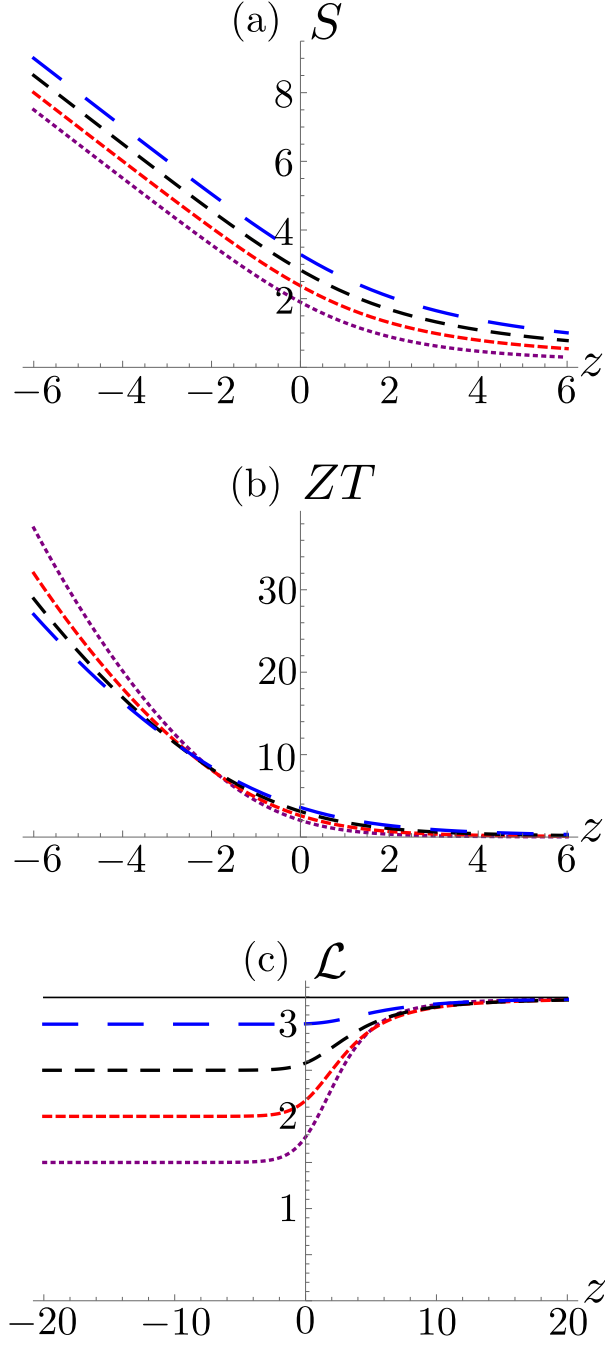


Figure 3.4: The leading universal dependences of the Seebeck coefficient S [in units of $k_B/|e|$, panel (a)], the figure of merit ZT [panel (b)], and the Wiedemann-Franz ratio \mathcal{L} [in units of $(k_B/|e|)^2$, panel (c)] versus $z = (\mu - E_c)/(k_B T)$, Eqs. (3.28), (3.29) and (3.30), with $x = 0.5$ [dotted (magenta) curve], $x = 1$ [small-dashed (red) curve], $x = 1.5$ [medium-dashed (black) curve], and $x = 2$ [large-dashed (blue) curve].

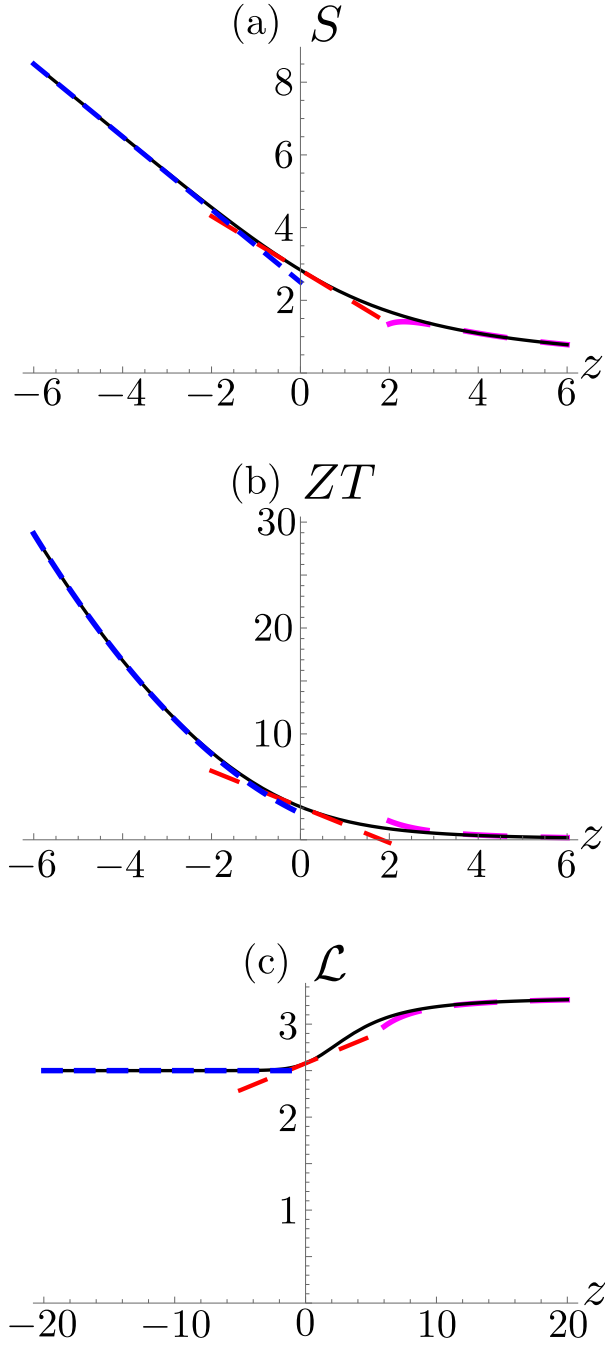


Figure 3.5: Comparisons of the full curves from Fig. 3.4, with $x = 1.5$ [solid (black) curves], with the various approximants (dashed lines). Each panel shows two leading terms in Eqs. (A.4), (A.5), or (A.6) for $z \gg 1$ [larger-dashed (magenta) curve] and in Eqs. (A.12), (A.14) or (A.16) for $|z| \ll 1$ [dashed (red) line], and one leading term in Eqs. (A.23), (A.24), or (3.39) for $z \ll -1$ [dotted (blue) line].

Note that the temperature dependence of μ , which is quadratic in T , is ignored [110, 114]. Plotting S/T versus T could help identify the leading correction exponent y .

The leading term in ZT decays for $\mu - E_c \gg k_B T$ as [125, 130]

$$ZT \approx \frac{\pi^2}{3} \frac{x^2}{z^2} = \frac{\pi^2}{3} \left(\frac{x k_B T}{\mu - E_c} \right)^2. \quad (3.36)$$

Equation (A.5) contains the two leading corrections to Eq. (3.36). The first (universal) correction modifies the quadratic temperature dependence of ZT , adding a new term of order T^4 . As seen on the right-hand side of Fig. 3.5(b), including this new term gives an excellent approximation for $z > 3$. The second correction, whose origin is the leading correction in Eq. (3.17), introduces a nonuniversal correction to the universal amplitude $\pi^2 x^2/3$ in Eq. (A.5), which varies with $t = k_B T/|E_c|$.

For $z \gg 1$, Eq. (A.6) shows the decrease of \mathcal{L} from the universal Lorenz value \mathcal{L}_0 . Interestingly enough, this x -dependent expression has not appeared in the literature (even for nonrandom band edges). Unlike the x -independent \mathcal{L}_0 , this correction term, which is of order $1/z^2 \propto T^2$, does depend on x . Note that the correction of order at^y vanishes.

2. $|z| \ll 1$: If one ignored the constraint $z \gg 1$, *i.e.*, $k_B T \ll \mu - E_c$ in Eq. (3.31), then one would wrongly conclude an apparent divergence of the Seebeck coefficient S for $\mu \rightarrow E_c + 0$ at fixed T . This led to some confusion in early papers based on the Sommerfeld approximation (*e.g.*, Ref. [124]). However, the situation was clarified in Refs. [114, 126], which showed that at the mobility edge $\mu = E_c$ (*i.e.*, $z = 0$), S approaches a *finite universal* value, which follows from the leading terms in Eq. (A.11):

$$S(z = 0) = \frac{k_B}{|e|} \frac{(x+1)I_{x+1}}{xI_x}, \quad (3.37)$$

where I_u is given in Eq. (A.8). The left panel in Fig. 3.6 shows $S_0 = S(z = 0)$ versus x . The Seebeck coefficient increases monotonically with x at $z = 0$. Measuring S at the mobility edge, $\mu = E_c$, can thus identify the exponent x .

The first (universal) correction gives a linear dependence on $z = (\mu - E_c)/(k_B T)$, for $|z| \ll 1$; see Eq. (A.13). Similar approximations of the form $S = S_0 - S_1 z$ but with wrong coefficients appeared in Refs. [114, 122, 129]. Reference [123] gave a linear expression, without specifying the coefficients S_0 and S_1 . The x dependences of the coefficients S_0 and S_1 calculated from Eq. (A.13) are displayed in Fig. 3.6. As seen in Fig. 3.5(a), the linear dependence of S on z fits the full curve reasonably well for $|z| < 1/2$. Measuring the slope of this curve for small z also yields information on the exponent x . The second correction comes from the leading correction to scaling. This correction introduces a small nonuniversal nonlinear variation of S with $t = k_B T/|E_c|$.

Similarly, ignoring the constraint $k_B T \ll \mu - E_c$ in Eq. (3.36), one would also find an apparent divergence of ZT for $\mu \rightarrow E_c$ at fixed T . However, the leading terms in Eq. (A.11)

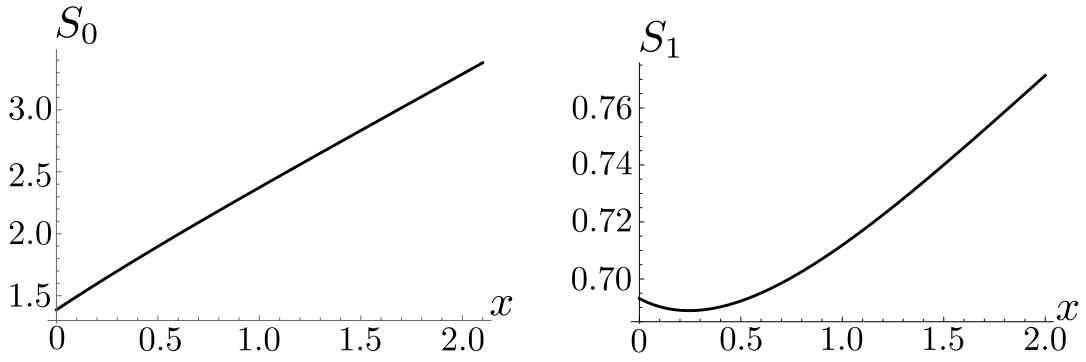


Figure 3.6: The x dependences of the coefficients S_0 (left) and S_1 (right) (in units of $k_B/|e|$) in Eq. (A.13).

imply that *at* the mobility edge $\mu = E_c$, ZT approaches a finite universal value:

$$ZT(z=0) = Z_0 = \frac{(x+1)^2 I_{x+1}^2}{(x+2)xI_{x+2}I_x - (x+1)^2 I_{x+1}^2}. \quad (3.38)$$

The left panel of Fig. 3.7 shows $Z_0 = ZT(z=0)$ versus x as given in Eq. (3.38). A few specific values were listed in Ref. [128]. As already seen in Fig. 3.4(b), the figure of merit increases monotonically with x .

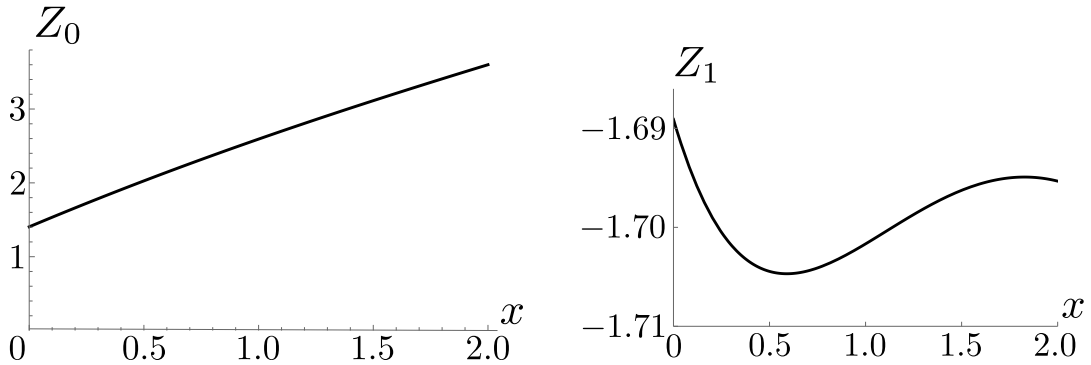


Figure 3.7: The x -dependences of the coefficients Z_0 and Z_1 in $ZT \approx Z_0 + Z_1 z$ for $|z| \ll 1$, Eq. (A.15).

For $|z| \ll 1$, Eqs. (A.15) also give the leading corrections to the figure of merit. The first (universal) correction practically gives a linear dependence on $z = (\mu - E_c)/(k_B T)$, for $|z| \ll 1$. Equation (A.15) is used to plot the x -dependence of Z_0 and of Z_1 ; see Fig. 3.7. Note that Z_1 is practically independent of x . The figure of merit decreases monotonically with increasing z . As seen in Fig. 3.5(b), the linear dependence of ZT on z fits the full curve (for $a = 0$) reasonably well for $|z| < 1/2$. The second correction, which comes from the leading correction to Eq. (3.17), introduces a small temperature-dependent nonuniversal nonlinear variation of ZT with $t = k_B T/|E_c|$.

3. $z \ll -1$: Finally, we turn to the “insulating” side of the mobility edge, $\mu < E_c$. Although the linear-response coefficients (including the conductivity) vanish in this regime at $T = 0$, they become nonzero for $T > 0$ due to the tail of the Fermi function. This regime, which apparently has not attracted much previous interest, deserves a close inspection. Equations (A.22) show that the linear-response coefficients decay exponentially in z for $z \ll -1$. However, as seen from Figs. 3.4(a) and 3.4(b), the Seebeck coefficient and the figure of merit grow significantly as z becomes more negative. Although Refs. [125, 127] mentioned that ZT may be large for negative z , no explicit expression for this increase was provided.

Equations (A.23) and (A.24) give analytic approximations for S and ZT for $z \ll -1$. Figure 3.5(a) shows the lowest-order (universal) term in Eq. (A.23), which is linear in z . Clearly, this linear term represents an excellent approximation for S for $z < -3$. The intercept of this straight line with the S -axis gives $(1 + x)$. Similarly, Fig. 3.5(b) shows the lowest-order (universal) term of the figure of merit, $ZT = (1 + x - z)^2/(1 + x)$, which is quadratic in z . This quadratic term represents an excellent approximation of ZT for $z < -2$. The intercept of this parabola with the ZT -axis, equal to $(1 + x)$, can be used to determine the value of the exponent x . For $z \ll -1$, Eqs. (A.22) also yield

$$\mathcal{L} = \left(\frac{k_B}{e} \right)^2 [x + 1 + \mathcal{O}(e^z, at^y)], \quad (3.39)$$

which approaches the constant limit $(k_B/e)^2(x + 1)$ [see Fig. 3.4(c)].

As already stated, the nonuniversal correction of order at^y introduces an additional small temperature-dependent nonlinear variation of S with $t = k_B T/|E_c|$. Figure 3.8 shows the Seebeck coefficient in Eq. (3.25) and the figure of merit in Eq. (3.26) for several values of $\mu - E_c$, y , and a . Increasing the temperature increases the Seebeck coefficient for $a > 0$ and decreases it for $a < 0$. The effect is much stronger for larger y . For $\mu - E_c > 0$, increasing temperature increases ZT for $a > 0$ and decreases it for $a < 0$. For $\mu - E_c \leq 0$, increasing temperature decreases ZT for $a > 0$ and increases it for $a < 0$. Again, the effect is much larger for larger y .

Figure 3.9 shows the temperature dependence of \mathcal{L} with $a \neq 0$. Interestingly, the corrections introduce a temperature dependence of the Wiedemann-Franz ratio even in regions where it was temperature independent in their absence.

3.3 Finite-size effects

With Eqs. (3.18) and (3.19), effects due to the finite size of the system can be taken into account upon replacing Eq. (3.24) by

$$\begin{aligned} K_n(x, z) &\rightarrow \tilde{K}_n(x, z, L) = \epsilon_L^x \int_{-z-\epsilon_L}^{-z+\epsilon_L} d\epsilon \, \epsilon^n \frac{1}{4 \cosh^2(\epsilon/2)} + \int_{-z+\epsilon_L}^{\infty} d\epsilon \, \epsilon^n (\epsilon + z)^x \frac{1}{4 \cosh^2(\epsilon/2)} \\ &= K_n(x, z) + \epsilon_L^x \int_{-z-\epsilon_L}^{-z+\epsilon_L} d\epsilon \, \epsilon^n \frac{1}{4 \cosh^2(\epsilon/2)} - \int_{-z}^{-z+\epsilon_L} d\epsilon \, \epsilon^n (\epsilon + z)^x \frac{1}{4 \cosh^2(\epsilon/2)}, \end{aligned} \quad (3.40)$$

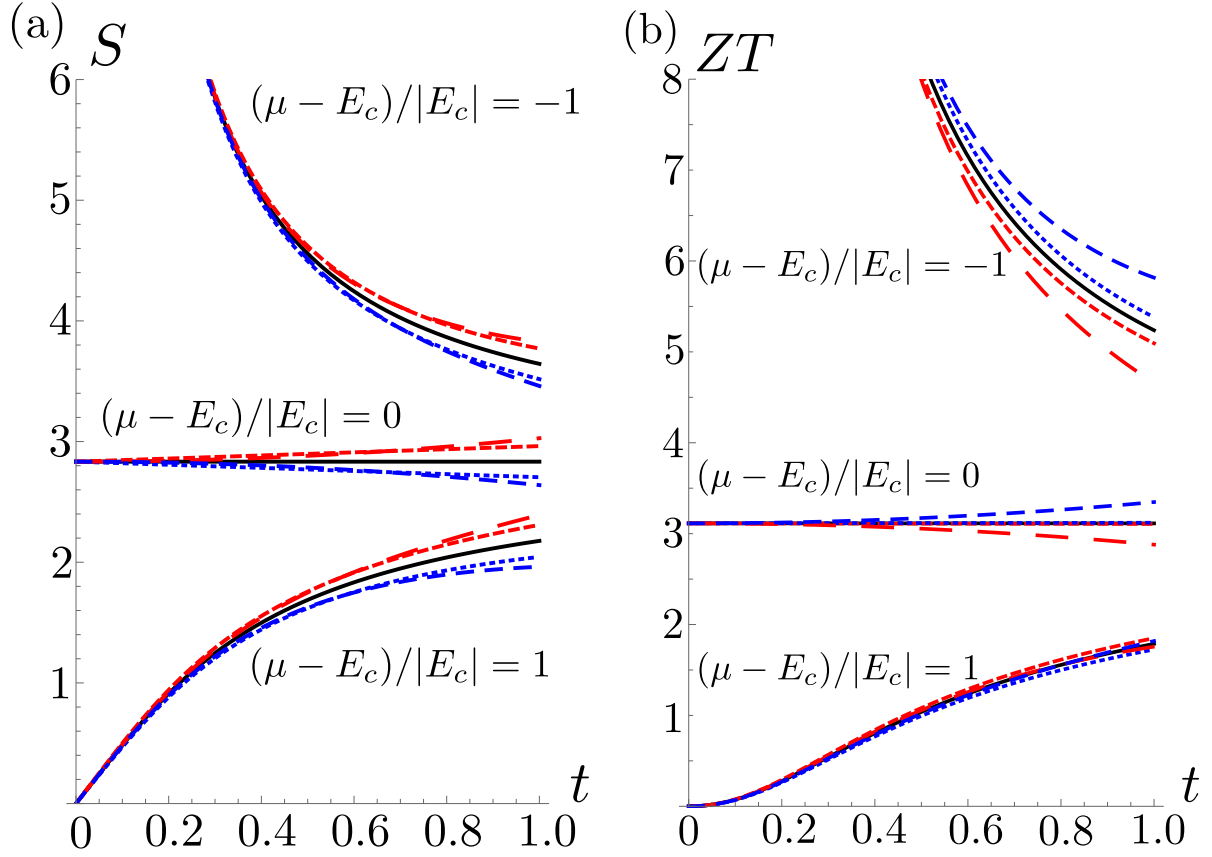


Figure 3.8: (a) The Seebeck coefficient in Eq. (3.25) and (b) the figure of merit in Eq. (3.26), versus $t = k_B T / |E_c|$ for $x = 1.5$, and $y = 1$, with $a = 0$ [solid (black) curves], $a = 0.05$ [dashed (red) curves], and $a = -0.05$ [dotted (blue) curves], as well as for $y = 2$, with $a = 0.01$ [largest-dashed (red) curves] and $a = -0.01$ [medium-dashed (blue) curves]: $(\mu - E_c) / |E_c| = -1$ (top), $(\mu - E_c) / |E_c| = 0$ (middle), $(\mu - E_c) / |E_c| = 1$ (bottom).

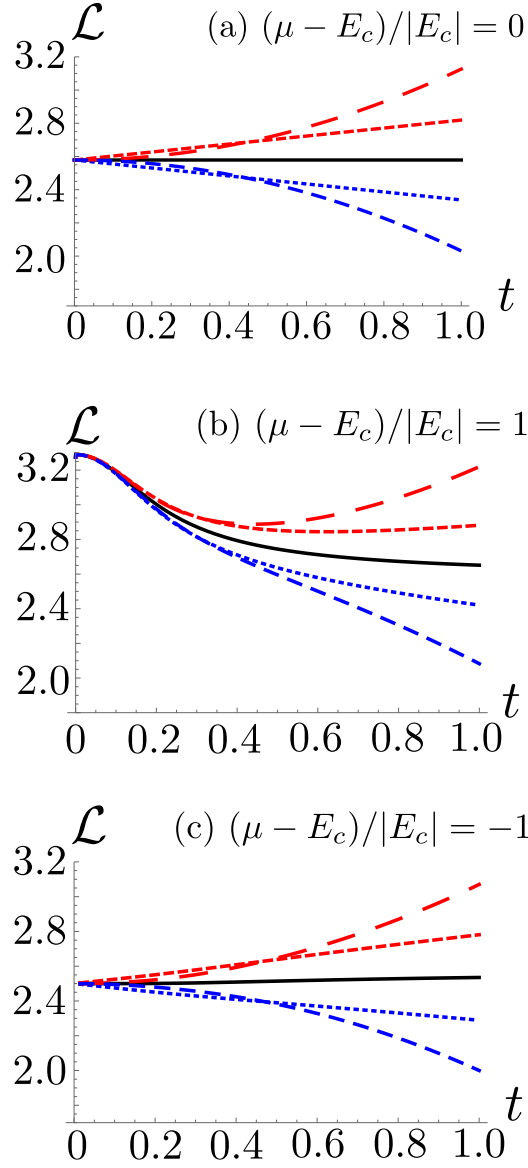


Figure 3.9: The Wiedemann-Franz ratio \mathcal{L} in Eq. (3.27) versus $t = k_B T / |E_c|$ for $x = 1.5$, $y = 1$, with $a = 0$ [solid (black) curve], $a = 0.05$ [dashed (red) curve] and $a = -0.05$ [dotted (blue) curve], as well as for $y = 2$, with $a = 0.01$ [largest-dashed (red) curve] and $a = -0.01$ [medium-dashed (blue) curve]. (a) $(\mu - E_c)/|E_c| = 0$, (b) $(\mu - E_c)/|E_c| = 1$, (c) $(\mu - E_c)/|E_c| = -1$.

where the exponentially small term in σ_0 of the insulating phase, which arises from finite-size effects, is neglected. Here

$$\epsilon_L = \frac{E_c}{k_B T} \left(\frac{\xi_0}{L} \right)^{1/\nu} \quad (3.41)$$

is a dimensionless energy, which is a measure of the finite-size effects. This energy determines the width of the plateaus in Fig. 3.3. Ignoring the corrections to scaling, we obtain the Seebeck coefficient, the figure of merit, and the Wiedemann-Franz ratio [Eqs. (3.27), (3.28), and (3.29)] as

$$S = \frac{k_B}{|e|} \frac{\tilde{K}_1(x, z, L)}{\tilde{K}_0(x, z, L)}, \quad (3.42)$$

$$ZT = \frac{\tilde{K}_1(x, z, L)^2}{\tilde{K}_0(x, z, L)\tilde{K}_2(x, z, L) - \tilde{K}_1(x, z, L)^2}, \quad (3.43)$$

and

$$\mathcal{L} = \left(\frac{k_B}{e} \right)^2 \frac{\tilde{K}_0(x, z, L)\tilde{K}_2(x, z, L) - \tilde{K}_1(x, z, L)^2}{\tilde{K}_0(x, z, L)^2}. \quad (3.44)$$

At $z = 0$, the first term in Eq. (3.40) vanishes for $n = 1$ because the integrand is odd in ϵ , so that

$$\tilde{K}_1(x, 0, L) - K_1(x, 0) = - \int_0^{\epsilon_L} d\epsilon \epsilon^{1+x} (\epsilon + z)^x \frac{1}{4 \cosh^2(\epsilon/2)}, \quad (3.45)$$

which becomes more negative as ϵ_L increases. In contrast, for $n = 0, 2$, one has

$$\tilde{K}_n(x, 0, L) - K_n(x, 0) = \int_0^{\epsilon_L} d\epsilon (2\epsilon_L^x - \epsilon^x) \epsilon^n (\epsilon + z)^x \frac{1}{4 \cosh^2(\epsilon/2)}, \quad (3.46)$$

which becomes more positive as ϵ_L increases. Since \tilde{K}_1 decreases and \tilde{K}_0 increases with ϵ_L , the Seebeck coefficient S decreases with decreasing system size. Since both \tilde{K}_0 and \tilde{K}_2 increase, while \tilde{K}_1 decreases, the electronic heat conductivity κ (proportional to $\tilde{K}_0\tilde{K}_2 - \tilde{K}_1^2$) also increases with decreasing size, and therefore the figure of merit ZT decreases with decreasing L . The situation is more complicated for the Wiedemann-Franz ratio \mathcal{L} ; both numerator and denominator in Eq. (3.44) increase with ϵ_L , and the result for \mathcal{L} is not monotonic.

For $z \gg 1$ the finite-size corrections are very small; the difference

$$\tilde{K}_n(x, z, L) - K_n(x, z) \approx \epsilon_L^x \int_{-z-\epsilon_L}^{-z+\epsilon_L} d\epsilon \epsilon^n e^\epsilon + \int_{-z}^{-z+\epsilon_L} d\epsilon \epsilon^n (\epsilon + z)^x e^\epsilon \quad (3.47)$$

is very small, of order e^{-z} , compared to the much larger expressions in Eq. (A.2). In contrast, for $z \ll -1$ both $K_n(x, z)$ [Eq. (A.21)] and the differences (3.47) for each $n = 1, 2, 3, \dots$ are

exponentially small, of order $e^{-|z|}$, and one therefore expects significant finite-size corrections. Using the same approximations as in Eq. (A.21), we find

$$\begin{aligned}\tilde{K}_0(x, z, L) &= e^z [\epsilon_L^x (e^{\epsilon_L} - e^{-\epsilon_L}) + \Gamma(x+1, \epsilon_L)] \equiv K_{00}, \\ \tilde{K}_1(x, z, L) &= e^z \left\{ \epsilon_L^x [(1 - \epsilon_L - z)e^{\epsilon_L} - (1 - z)e^{-\epsilon_L}] + (x+1-z)\Gamma(x+1, \epsilon_L) \right\} \equiv K_{10} - K_{00}z, \\ \tilde{K}_2(x, z, L) &= e^z \left\{ \epsilon_L^x [(\epsilon_L^2 - 2\epsilon_L + 2 + 2(\epsilon_L - 1)z + z^2)e^{\epsilon_L} + (x\epsilon_L - 2 + 2z - z^2)e^{-\epsilon_L}] \right. \\ &\quad \left. + [(x+1)(x+2) - 2(x+1)z + z^2]\Gamma(x+1, \epsilon_L) \right\} \equiv K_{20} - 2K_{10}z + K_{00}z^2, \quad (3.48)\end{aligned}$$

where

$$\Gamma(s, r) \equiv \int_r^\infty dt \, t^{s-1} e^{-t} \quad (3.49)$$

is the upper incomplete Gamma function. Note that $\Gamma(s+1, r) = s\Gamma(s, r) + r^s e^{-r}$.

Figure 3.10 displays the size dependence of S , ZT , and \mathcal{L} , for several nonpositive values of z . We show the results only for small values of ϵ_L , because the power laws are applicable only near the transition point. As Fig. 3.10(a) shows, the Seebeck coefficient S continues to decrease with increasing ϵ_L also for $z \ll -1$. An explicit calculation of Eqs. (3.48) shows that \tilde{K}_0 , \tilde{K}_1 , \tilde{K}_2 , and κ all increase with ϵ_L . However, as seen in Figs. 3.10(b) and 3.10(c), their ratios for ZT and for \mathcal{L} are not monotonic in ϵ_L . In particular, at $z = -10$, the figure of merit becomes comparable to its value for the infinite system around $\epsilon_L \approx 2$. For relatively large ϵ_L ($1 \leq \epsilon_L \leq 2$), the figure of merit increases [Fig. 3.10(b)] and the Wiedemann-Franz ratio decreases [Fig. 3.10(c)] with decreasing size.

Figure 3.11 displays S , ZT , and \mathcal{L} versus z for several values of the system size. As expected, for $z \gg 1$, all three quantities are almost size independent. For $z \ll -1$, Eqs. (3.48) give

$$S = \frac{L_{12}}{TL_{11}} = \frac{k_B}{|e|} \left\{ \frac{\epsilon_L^x [(1 - \epsilon_L)e^{\epsilon_L} - e^{-\epsilon_L}] + (x+1)\Gamma(x+1, \epsilon_L)}{\epsilon_L^x (e^{\epsilon_L} - e^{-\epsilon_L}) + \Gamma(x+1, \epsilon_L)} - z \right\}. \quad (3.50)$$

The Seebeck coefficient is linear in z , with a size-independent slope. As seen in Fig. 3.11(a), the magnitude of S decreases with decreasing size.

In contrast to S , as already seen in Fig. 3.10(b), ZT exhibits a nontrivial nonmonotonic size dependence for $z < 0$. For large negative z , Eqs. (3.4) and (3.48) show that

$$ZT = \frac{(K_{10} - K_{00}z)^2}{K_{00}K_{20} - K_{10}^2}. \quad (3.51)$$

Numerically, this function is found to decrease with ϵ_L for small ϵ_L , but then to increase for $\epsilon_L \gtrsim 1$, thus explaining the nonmonotonic size dependence of ZT . In this range, smaller devices are more efficient.

Figure 3.11(c) presents the z dependence of the Wiedemann-Franz ratio for several system sizes. Note again that there is almost no size dependence for $z \gg 1$. For large negative z the ratio \mathcal{L} approaches the z -independent limit $\mathcal{L} \approx (K_{00}K_{20} - K_{10}^2)/K_{00}^2$. As can be seen in Fig. 3.11(c), this value is also not monotonic in ϵ_L .

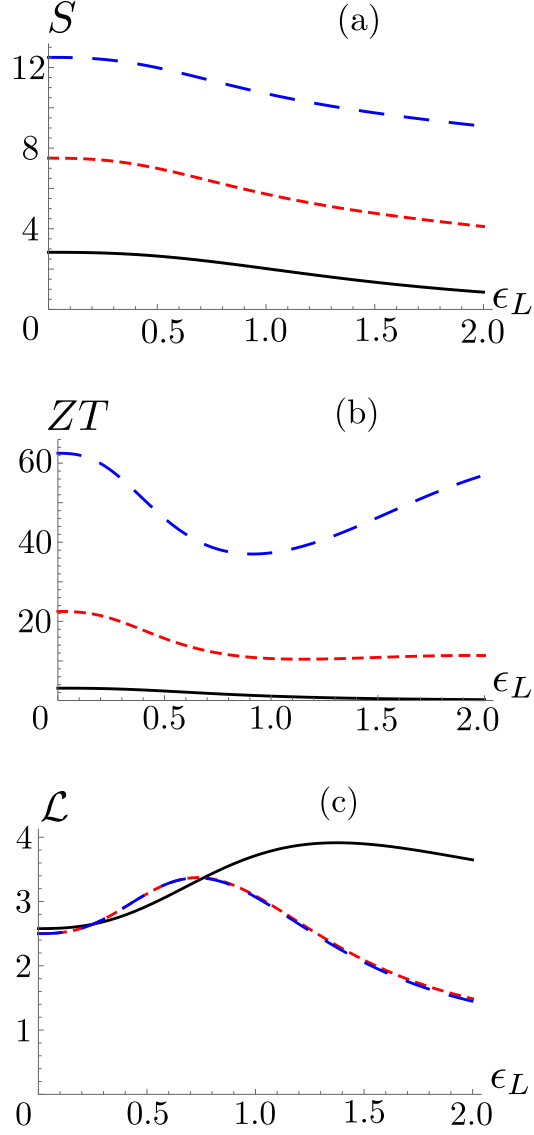


Figure 3.10: The Seebeck coefficient S [in units of $k_B/|e|$, panel (a)], the figure of merit ZT [panel (b)] and the Wiedemann-Franz ratio \mathcal{L} [in units of $(k_B/|e|)^2$, panel (c)] as functions of the dimensionless energy ϵ_L , Eqs. (3.42), (3.43), and (3.44), for $x = 1.5$ and $z = 0$ [solid (black) curve], $z = -5$ [small-dashed (red) curve], and $z = -10$ [large-dashed (blue) curve]. Note that \mathcal{L} is practically independent of z for $z \ll -1$.

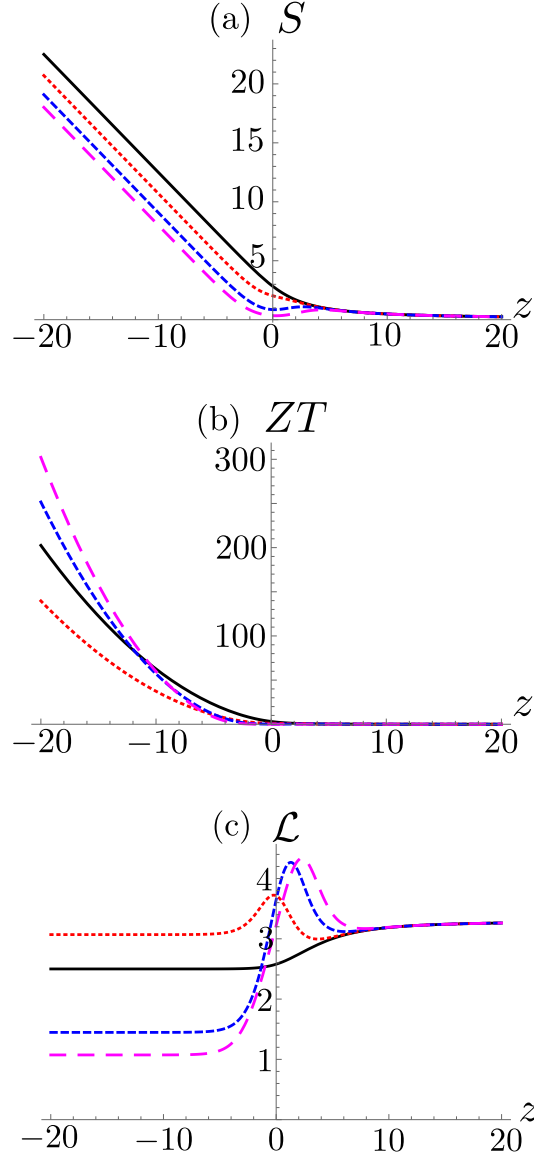


Figure 3.11: The Seebeck coefficient S [in units of $k_B/|e|$, panel (a)], the figure of merit ZT [panel (b)] and the Wiedemann-Franz ratio \mathcal{L} [in units of $(k_B/|e|)^2$, panel (c)] versus $z = (\mu - E_c)/(k_B T)$ with $x = 1.5$ for $\epsilon_L = 0$ [solid (black) curve], $\epsilon_L = 1$ [dotted (red) curve], $\epsilon_L = 2$ [dashed (blue) curve], and $\epsilon_L = 3$ [large-dashed (magenta) curve].

3.4 A band with two mobility edges

As discussed in Subsection 3.1.4, the case of two mobility edges is described by inserting Eq. (3.20) into Eqs. (3.8), which gives

$$\begin{aligned} L_{11} &= At^x \mathcal{K}_0(x, \bar{E}_c, \bar{\mu}), \\ L_{12} &= A \frac{k_B T}{|e|} t^x \mathcal{K}_1(x, \bar{E}_c, \bar{\mu}), \\ L_{22} &= A \left(\frac{k_B T}{e} \right)^2 t^x \mathcal{K}_2(x, \bar{E}_c, \bar{\mu}), \end{aligned} \quad (3.52)$$

where

$$\bar{E}_c = \frac{E_c}{k_B T}, \quad \bar{\mu} = \frac{\mu}{k_B T}. \quad (3.53)$$

We should note that the chemical potential μ is now measured relative to the center of the band, $E = (E_{c1} + E_{c2})/2 = 0$ and

$$\mathcal{K}_n(x, \bar{E}_c, \bar{\mu}) = \int_{-\bar{\mu}-\bar{E}_c}^{-\bar{\mu}+\bar{E}_c} d\epsilon \frac{(\bar{E}_c - |\epsilon + \bar{\mu}|)^x \epsilon^n}{4 \cosh(\epsilon/2)}. \quad (3.54)$$

For the present case, the Seebeck coefficient S , the figure of merit ZT , and the Wiedemann-Franz ratio \mathcal{L} for specific values of x , \bar{E}_c , and $\bar{\mu}$ are displayed in Fig. 3.12. All three plots exhibit a crossover around the mobility edges, $|\bar{\mu}| \sim \pm \bar{E}_c$. For $|\bar{\mu}| < \bar{E}_c$, S , and ZT are small, while \mathcal{L} has a minimum. For $|\bar{\mu}| > \bar{E}_c$, $|S|$, and ZT increase with $|\bar{\mu}|$, while \mathcal{L} approaches a plateau at values, which decrease with decreasing \bar{E}_c . This latter decrease indicates a decrease in the heat conductivity κ . As expected by Mahan and Sofo [109], this causes a fast increase in the figure of merit.

The dashed lines in Fig. 3.12(a) show the Seebeck coefficient calculated with the single-threshold expression in Eq. (3.15). As might be expected, the two calculations coincide for $\mu < 0$ in the limit $E_c \gg k_B T$; the difference between Eq. (3.54) and the single-band case (3.24) becomes of order $e^{-|\bar{\mu}|}$, owing to the decay of $1/[4 \cosh^2(\epsilon/2)] \approx e^{-|\epsilon|}$.

When $|\bar{\mu}| \gg \bar{E}_c$, Eq. (3.54) can be expanded to the lowest order in \bar{E}_c , as in

$$\mathcal{K}_n(x, \bar{E}_c, \bar{\mu}) \approx \bar{E}_c^{x+1} \frac{(-\bar{\mu})^n}{2 \cosh^2(\bar{\mu}/2)}. \quad (3.55)$$

With this approximation, one indeed finds that the electronic heat conductivity vanishes, $\mathcal{K}_0 \mathcal{K}_2 - \mathcal{K}_1^2 = 0$, and therefore $\mathcal{L} = 0$ and $ZT = \infty$. It should be kept in mind that the phononic heat conductivity should be included in the definition of the figure of merit, in particular in this limit. In this regime, $S = -(k_B/|e|)\bar{\mu}$, which fully agrees with Fig. 3.12.

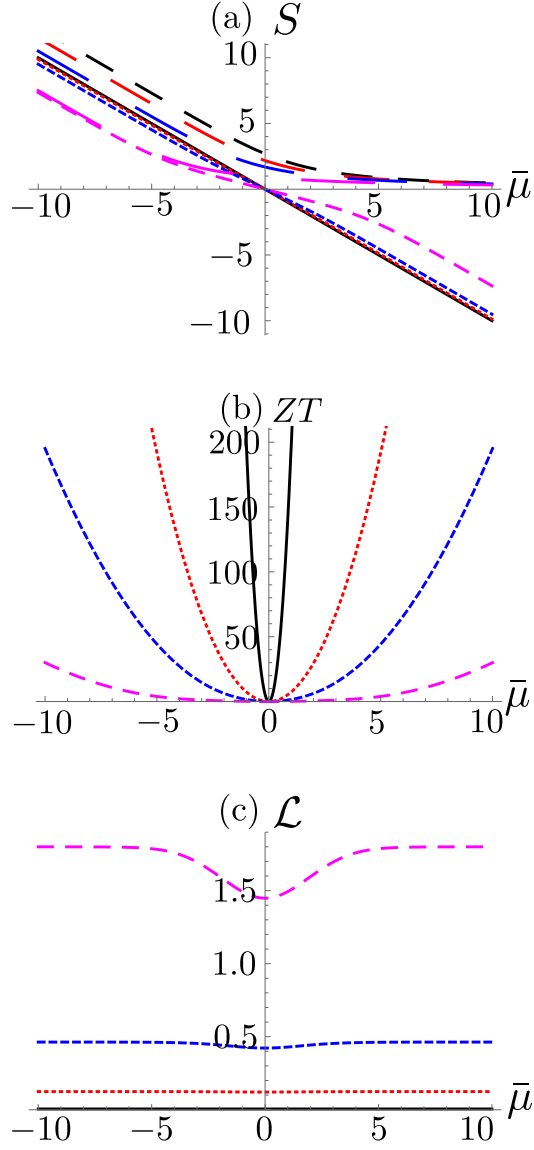


Figure 3.12: The Seebeck coefficient S [in units of $k_B/|e|$, panel (a)], the figure of merit ZT [panel (b)] and the Wiedemann-Franz ratio \mathcal{L} [in units of $(k_B/|e|)^2$, panel (c)] versus $\bar{\mu} = \mu/(k_B T)$ for $x = 1.5$ and for $\bar{E}_c = E_c/(k_B T) = 0.2$ [solid (black) line], 1 [small-dashed (red) line], 2 [medium-dashed (blue) line], and 5 [large-dashed (magenta) line]. The larger-dashed four curves in the plot of the Seebeck coefficient [panel (a)] are calculated with the single-threshold expression.

3.5 Summary and discussions

In the present chapter, we have investigated thermoelectricity near Anderson localization transitions, with which we expect to obtain a high Seebeck coefficient and a high figure of merit. A high figure of merit gives a high maximum efficiency and a high efficiency at the maximum power as shown in Eqs. (2.15) and (2.22).

In Section 3.1, we have represented familiar transport coefficients, such as the electric conductivity, the Seebeck coefficient, and the thermal conductivity, in terms of the linear-response coefficients. We have next obtained an expression of the linear-response coefficients from the Chester-Thellung-Kubo-Greenwood (CTKG) formulation. Using this expression, we have shown that the Carnot efficiency is achieved with the delta-like density of states, which may not be achieved in real materials. We have next focused on thermoelectricity near the Anderson localization, which may make a high Seebeck coefficient thanks to broken electron-hole symmetry.

In Section 3.2, for an isolated localization edge in an infinite system, we have presented a detailed analysis of the universal functions, which describe various thermoelectric coefficients as functions of the distance of the energy of the mobility edge E_c from the chemical potential in units of $k_B T$: $z = (\mu - E_c)/(k_B T)$. In particular, we have corrected certain expressions which appeared in the earlier literature and added several new approximations for specific values of $z = (\mu - E_c)/(k_B T)$. We have also added a new detailed discussion on the “insulating” region $z < 0$, where we have found large values of the Seebeck coefficient and the figure of merit. In addition, we have introduced corrections to scaling, which generate additional nonuniversal temperature dependences of the various coefficients. Such corrections may be needed when we move away from the vicinity of the localization edge.

In Section 3.3, we have introduced finite-size effects. These results are highly relevant to future mesoscopic thermoelectric devices. As the system becomes smaller, we have found that the Seebeck coefficient becomes smaller, but the figure of merit and the Wiedemann-Franz ratio behave nonmonotonically with the system size. In particular, electronic heat conductivity decreases and the figure of merit increases for smaller systems. It would be very interesting to probe these predictions experimentally.

Surprisingly, we could not find earlier analyses of thermoelectricity in the common situation of a disorder-generated narrow zero-temperature mobility range near the center of an energy band. In Section 3.4, it turns out that disorder enhances the thermoelectric efficiency, particularly near the value of the disorder at which the mobility range shrinks to zero and the system is always an insulator.

It should be emphasized that in the present chapter we have considered only noninteracting electrons and ignored any inelastic processes. The issue of inelastic processes is particularly important for high temperatures. One way to include such processes is to replace the size L by the inelastic length $L_i \sim T^{-p}$ [122, 125]. We leave this discussion for the future.

Although we have found a large electronic figure of merit for large negative z , *i.e.*, deep in the insulating phase, this result should be considered with care. First, we have ignored the phononic thermal conductivity κ_{ph} . Since this conductivity should be added to κ in the denominator of Eq. (3.4), it becomes important when the electronic thermal conductivity κ becomes very small, which happens for large negative z . We expect a significant decrease of

our calculated value of ZT when $\kappa_{\text{ph}}/\kappa \geq 1$ [138]. Secondly, at finite temperatures and deep in the insulating regime, the main mechanism for electronic conduction is the phonon-assisted (or variable-range) hopping [139–142]. Although the mechanism described in the present chapter should dominate the charge and heat transport at sufficiently low temperatures, there must exist a cross-over temperature, above which the transport is dominated by the phonon-assisted hopping. This cross-over temperature may depend on the system.

Although noninteracting electronic states are fully localized in a random macroscopic two-dimensional electron gas, large localization lengths and sufficiently small systems have recently been observed to exhibit large thermoelectric and electric transport [143]. It may be interesting to apply our analysis in the vicinity of such an effective ‘2D metal-insulator transition’.

Chapter 4

Efficiency bounds on thermoelectric transport in magnetic fields: The role of inelastic processes

In the present chapter, we investigate the possibility of the Carnot efficiency with nonvanishing power, which was argued by Benenti *et al.* [90]; see also Section 2.3 in the present thesis. They argue that we can achieve the Carnot efficiency with nonvanishing power if the linear-response coefficients satisfy $|x| > 1$ and $y = 4x/(x - 1)^2$ simultaneously [see Eqs. (2.66) and (2.87)], where

$$x \equiv \frac{L_{12}}{L_{21}}, \quad y = \frac{L_{12}L_{21}}{L_{11}L_{22} - L_{12}L_{21}} \quad (4.1)$$

from Eq. (2.33) with L_{ij} denoting the element of the 2×2 linear-response matrix. In other words, we can achieve the Carnot efficiency with nonvanishing power if we can achieve zero entropy production $\dot{S} = 0$ with $|x| > 1$; see Eqs. (2.66), (2.77) and (2.87). We investigate whether or not a specific model can satisfy these conditions.

In Section 4.1, we review the previous attempts to achieve the Carnot efficiency with nonvanishing power. In Section 4.2, we focus on the attempts with quantum thermoelectricity in mesoscopic transport systems in the realm of the Landauer-Büttiker formula, that is, with elastic scatterings, which we explained in Section 2.4. We mainly review Brandner *et al.*'s work [10] in details because they have considered the model with three reservoirs, which is the same number of reservoirs as our work in Section 4.3; the model itself is different but their results, particularly the bound of the efficiency at the maximum power, may be a good benchmark for our work. Brandner *et al.* have derived a strong bound for the linear-response coefficients from the unitarity of the scattering matrix, which prohibits y from attaining $y = 4x^2/(x - 1)^2$ for $|x| > 1$. They have thus proved that we cannot attain the Carnot efficiency with nonvanishing power in the realm of the Landauer-Büttiker formula.

However, there was no research for the case to which we cannot apply the Landauer-Büttiker formula. In Section 4.3, we explain our result, in which we consider electron-phonon interactions as inelastic scatterings. Since the Landauer-Büttiker formula cannot be applied to the case with inelastic scatterings, the bound of Brandner *et al.*'s cannot be applied to our case. We prove that we cannot attain the Carnot efficiency with nonvanishing power for energy-independent

symmetric resonant widths within the approximations that the vertex corrections are neglected and the electron-phonon coupling is taken into account only up to the second order; we prove that the entropy production (of the effective 2×2 linear-response matrix) cannot be zero for $|x| > 1$. In Section 4.4, we consider two different setups from Section 4.3. In Section 4.5, we generalize our result of Section 4.3, finding the condition for the Carnot efficiency with nonvanishing power, which we show that our specific model in Section 4.3 cannot satisfy. We give a summary and conclusion in Section 4.6.

4.1 Exploring the possibility of the Carnot efficiency with nonvanishing power under a magnetic field

As we showed in Section 2.3, we cannot rule out the possibility to obtain the Carnot efficiency with nonvanishing power in the linear-response regime under a magnetic field. Since this may not be consistent with our intuition, there are several works to investigate this argument, which we review below.

The attempts started with quantum thermoelectricity in mesoscopic transport systems in the framework of the Landauer-Büttiker formula. As we explained the formula in Section 2.4, it is a famous formula for mesoscopic transport systems without inelastic scatterings. It can be applied to the system attached to several semi-infinite one-dimensional leads with the following situation: the electrons experience only elastic scatterings in the system; in the leads, electrons do not interact each other; at the end of the leads, there are electronic reservoirs, so that the incoming electrons have its Fermi distribution.

The first attempt in the realm of the Landauer-Büttiker formula might have been Saito *et al.*'s [144]. They numerically found that the efficiency decreases with the asymmetry parameter x increased. Brandner *et al.* later proved [10] that we cannot attain the Carnot efficiency with nonvanishing power owing to a strong bound of the linear-response coefficients. At almost the same time, Balachandran *et al.* found the same bound numerically in Ref. [145].

Then the investigation was extended to cyclic heat engines, all of which proved that we cannot achieve the Carnot efficiency with nonvanishing power. The first attempt with cyclic engines might have been that of Brandner *et al.*'s [146], in which they treated a Brownian motor. Then several researches for a system with periodic driving were given by the Belgian group [147, 148]. One of the milestones is Shiraishi *et al.*'s work [149], which proved that we cannot achieve the Carnot efficiency with nonvanishing power for any engines described by classical Markov jumps. This can be applied to both thermoelectric and cyclic heat engines as long as they are described by classical Markov jumps. He later proved the no-go theorem in collaboration with Tajima for non-Markov quantum cyclic engines [150].

Let us focus on the attempts with quantum thermoelectricity in mesoscopic transport systems in details. One may incorporate an Aharonov-Bohm ring in the framework of the Landauer-Büttiker formula with two reservoirs in order to include a magnetic field. As shown in Section 2.4, however, we cannot obtain an asymmetric linear-response matrix in this case. Saito *et al.* came up with an idea in Ref. [144] to use a model with three reservoirs in the framework of the Landauer-Büttiker formula and used the technique called the ‘Büttiker probe’ condition [151]. By this method, Brandner *et al.* later proved [10] that we cannot obtain the Carnot

efficiency with nonvanishing power in the case of three reservoirs because of the unitarity of the scattering matrix, which we will review in Subsection 4.2.1. Brandner *et al.* also proved the no-go theorem in the case of many reservoirs [14, 107, 152]. However, there was no research for the case to which we cannot apply the Landauer-Büttiker formula.

Our work [36] includes an electron-phonon interaction as an inelastic scattering directly in the Hamiltonian, so that we cannot apply the Landauer-Büttiker formula. Therefore, the bound that Brandner *et al.* found in the framework of the formula cannot be applied to our case. As shown in Section 4.3, we cannot achieve the Carnot efficiency with nonvanishing power for a specific situation. We show that there is a possibility to attain a high maximum efficiency and a high efficiency at the maximum power under a magnetic field and electron-phonon interaction within our framework.

4.2 Analysis of mesoscopic transport systems under a magnetic field using the Landauer-Büttiker formula

In the present section, we review analyses [10, 107, 152] of mesoscopic transport systems under a magnetic field in the framework of the Landauer-Büttiker formula.

4.2.1 The case of three reservoirs

As shown in Section 2.4, we cannot obtain an asymmetric linear-response matrix in the framework of the Landauer-Büttiker formula with *two* reservoirs. Saito *et al.* [144] considered the model with *three* reservoirs in Fig. 4.1, in which they took an Aharonov-Bohm ring as the scattering region. As we will explain later, this model gives a 4×4 asymmetric linear-response matrix. They also used a technique called the Büttiker probe [151] condition to obtain an effective 2×2 linear-response matrix, in which we set the temperature and the chemical potential of the third reservoir so that the electric and heat current into the reservoir can be zero. Brandner *et al.*, however, proved [10] that a strong bound for the linear-response coefficients from the unitarity of the scattering matrix prevents us from attaining the Carnot efficiency with nonvanishing power.

Let us review Brandner *et al.*'s work for the case of three reservoirs [10] in details in the present subsection. Since we will consider another model with three reservoirs in Section 4.3, Brandner *et al.*'s work, particularly the bound of the efficiency at the maximum power, may be a good benchmark for our work. Note that the way of proof itself is not applicable to our case.

They consider the model with three reservoirs in Fig. 4.1; we will call the third reservoir a probe reservoir hereafter in the present section. We first show that we can make an asymmetric effective 2×2 linear-response matrix with the 'Büttiker probe' condition. We next derive a bound for the linear-response coefficients from the unitarity of the scattering matrix and show that it prohibits the Carnot efficiency with nonvanishing power.

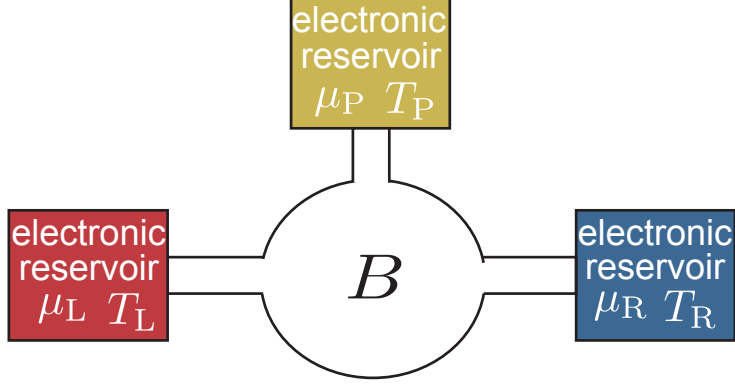


Figure 4.1: Three-terminal setup with the third probe reservoir. There is a scattering region in the center including a magnetic field, where we assume that there is no inelastic scattering. For example, Saito *et al.* chose an Aharonov-Bohm ring as the scattering region [144].

Construction of the linear-response matrix and finding an asymmetric matrix

Let us construct the linear-response matrix in the present case. Since there are three electronic reservoirs in the model in Fig. 4.1, there are six currents: one electric and one energy current from each reservoir. Because of the conservation laws of particle and energy, the number of independent currents is four. We choose the electric and heat currents from the left and the third, probe reservoirs as the independent currents. Let us express the entropy production \dot{S} with these currents in order to obtain the conjugate affinities to them. We start from the expression as

$$\dot{S} = -\frac{J_Q^L}{T_L} - \frac{J_Q^P}{T_P} + \frac{J_Q^R}{T_R}, \quad (4.2)$$

where J_Q^L , J_Q^P , J_Q^R are heat currents from the left reservoir, one from the probe reservoir, and one *into* the right reservoir, respectively, while T_L , T_P , T_R are the temperatures of the left, the probe, and the right reservoirs, respectively. The derivation of this expression of the entropy production was explained in Eq. (1.16) in Subsection 1.2.1. Since $J_Q^i = J_E^i - \mu_i J_N^i$ with J_E^i and J_N^i denoting the energy and the particle currents from the reservoir i ($i = L, P$) and *into* the reservoir i ($i = R$), respectively, we find that the first law of thermodynamics is satisfied as

$$J_Q^L + J_Q^P - J_Q^R = -\mu_L J_N^L - \mu_P J_N^P + \mu_R J_N^R \quad (4.3)$$

$$= -(\mu_L - \mu_R) J_N^L - (\mu_P - \mu_R) J_N^P, \quad (4.4)$$

where μ_L, μ_P, μ_R are the chemical potentials of the left, the probe, and the right reservoirs, respectively. In the second line, we used the relation $J_N^R = J_N^L + J_N^P$ from the conservation of particle. Inserting Eq. (4.4) into Eq. (4.2), we express the entropy production as

$$\dot{S} = -\frac{J_Q^L}{T_L} - \frac{J_Q^P}{T_P} + \frac{J_Q^L + J_Q^P + (\mu_L - \mu_R) J_N^L + (\mu_P - \mu_R) J_N^P}{T_R} \quad (4.5)$$

$$= \frac{\mu_L - \mu_R}{T_R} J_N^L + \frac{\mu_P - \mu_R}{T_R} J_N^P + \frac{T_L - T_R}{T_L T_R} J_Q^L + \frac{T_P - T_R}{T_P T_R} J_Q^L \quad (4.6)$$

$$= \frac{1}{T_R} \left(V_{LR} J_e^L + V_{PR} J_e^P + \frac{T_L - T_R}{T_L} J_Q^L + \frac{T_P - T_R}{T_P} J_Q^L \right), \quad (4.7)$$

where we defined the voltage difference between the left and right reservoirs as $V_{LR} \equiv (\mu_L - \mu_R)/e$ and one between the probe and the right reservoirs as $V_{PR} \equiv (\mu_P - \mu_R)/e$ as well as the electric current from the left reservoir as $J_e^L \equiv eJ_N^L$ and one from the probe reservoir as $J_e^P \equiv eJ_N^P$. As we did in Section 2.1, we obtain the conjugate affinities from the entropy production (multiplied by T_R) in the form

$$T_R \dot{S} = J_e^L A_e^L + J_Q^L A_Q^L + J_e^P A_e^P + J_Q^P A_Q^P, \quad (4.8)$$

from which we identify $A_e^L \equiv V_{LR}$, $A_Q^L \equiv (T_L - T_R)/T_L$, $A_e^P \equiv V_{PR}$, and $A_Q^P \equiv (T_P - T_R)/T_P$ to be conjugate affinities to J_e^L , J_Q^L , J_e^P , and J_Q^P , respectively. Finally, we obtain the following linear-response form:

$$\begin{pmatrix} J_e^L \\ J_Q^L \\ J_e^P \\ J_Q^P \end{pmatrix} = \mathbb{G} \begin{pmatrix} A_e^L \\ A_Q^L \\ A_e^P \\ A_Q^P \end{pmatrix}, \quad (4.9)$$

where \mathbb{G} is a 4×4 matrix that satisfies the Onsager-Casimir relations [92] $G_{ij}(B) = G_{ji}(-B)$ with $(i, j = 1, 2, 3, 4)$. We later obtain the elements of \mathbb{G} in the framework of the Landauer-Büttiker formula.

Let us construct the effective 2×2 linear-response formalism by starting from the 4×4 one in the form

$$\begin{pmatrix} \mathbf{J}^L \\ \mathbf{J}^P \end{pmatrix} = \mathbb{G} \begin{pmatrix} \mathbf{A}^L \\ \mathbf{A}^P \end{pmatrix}, \quad \mathbb{G} \equiv \begin{pmatrix} \mathbb{G}_{LL} & \mathbb{G}_{LP} \\ \mathbb{G}_{PL} & \mathbb{G}_{PP} \end{pmatrix}, \quad (4.10)$$

where we defined $\mathbf{J}^L \equiv (J_e^L \ J_Q^L)^T$, $\mathbf{J}^P \equiv (J_e^P \ J_Q^P)^T$, $\mathbf{A}^L \equiv (A_e^L \ A_Q^L)^T$ and $\mathbf{A}^P \equiv (A_e^P \ A_Q^P)^T$ whereas G_{AB} ($A, B = L, P$) is a 2×2 block matrix of \mathbb{G} . Note that A^T with A denoting a matrix means the transpose of A . Here we take the ‘Büttiker probe’ condition [151], which we denote as the probe condition hereafter. In the probe condition, we set the affinity to make the conjugate current zero in order to make the effective smaller matrix from the original linear-response matrix. Let us here set the affinities \mathbf{A}^P to make the conjugate currents \mathbf{J}^P zero. With the condition

$$\mathbf{J}^P = \mathbb{G}_{PL} \mathbf{A}^L + \mathbb{G}_{PP} \mathbf{A}^P = 0, \quad (4.11)$$

which leads to

$$\mathbf{A}^P = -\mathbb{G}_{PP}^{-1} \mathbb{G}_{PL} \mathbf{A}^L, \quad (4.12)$$

we find

$$\mathbf{J}^L = \mathbb{G}_{LL} \mathbf{A}^L + \mathbb{G}_{LP} \mathbf{A}^P \quad (4.13)$$

$$= \mathbb{G}_{LL} \mathbf{A}^L + \mathbb{G}_{LP} [-\mathbb{G}_{PP}^{-1} \mathbb{G}_{PL} \mathbf{A}^L] \quad (4.14)$$

$$= [\mathbb{G}_{LL} - \mathbb{G}_{LP} \mathbb{G}_{PP}^{-1} \mathbb{G}_{PL}] \mathbf{A}^L \quad (4.15)$$

$$\equiv \mathbb{L} \mathbf{A}^L. \quad (4.16)$$

In this way, we obtain the effective 2×2 matrix as

$$\mathbb{L} \equiv \mathbb{G}_{LL} - \mathbb{G}_{LP} \mathbb{G}_{PP}^{-1} \mathbb{G}_{PL} \equiv \begin{pmatrix} L_{11} & L_{12} \\ L_{21} & L_{22} \end{pmatrix}. \quad (4.17)$$

The Landauer-Büttiker formula for three reservoirs

In order to find the expressions of the linear-response coefficients in \mathbb{G} , we need the multi-terminal Landauer-Büttiker formula [153, 154] as shown in Section 2.4. Let us consider the case of three reservoirs, in which there is the left reservoir L, the probe one P, and the right one R, as shown in Fig. 4.1. The particle current from the left reservoir is calculated from Eq. (2.126) as

$$J_N^L = \sum_{\beta=L,P,R} \int dE j_{\beta}(x_L, E, B) f_{\beta}(E) \quad (4.18)$$

$$= \frac{1}{h} \int dE \{ [1 - |S_{LL}(E, B)|^2] f_L(E) - |S_{LP}(E, B)|^2 f_P(E) - |S_{LR}(E, B)|^2 f_R(E) \} \quad (4.19)$$

$$= \frac{1}{h} \int dE \{ |S_{LP}(E, B)|^2 [f_L(E) - f_P(E)] + |S_{LR}(E, B)|^2 [f_L(E) - f_R(E)] \}, \quad (4.20)$$

where h is the Planck constant. In the last equality, we used the relation $1 - |S_{LL}(E, B)|^2 = |S_{LP}(E, B)|^2 + |S_{LR}(E, B)|^2$, which we find from the unitarity of the scattering matrix $\sum_{\beta=L,P,R} |S_{\alpha\beta}(E, B)|^2 = \sum_{\alpha=L,P,R} |S_{\alpha\beta}(E, B)|^2 = 1$ in Eq. (2.122). Note that $|S_{\alpha\beta}|^2$ ($\alpha \neq \beta$) is the transmission probability from the β reservoir to the α one ($\alpha, \beta = L, P, R$). In the same way, we obtain the particle current from the probe reservoir as

$$J_N^P = \sum_{\beta=L,P,R} \int dE j_{\beta}(x_P, E, B) f_{\beta}(E) \quad (4.21)$$

$$= \frac{1}{h} \int dE \{ [1 - |S_{PP}(E, B)|^2] f_P(E) - |S_{PL}(E, B)|^2 f_L(E) - |S_{PR}(E, B)|^2 f_R(E) \} \quad (4.22)$$

$$= \frac{1}{h} \int dE \{ |S_{PL}(E, B)|^2 [f_P(E) - f_L(E)] + |S_{PR}(E, B)|^2 [f_P(E) - f_R(E)] \}. \quad (4.23)$$

In the last equality, we used the relation $1 - |S_{PP}(E, B)|^2 = |S_{PL}(E, B)|^2 + |S_{PR}(E, B)|^2$, which we find from the unitarity of the scattering matrix $\sum_{\beta=L,P,R} |S_{\alpha\beta}(E, B)|^2 = \sum_{\alpha=L,P,R} |S_{\alpha\beta}(E, B)|^2 = 1$. The electric and heat currents from the left reservoir are

$$J_e^L = \frac{e}{h} \int dE \{ |S_{LP}(E, B)|^2 [f_L(E) - f_P(E)] + |S_{LR}(E, B)|^2 [f_L(E) - f_R(E)] \} \quad (4.24)$$

$$J_Q^L = \frac{1}{h} \int dE (E - \mu_L) \{ |S_{LP}(E, B)|^2 [f_L(E) - f_P(E)] + |S_{LR}(E, B)|^2 [f_L(E) - f_R(E)] \}, \quad (4.25)$$

while the electric and the heat currents from the probe reservoir are

$$J_e^P = \frac{e}{h} \int dE \{ |S_{PL}(E, B)|^2 [f_P(E) - f_L(E)] + |S_{PR}(E, B)|^2 [f_P(E) - f_R(E)] \} \quad (4.26)$$

$$J_Q^P = \frac{e}{h} \int dE (E - \mu_P) \left\{ |S_{PL}(E, B)|^2 [f_P(E) - f_L(E)] + |S_{PR}(E, B)|^2 [f_P(E) - f_R(E)] \right\}. \quad (4.27)$$

Let us calculate the linear-response coefficients from these expressions. With the expansion of the Fermi function as

$$f_i - f_R = \frac{\partial f_R}{\partial \mu_R} \Delta \mu_i + \frac{\partial f_R}{\partial T_R} \Delta T_i \quad (4.28)$$

$$\equiv F(E) \Delta \mu_i + \frac{E - \mu_R}{T_R} F(E) \Delta T_i, \quad (4.29)$$

where k_B is the Boltzmann constant, $i = L, P$, $\Delta \mu_i \equiv \mu_i - \mu_R$, $\Delta T_i \equiv T_i - T_R$, and

$$F(E) \equiv \frac{1}{4k_B T_R \cosh^2 \left(\frac{E - \mu_R}{2k_B T_R} \right)}, \quad (4.30)$$

we find the linear-response coefficients as follows:

$$\mathbb{G}_{\alpha\beta} = \frac{e^2}{h} \int dE F(E) \begin{pmatrix} 1 & \frac{E - \mu_R}{e} \\ \frac{E - \mu_R}{e} & \left(\frac{E - \mu_R}{e} \right)^2 \end{pmatrix} [\delta_{\alpha\beta} - |S_{\alpha\beta}(E, B)|^2], \quad (4.31)$$

where $\alpha, \beta = L, P, R$. Since there are three reservoirs, the scattering matrix satisfies

$$S_{\alpha\beta}(E, B) \neq S_{\beta\alpha}(E, B), \quad (4.32)$$

which makes $\mathbb{G}_{\alpha\beta} \neq \mathbb{G}_{\beta\alpha}$. The original 4×4 linear-response matrix \mathbb{G} is therefore asymmetric, so that the effective 2×2 linear-response matrix \mathbb{L} is also asymmetric. Note that each 2×2 block matrix $\mathbb{G}_{\alpha\beta}$ (4.31) is symmetric.

The restriction for the effective 2×2 matrix \mathbb{L} from the unitarity of the scattering matrix

Let us find the restriction for \mathbb{L} in (4.17) from the unitarity of the scattering matrix [10]. The restriction comes from the positive semi-definiteness of the 2×2 Hermitian matrix \mathbb{K} defined by [10]

$$\mathbb{K} \equiv (\mathbb{L} + \mathbb{L}^T) + i\sqrt{3}(\mathbb{L} - \mathbb{L}^T) \equiv \begin{pmatrix} K_{11} & K_{12} \\ K_{12}^* & K_{22} \end{pmatrix}. \quad (4.33)$$

In order to prove the positive semi-definiteness of \mathbb{K} , we use the positive semi-definiteness of the 4×4 Hermitian matrix \mathbb{H} defined by [10]

$$\mathbb{H} \equiv (\mathbb{G} + \mathbb{G}^T) + i\sqrt{3}(\mathbb{G} - \mathbb{G}^T), \quad (4.34)$$

the proof of which is given in the supplementary material of Ref. [10] using the unitarity of the scattering matrix \mathbb{S} . From the positive semi-definiteness of \mathbb{H} , we find the positive semi-

definiteness of \mathbb{K} because of the following relation [10]:

$$\mathbf{k}^\dagger \mathbb{K} \mathbf{k} = \mathbf{h}^\dagger \mathbb{H} \mathbf{h} \geq 0 \quad (4.35)$$

for any $\mathbf{k} \in \mathbb{C}^2$, where

$$\mathbf{h} = \begin{pmatrix} \mathbf{k} \\ -\mathbb{G}_{\text{PP}}^{-1} \mathbb{G}_{\text{PL}} \mathbf{k} \end{pmatrix}. \quad (4.36)$$

The positive semi-definiteness of \mathbb{K} gives the restriction for L_{ij} as follows. From the definition of \mathbb{K} in Eq. (4.33), we find

$$\begin{pmatrix} K_{11} & K_{12} \\ K_{12}^* & K_{22} \end{pmatrix} = \begin{pmatrix} 2L_{11} & (L_{12} + L_{21}) + i\sqrt{3}(L_{12} - L_{21}) \\ (L_{12} + L_{21}) - i\sqrt{3}(L_{12} - L_{21}) & 2L_{22} \end{pmatrix}. \quad (4.37)$$

The positive semi-definiteness of \mathbb{K} gives the conditions

$$K_{11} \geq 0, \quad K_{22} \geq 0, \quad K_{11}K_{22} - K_{12}K_{12}^* \geq 0, \quad (4.38)$$

which leads to

$$L_{11} \geq 0, \quad L_{22} \geq 0, \quad (4.39)$$

and

$$K_{11}K_{22} - K_{12}K_{12}^* = 4L_{11}L_{22} - [(L_{12} + L_{21})^2 + 3(L_{12} - L_{21})^2] \quad (4.40)$$

$$= 4[L_{11}L_{22} + L_{12}L_{21} - L_{12}^2 - L_{21}^2] \geq 0. \quad (4.41)$$

Therefore, we finally find the inequality [10]

$$L_{11}L_{22} - \frac{1}{4}(L_{12} + L_{21})^2 \geq \frac{3}{4}(L_{12} - L_{21})^2. \quad (4.42)$$

We find that this inequality is stronger than the inequality (2.32) from the nonnegativity of the entropy production except for the case of $L_{12} = L_{21}$.

This inequality bounds the maximum efficiency and the efficiency at the maximum power as follows [10]. First, we obtain the following inequality by dividing the inequality (4.42) by L_{12}^2 :

$$\left(\frac{1}{y} + 1\right)x - \frac{1}{4}(x^2 + 1 + 2x) \geq \frac{3}{4}(x - 1)^2, \quad (4.43)$$

which leads to

$$0 \leq y \leq \frac{x}{(x - 1)^2} \quad \text{for } y \geq 0, \quad (4.44)$$

$$\frac{x}{(x - 1)^2} \leq y < 0 \quad \text{for } y < 0. \quad (4.45)$$

We here repeat the definitions of x and y as

$$x \equiv \frac{L_{12}}{L_{21}}, \quad y \equiv \frac{L_{12}L_{21}}{L_{11}L_{22} - L_{12}L_{21}}. \quad (4.46)$$

This inequality is of course stricter than the inequality (2.38), which is

$$0 \leq y \leq \frac{4x}{(x-1)^2} \quad \text{for } y \geq 0, \quad (4.47)$$

$$\frac{4x}{(x-1)^2} \leq y \leq 0 \quad \text{for } y \leq 0. \quad (4.48)$$

Let us remember Benenti *et al.*'s claim that if $|x| > 1$ and $y = 4x/(x-1)^2$ are satisfied, we can attain the Carnot efficiency with nonvanishing power. However, for the present case in the framework of the Landauer-Büttiker formula, the parameter y cannot attain a value $y = 4x/(x-1)^2$ because of the strong bound (4.45) from the unitarity of the scattering matrix (4.45). We thus conclude that we cannot attain the Carnot efficiency with nonvanishing power in the present case [10].

The upper bound of the maximum efficiency

Let us calculate the upper bound of the maximum efficiency. It is sufficient to consider $|x| \geq 1$ because the inequality (2.38) is looser than the inequality (4.45) and we cannot achieve the Carnot efficiency for $|x| < 1$ even with the looser inequality (2.38). As explained in Chapter 2, since the maximum efficiency is an increasing function of y , we find from the inequality (4.45) that the maximum efficiency takes its maximum at $y = x/(x-1)^2$. The upper bound of the maximum efficiency becomes

$$\eta \left(V = V_{\max}, y = \frac{x}{(x-1)^2} \right) = \eta_c x \frac{\sqrt{1 + x/(x-1)^2} - 1}{\sqrt{1 + x/(x-1)^2} + 1} \quad (4.49)$$

$$\leq \eta_c, \quad (4.50)$$

where the equality is achieved if and only if $x = 1$ [10]. This means that we can achieve the Carnot efficiency only with a symmetric linear-response matrix in the present case, that is, we can achieve it only with vanishing power.

The upper bound of the efficiency at the maximum power

Let us also calculate the upper bound of the efficiency at the maximum power [10]. The same discussion as Subsection 2.3.6 tells us that the upper bound of the efficiency at maximum power takes its maximum at $y = x/(x-1)^2$ [10];

$$\eta \left(V_{\max p}, y = \frac{x}{(x-1)^2} \right) \leq \frac{\eta_c}{2} \frac{x \frac{x}{(x-1)^2}}{2 + \frac{x}{(x-1)^2}} \quad (4.51)$$

$$= \eta_c \frac{x^2}{4x^2 - 6x + 4}. \quad (4.52)$$

This upper bound takes its maximum [10]

$$\max_x \eta \left(V_{\max p}, y = \frac{x}{(x-1)^2} \right) = \frac{4}{7} \eta_c, \quad (4.53)$$

at $x = 4/3$ because

$$\frac{d}{dx}\eta\left(V_{\text{maxp}}, y = \frac{x}{(x-1)^2}\right) = 2x\eta_c \frac{-3x+4}{(4x^2-6x+4)^2} = 0. \quad (4.54)$$

This value is a bit larger than the Curzon-Ahlborn bound $\eta_c/2$ [89] explained in Section 2.2. We should note that Balachandran *et al.* have numerically found the transmission probabilities $|S_{\alpha\beta}(E, B)|^2$ ($\alpha, \beta = \text{L, P, R}$) that give the bound (4.53) [145].

To summarize the present review of Ref. [10], in the setup of three reservoirs in the framework of the Landauer-Büttiker formula, although we can obtain an asymmetric linear-response matrix and break the Curzon-Ahlborn bound [89], we cannot obtain the Carnot efficiency with nonvanishing power. In the next section, we will consider a model with inelastic electron-phonon interactions, to which we cannot apply the Landauer-Büttiker formula. We regard Brandner *et al.*'s result, particularly the maximum value of the efficiency at the maximum power, as a benchmark for our work in the next section.

4.2.2 The case of many reservoirs

In the case of many reservoirs, Brandner and his colleagues showed numerically [152] and analytically [14, 107] that we cannot achieve the Carnot efficiency with nonvanishing power. The analytical proof is a bit complicated and too mathematical to review here; please see Chapter 3 of Brandner's thesis [107] for details.

4.3 Efficiency bounds on thermoelectric transport in magnetic fields with electron-phonon interaction

In the section above, we have reviewed the work in the framework of the Landauer-Büttiker formula [10], in which it was proved that we cannot achieve the Carnot efficiency with nonvanishing power due to the unitarity of the scattering matrix. Here we incorporate the inelastic electron-phonon interaction directly into the Hamiltonian, to which we cannot apply the Landauer-Büttiker formula. The bound of Brandner *et al.*'s [10] therefore does not work in this case; it is possible to break the bound (4.53) and achieve a high efficiency. We show, however, that we cannot achieve the Carnot efficiency with nonvanishing power even in the presence of an electron-phonon coupling [36] and a magnetic field under a specific setup explained before Eq. (4.113) and with the approximation that vertex corrections are neglected and the electron-phonon coupling is taken into account only up to the second order. We also show that a magnetic field and phonons enables us to achieve a high efficiency at the maximum power and a high maximum efficiency within our framework.

We here remark the difference between our work and the previous research [155]. Although the linear-response coefficients in the model used in the present section were calculated in Ref. [155], they used $J_Q = (J_Q^L + J_Q^R)/2$ as the electronic heat current. Moreover, they did not calculate the efficiency. When we calculate the efficiency, we should take J_Q^L as the electronic heat current as explained in Sec. 1.2. In our work [36], we follow the rule and calculate the

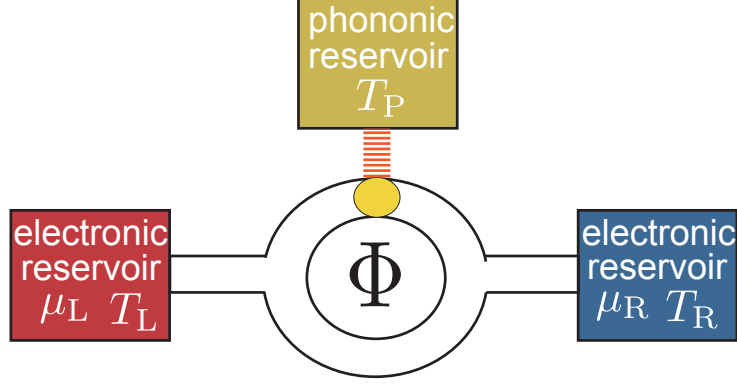


Figure 4.2: A thermoelectric device, comprising two electronic reservoirs (held at chemical potentials μ_L and μ_R , and at temperatures T_L and T_R), and a Bosonic reservoir held at a temperature T_P , with which the electrons exchange energy. The model has an Aharonov-Bohm ring threaded by a magnetic flux Φ . The electrons exchange energy with vibrational modes on a dot placed on the upper arm of the ring.

linear-response coefficients with appropriate affinities and the efficiency. We also assume two specific conditions as shown before Eq. (4.113) to make the linear-response matrix simple.

4.3.1 Model and the Hamiltonian

We use the model in Ref. [155] shown in Fig. 4.2, in which there is an Aharonov-Bohm ring threaded by a magnetic flux Φ . The ring is attached to two electronic reservoirs and has a quantum dot on one of its arms; when the electrons are on the quantum dot, they interact with the phonons there, which are tightly coupled to a Bosonic bath that fixes the population to the Bose distribution [156]. In this model, the dot is replaced by a single localized electronic level of energy ϵ_d and its vibrational modes are the Einstein phonons of frequency ω_0 ; the electronic reservoirs are assumed to contain free electron gases. With γ denoting the coupling strength of an electron with the vibrational modes, whose creation (annihilation) operators are b^\dagger (b) and the creation (annihilation) operators of the electron on the localized level by c_d^\dagger (c_d), the Hamiltonian (using $\hbar = 1$) is

$$\begin{aligned} \mathcal{H} = & [\epsilon_d + \gamma(b^\dagger + b)]c_d^\dagger c_d + \omega_0 \left(b^\dagger b + \frac{1}{2} \right) + \sum_{k_L} \epsilon_{k_L} c_{k_L}^\dagger c_{k_L} + \sum_{k_R} \epsilon_{k_R} c_{k_R}^\dagger c_{k_R} \\ & + \sum_{k_L} (V_{k_L} c_{k_L}^\dagger c_d + \text{H.c.}) + \sum_{k_R} (V_{k_R} c_{k_R}^\dagger c_d + \text{H.c.}) + \sum_{k_L, k_R} (V_{k_L k_R} e^{i\Phi} c_{k_L}^\dagger c_{k_R} + \text{H.c.}). \end{aligned} \quad (4.55)$$

The operators that create (annihilate) a conduction electron in the left (right) reservoir of energy $\epsilon_{k_L(k_R)}$ are $c_{k_L(k_R)}^\dagger$ ($c_{k_L(k_R)}$). The tunneling matrix elements between the dot and the left (right) electronic reservoir are denoted by V_{k_L} (V_{k_R}). The lower arm of the ring in Fig. 4.2 connects the two reservoirs with the tunneling matrix element $V_{k_L k_R}$; the magnetic flux Φ (in units of c/e) penetrating the ring is assigned to these elements. Since the magnetic field giving

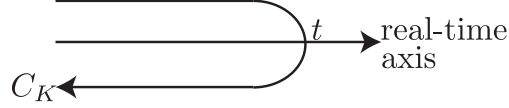


Figure 4.3: The Keldysh contour C_K . It goes from the infinite past to the time t , and then goes back to the infinite past.

rise to the Aharonov-Bohm effect is usually small, one may neglect the tiny Zeeman effect on the spins of the conduction electrons.

4.3.2 Brief introduction of the Keldysh Green's function

The electric and heat currents flowing through the Aharonov-Bohm ring are found within the Keldysh formalism, which is particularly suitable for treating nonequilibrium configurations with inelastic scatterings [79]; we explain the Keldysh formalism briefly in the present subsection.

Let us introduce the following Green's function, which is defined on the *Keldysh contour* as shown in Fig. 4.3:

$$G_{AB}(\tau_1, \tau_2) = -i \langle T_C A(\tau_1) B(\tau_2) \rangle, \quad (4.56)$$

where A and B are field operators and T_C denotes the time-ordering on the *Keldysh contour* shown in Fig. 4.3, which goes from the infinite past to the time t , and then goes back to the infinite past. Here τ_1, τ_2 are the 'time' variables on the Keldysh contour. We use Greek characters to denote the 'time' on the Keldysh contour and Roman characters to denote the time on the real-time axis hereafter. The Green's function (4.56) is called the contour-ordered Green's function. We can produce the Dyson equation of it as for the equilibrium Green's function [79].

Since the contour-ordered Green's function is defined not on the real-time axis but on the Keldysh contour, we need to project it to the real-time axis because any physical quantities are defined on the real-time axis, not on the Keldysh contour. Let us denote t_1, t_2 as the time of τ_1, τ_2 projected on the real-time axis. Since the Keldysh contour has forward and backward paths, when we would like to express the contour-ordered Green's function with respect to the real times t_1, t_2 , we have to consider the following four Green's functions depending on which path (forward and backward) τ_1, τ_2 are on. For τ_1, τ_2 on the same path, we define the following two Green's functions: For τ_1, τ_2 on the forward path [Fig. 4.4 (a)],

$$G_{AB}(t_1, t_2) = G_{AB}^c(t_1, t_2) \equiv -i \langle T B(t_2) A(t_1) \rangle, \quad (4.57)$$

where T means the time-ordering on the *real-time axis*; for τ_1, τ_2 on the backward path [Fig. 4.4 (b)],

$$G_{AB}(t_1, t_2) = G_{AB}^{\bar{c}}(t_1, t_2) \equiv -i \langle \tilde{T} B(t_2) A(t_1) \rangle, \quad (4.58)$$

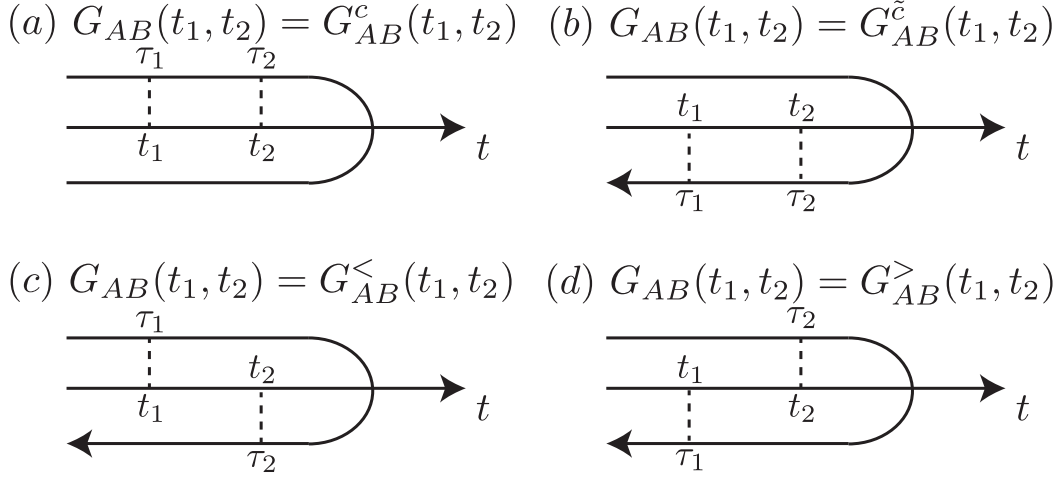


Figure 4.4: The definitions of the each Green's function depending on which path τ_1, τ_2 are on. (a) the definition of $G_{AB}^c(\tau_1, \tau_2)$. (b) the definition of $G_{AB}^{\tilde{c}}(\tau_1, \tau_2)$ (c) the definition of $G_{AB}^<(\tau_1, \tau_2)$. (d) the definition of $G_{AB}^>(\tau_1, \tau_2)$.

where \tilde{T} denotes the *anti*-time ordering on the *real-time axis*. For τ_1, τ_2 on the different path, we define the following two Green's functions:

$$G_{AB}(t_1, t_2) = G_{AB}^<(t_1, t_2) \equiv i \langle B(t_2) A(t_1) \rangle \quad (4.59)$$

for $\tau_1 < \tau_2$ [Fig. 4.4 (c)] in the sense on Keldysh contour, which is called the lesser Green's function, while

$$G_{AB}(t_1, t_2) = G_{AB}^>(t_1, t_2) \equiv -i \langle A(t_2) B(t_1) \rangle \quad (4.60)$$

for $\tau_1 > \tau_2$ [Fig. 4.4 (d)] in the sense on Keldysh contour, which is called the greater Green's function. When we consider a problem, we often use the retarded and advanced Green's functions instead of $G_{AB}^c(t_1, t_2)$ and $G_{AB}^{\tilde{c}}(t_1, t_2)$, which are defined as

$$G_{AB}^r(t_1, t_2) \equiv -i\theta(t_1 - t_2) \langle \{A(t_1), B(t_2)\} \rangle \quad (4.61)$$

$$G_{AB}^a(t_1, t_2) \equiv i\theta(t_2 - t_1) \langle \{A(t_1), B(t_2)\} \rangle. \quad (4.62)$$

Here $\{A, B\} = AB + BA$ denotes the anticommutation relation. These four Green's functions are not independent and have the relation as

$$G_{AB}^r(t_1, t_2) - G_{AB}^a(t_1, t_2) = G_{AB}^>(t_1, t_2) - G_{AB}^<(t_1, t_2). \quad (4.63)$$

Note that as the contour Green's function satisfy the Dyson equation (on the Keldysh contour) [79], a self-energy also satisfy the relation (4.63).

In the next subsection, we show that the current is expressed in terms of the lesser components of the Keldysh Green's functions.

4.3.3 Expressions of the Green's functions and the currents

The electric current emerging from the left reservoir is expressed as

$$J_e = -e\langle \dot{N}_L \rangle = -e \frac{d\langle \sum_{k_L} c_{k_L}^\dagger c_{k_L} \rangle}{dt} = -e \int \frac{d\omega}{2\pi} J_L(\omega, \Phi), \quad (4.64)$$

where

$$J_L(\omega, \Phi) = \sum_k V_{k_L} [G_{k_L d}^<(\omega) - G_{dk_L}^<(\omega)] + \sum_{k_L, k_R} V_{k_L k_R} [e^{-i\Phi} G_{k_L k_R}^<(\omega) - e^{i\Phi} G_{k_R k_L}^<(\omega)]. \quad (4.65)$$

Here, $G_{ab}^<(\omega)$ is the lesser component of the contour-ordered Green's function in the energy space, which is the Fourier transform of $G_{ab}^<(t-t') = i\langle c_b^\dagger(t')c_a(t) \rangle$ with a and b denoting the relevant operators ($a, b = d, k_L, k_R$; see Eq. (4.55)); see the definition of the lesser component of the contour-ordered Green's function (4.59). The energy current emerging from the left reservoir is given by $-\langle \dot{E}_L \rangle = d\langle \sum_{k_L} E_{k_L} c_{k_L}^\dagger c_{k_L} \rangle / dt$; it attains the same form as the electric current except for an extra factor ω in the integrand in Eq. (4.64) (and without the electron's charge e). The energy current from the Bosonic reservoir J_Q^P is obtained so that it may satisfy the energy conservation $\langle \dot{E}_L + \dot{E}_R + \dot{E}_P \rangle = 0$. Here \dot{E}_i ($i = L, R, P$) means the energy current going *into* the i th reservoir.

In order to calculate the current, we need the lesser components of the Green's functions as shown above. We calculate the lesser components by obtaining each (contour-ordered) Green's function from their Dyson equations and then project them to their lesser components. The calculation is, however, so complex that we relegate it to Appendix B. Here we summarize the results. Since the results of the currents include many new notations, we explain them below for preparation.

Each component of the contour-ordered Green's function of the dot $G_{dd}(\tau_1, \tau_2) = -i\langle T_C c_d(\tau_1) c_d^\dagger(\tau_2) \rangle$ in energy space is given by [155]

$$G_{dd}^r(\omega, \Phi) = \frac{1}{[\mathcal{G}_{dd}^r(\omega, \Phi)]^{-1} - \Delta\epsilon_V(\omega, \Phi) - \Sigma_V^r(\omega, \Phi)}, \quad G_{dd}^a(\omega, \Phi) = [G_{dd}^r(\omega, \Phi)]^*, \quad (4.66)$$

$$G_{dd}^<(\omega, \Phi) = G_{dd}^r(\omega, \Phi) [\Sigma_l^<(\omega, \Phi) + \Sigma_V^<(\omega, \Phi)] G_{dd}^a(\omega, \Phi), \quad (4.67)$$

as shown in Eqs. (B.101) and (B.103). Here $\mathcal{G}_{dd}(\omega, \Phi)$ is the contour-ordered Green's function of the dot in the absence of the electron-phonon coupling, whose components are given by [155]

$$\mathcal{G}_{dd}^r(\omega, \Phi) = \frac{1}{\omega - \epsilon_d - \Sigma_l^r(\omega, \Phi)}, \quad \mathcal{G}_{dd}^a(\omega, \Phi) = [\mathcal{G}_{dd}^r(\omega, \Phi)]^*, \quad (4.68)$$

$$\mathcal{G}_{dd}^<(\omega, \Phi) = \mathcal{G}_{dd}^r(\omega, \Phi) \Sigma_l^<(\omega, \Phi) \mathcal{G}_{dd}^a(\omega, \Phi), \quad (4.69)$$

as shown in Eqs. (B.79) and (B.80), where

$$\Sigma_l^r(\omega, \Phi) \equiv \frac{-i}{2[1 + \lambda(\omega)]} [\Gamma_L(\omega) + \Gamma_R(\omega) - 2i\sqrt{\lambda(\omega)\Gamma_L(\omega)\Gamma_R(\omega)} \cos \Phi], \quad (4.70)$$

$$\Sigma_l^<(\omega, \Phi) \equiv \frac{i}{[1 + \lambda(\omega)]^2} \{f_L(\omega)[\Gamma_L(\omega) + \lambda(\omega)\Gamma_R(\omega)] + f_R(\omega)[\Gamma_R(\omega) + \lambda(\omega)\Gamma_L(\omega)]\}$$

$$+ 2\sqrt{\lambda(\omega)\Gamma_L(\omega)\Gamma_R(\omega)}[f_R(\omega) - f_L(\omega)]\sin\Phi\}, \quad (4.71)$$

are the retarded and the lesser components of the self-energy [155] from the couplings of the left and the right reservoirs as shown in Eqs. (B.76) and (B.77). Here $f_{L(R)}(\omega) = \{1 + \exp[\beta_{L(R)}(\omega - \mu_{L(R)})]\}^{-1}$ is the Fermi distribution of the left (right) reservoir and the resonance width from the coupling between the left (right) reservoir and the dot is

$$\Gamma_{L(R)}(\omega) = \frac{\pi}{2} \sum_{k_L(k_R)} |V_{k_L(k_R)}|^2 \delta(\omega - \epsilon_{k_L(k_R)}), \quad (4.72)$$

as shown in Eq. (B.69), as well as that between the left and the right reservoirs is [155]

$$\lambda(\omega) = \pi^2 \sum_{k_L, k_R} |V_{k_L k_R}|^2 \delta(\omega - \epsilon_{k_L}) \delta(\omega - \epsilon_{k_R}) \quad (4.73)$$

as shown in Eq. (B.70). With these resonance widths, we define the following quantities: the total width [155],

$$\Gamma(\omega) = \frac{\Gamma_L(\omega) + \Gamma_R(\omega)}{1 + \lambda(\omega)} \quad (4.74)$$

as shown in Eq. (B.106); the transmission and the reflection amplitudes of the lower arm of the Aharonov-Bohm ring [155],

$$t_0^2(\omega) = \frac{4\lambda(\omega)}{[1 + \lambda(\omega)^2]}, \quad r_0^2(\omega) = 1 - t_0^2(\omega) \quad (4.75)$$

as shown in Eq. (B.107); the parameters that characterize the asymmetry of the resonance widths $\Gamma_{L(R)}$ [155],

$$\alpha(\omega) = \frac{2\sqrt{\Gamma_L(\omega)\Gamma_R(\omega)}}{\Gamma_L(\omega) + \Gamma_R(\omega)}, \quad \bar{\alpha}(\omega) = \frac{\Gamma_L(\omega) - \Gamma_R(\omega)}{\Gamma_L(\omega) + \Gamma_R(\omega)} \quad (4.76)$$

as shown in Eq. (B.108), which satisfy

$$\alpha^2(\omega) + \bar{\alpha}^2(\omega) = 1. \quad (4.77)$$

The retarded and the lesser components of the self-energy of phonons, which appears in Eq. (4.66) and (4.67), are given in Eqs. (B.93), (B.90), (B.92) and (B.95) as [155, 156]

$$\begin{aligned} \Sigma_V^r(\omega, \Phi) = i\gamma^2 \int \frac{d\omega'}{2\pi} \left[\mathcal{G}_{dd}^>(\omega', \Phi) \left(\frac{1+N}{\omega - \omega' - \omega_0 + i0^+} + \frac{N}{\omega - \omega' + \omega_0 + i0^+} \right) \right. \\ \left. - \mathcal{G}_{dd}^<(\omega', \Phi) \left(\frac{1+N}{\omega - \omega' + \omega_0 + i0^+} + \frac{N}{\omega - \omega' - \omega_0 + i0^+} \right) \right], \end{aligned} \quad (4.78)$$

$$\Sigma_V^<(\omega, \Phi) = \gamma^2 [N \mathcal{G}_{dd}^<(\omega - \omega_0, \Phi) + (1+N) \mathcal{G}_{dd}^<(\omega + \omega_0, \Phi)], \quad (4.79)$$

where $N \equiv [e^{\beta_P \omega_0} - 1]^{-1}$ is the Bose-Einstein distribution of the Bosonic reservoir.

Another term that appears in Eq. (4.66) is the porolon shift $\Delta\epsilon_V$, which is given by [157]

$$\Delta\epsilon_V(\omega, \Phi) = -\frac{2\gamma^2}{\omega_0} \langle c_d^\dagger c_d \rangle = \frac{2i\gamma^2}{\omega_d} \int \frac{d\omega}{2\pi} \mathcal{G}_{dd}^<(\omega, \Phi), \quad (4.80)$$

as shown in Eq. (B.81).

The expressions of the electric current, J_e , and the heat current from the left reservoir, J_Q^L , J_Q^P are given by Eqs. (B.132), and (B.134), respectively, as

$$J_e = e \int \frac{d\omega}{2\pi} [f_L(\omega) - f_R(\omega)] J_l(\omega, \Phi) + e \int \frac{d\omega}{2\pi} c(\omega, \Phi) J_{V0}^L(\omega, \Phi), \quad (4.81)$$

$$J_Q^L = \int \frac{d\omega}{2\pi} (\omega - \mu_L) [f_L(\omega) - f_R(\omega)] J_l(\omega, \Phi) + \int \frac{d\omega}{2\pi} c(\omega, \Phi) [J_{V1}^L(\omega, \Phi) - \mu_L J_{V0}^L(\omega, \Phi)], \quad (4.82)$$

where the elastic part of the integrand of the current are given in Eq. (B.128) as [155]

$$J_l(\omega, \Phi) = t_0^2 \left(1 - \Gamma \operatorname{Im} G_{dd}^a + \frac{\Gamma^2}{4} [1 - \alpha^2 \cos^2 \Phi] |G_{dd}^a|^2 \right) + t_0 r_0 \Gamma \alpha \cos \Phi \operatorname{Re} G_{dd}^a + \frac{\Gamma^2 \alpha^2}{4} |G_{dd}^a|^2, \quad (4.83)$$

while the inelastic part are given in Eq. (B.135) as

$$\begin{aligned} J_{Vs}^L(\omega, \Phi) = & F_{LL}(\omega) \{ -\omega_+^s a_+(\omega_+) g_{+-}(\omega_-, \Phi) + \omega_-^s a_+(\omega_-) g_{+-}(\omega_+, \Phi) \} \\ & + F_{RR}(\omega) \{ -\omega_+^s b(\omega_+) \sin \Phi g_{-+}(\omega_-, \Phi) + \omega_-^s b(\omega_-) \sin \Phi g_{-+}(\omega_+, \Phi) \} \\ & + F_{LR}(\omega) \{ -\omega_+^s a_+(\omega_+) g_{-+}(\omega_-, \Phi) + \omega_-^s b(\omega_-) \sin \Phi g_{+-}(\omega_+, \Phi) \} \\ & + F_{RL}(\omega) \{ -\omega_+^s b(\omega_+) \sin \Phi g_{+-}(\omega_-, \Phi) + \omega_-^s a_+(\omega_-) g_{-+}(\omega_+, \Phi) \}. \end{aligned} \quad (4.84)$$

The heat current from the Bosonic reservoir, J_Q^P , is given by Eq. (B.120) as

$$\begin{aligned} J_Q^P = & \omega_0 \int \frac{d\omega}{2\pi} c(\omega, \Phi) \{ F_{LL}(\omega) [g_{+-}(\omega_+, \Phi) g_{+-}(\omega_-, \Phi)] + F_{RR}(\omega) [g_{-+}(\omega_+, \Phi) g_{-+}(\omega_-, \Phi)] \\ & + F_{LR}(\omega) [g_{+-}(\omega_+, \Phi) g_{-+}(\omega_-, \Phi)] + F_{RL}(\omega) [g_{-+}(\omega_+, \Phi) g_{+-}(\omega_-, \Phi)] \}. \end{aligned} \quad (4.85)$$

Here we defined the following parameters [155] as shown below Eq. (B.120):

$$c(\omega, \Phi) \equiv \gamma^2 \frac{\Gamma(\omega_+) \Gamma(\omega_-)}{4} |\mathcal{G}_{dd}^a(\omega_+, \Phi) \mathcal{G}_{dd}^a(\omega_-, \Phi)|^2, \quad (4.86)$$

$$\omega_{\pm} \equiv \omega \pm \frac{\omega_0}{2}, \quad (4.87)$$

$$g_{\pm\pm}(\omega, \Phi) \equiv a_{\pm}(\omega) \pm b(\omega) \sin \Phi, \quad g_{\pm\mp}(\omega, \Phi) \equiv a_{\pm}(\omega) \mp b(\omega) \sin \Phi, \quad (4.88)$$

$$a_{\pm}(\omega) = 1 \pm \bar{\alpha}(\omega) r_0(\omega), \quad b(\omega) = \alpha(\omega) t_0(\omega), \quad (4.89)$$

$$F_{\alpha\beta}(\omega) \equiv N[1 - f_{\alpha}(\omega_+)] f_{\beta}(\omega_-) - (1 + N)[1 - f_{\beta}(\omega_-)] f_{\alpha}(\omega_+). \quad (4.90)$$

4.3.4 Construction of the linear-response matrix in the case of three reservoirs

Since we have the expressions of the current, let us go to the linear-response regime and obtain the linear-response matrix. We first construct the linear-response formalism for the case of three reservoirs as in Section 2.1. Since there are two electronic reservoirs and one Bosonic reservoir, there are five currents: the electric and heat currents from the left and right reservoirs and the heat current from the bosonic reservoir. With the particle and energy conservations, the number of the independent currents are three. We here take the independent currents as the electric current between the reservoir J_e and the heat currents from the left and the Bosonic reservoirs J_Q^L and J_Q^P .

Let us next obtain the conjugate affinities to these three independent currents. The entropy production of the model is

$$\dot{S} = -\frac{J_Q^L}{T_L} + \frac{J_Q^R}{T_R} - \frac{J_Q^P}{T_P}, \quad (4.91)$$

where J_Q^L , J_Q^R , J_Q^P are the heat currents from the left reservoir, one *into* the right reservoir, and one from the Bosonic reservoir, respectively, while T_L , T_R , T_P are the temperatures of the left, the right, and the Bosonic reservoirs, respectively. The derivation of this expression was explained in Eq. (1.16) in Subsection 1.2.1. With inserting the first law of thermodynamics $J_Q^L - J_Q^R + J_Q^P = -(\mu_L - \mu_R)/eJ_e$ to Eq. (4.91), we obtain the following form:

$$\dot{S} = -\frac{J_Q^L}{T_L} + \frac{J_Q^L + J_Q^P + (\mu_L - \mu_R)/eJ_e}{T_R} - \frac{J_Q^P}{T_P} \quad (4.92)$$

$$= J_e \frac{V}{T_R} + J_Q^L \frac{T_L - T_R}{T_L T_R} + J_Q^P \frac{T_P - T_R}{T_P T_R} \quad (4.93)$$

$$\equiv \frac{1}{T_R} (J_e V + J_Q^L \delta t_{\text{el}} + J_Q^P \delta t_{\text{e-p}}), \quad (4.94)$$

where $V \equiv (\mu_L - \mu_R)/e$, $\delta t_{\text{el}} \equiv (T_L - T_R)/T_L$, $\delta t_{\text{e-p}} = (T_P - T_R)/T_P$ are conjugate affinities to J_e , J_Q^L , J_Q^P , respectively. Here μ_L, μ_R are chemical potentials of the left and the right reservoirs, respectively.

Once we obtain the expressions for the currents, we expand them to the linear order in the three affinities to obtain the linear-response coefficients. Let us expand the currents (4.81), (4.82), and (4.85) with respect to the conjugate affinities $V \equiv (\mu_L - \mu_R)/e$, $\delta t_{\text{el}} \equiv (T_L - T_R)/T_L$, $\delta t_{\text{e-p}} = (T_P - T_R)/T_P$. In order to make the expressions of the linear-response coefficients simple, we introduce the following notations for preparation:

$$T_l(\omega, \Phi) \equiv \beta_R f_R(\omega) [1 - f_R(\omega)] J^l(\omega, \Phi), \quad (4.95)$$

$$\mathcal{T}_P(\omega, \Phi) \equiv \beta_R N f_R(\omega_-) [1 - f_R(\omega_+)] c(\omega, \Phi), \quad (4.96)$$

which describe the transmission for elastic and inelastic scatterings, respectively.

When we expand the currents to the first order of the differences $\Delta\mu \equiv \mu_L - \mu_R$, $\Delta T \equiv T_L - T_R$, $\Delta T_P \equiv T_P - T_R$, they come only from F_{ij} . The expansion of F_{ij} [multiplied by $c(\omega, \Phi)$]

is in the form

$$c(\omega, \Phi)F_{\text{LL}}(\omega) = \mathcal{T}_{\text{P}}(\omega, \Phi) \left(-\omega_0 \frac{\Delta T}{T_{\text{R}}} + \omega_0 \frac{\Delta T_{\text{P}}}{T_{\text{R}}} \right), \quad (4.97)$$

$$c(\omega, \Phi)F_{\text{RR}}(\omega) = \mathcal{T}_{\text{P}}(\omega, \Phi) \left(\omega_0 \frac{\Delta T_{\text{P}}}{T_{\text{R}}} \right), \quad (4.98)$$

$$c(\omega, \Phi)F_{\text{LR}}(\omega) = \mathcal{T}_{\text{P}}(\omega, \Phi) \left[-\Delta\mu - (\omega_+ - \mu_{\text{R}}) \frac{\Delta T}{T_{\text{R}}} + \omega_0 \frac{\Delta T_{\text{P}}}{T_{\text{R}}} \right], \quad (4.99)$$

$$c(\omega, \Phi)F_{\text{RL}}(\omega) = \mathcal{T}_{\text{P}}(\omega, \Phi) \left[\Delta\mu + (\omega_- - \mu_{\text{R}}) \frac{\Delta T}{T_{\text{R}}} + \omega_0 \frac{\Delta T_{\text{P}}}{T_{\text{R}}} \right]. \quad (4.100)$$

With these expansions and the above notations, we obtain the linear-response coefficients in

$$\begin{pmatrix} J_e \\ J_Q^{\text{L}} \\ J_Q^{\text{P}} \end{pmatrix} = \mathbb{M} \begin{pmatrix} V \\ \delta t_{\text{el}} \\ \delta t_{\text{e-p}} \end{pmatrix} = \begin{pmatrix} M_{11} & M_{12} & M_{13} \\ M_{21} & M_{22} & M_{23} \\ M_{31} & M_{32} & M_{33} \end{pmatrix} \begin{pmatrix} V \\ \delta t_{\text{el}} \\ \delta t_{\text{e-p}} \end{pmatrix} \quad (4.101)$$

as follows:

$$M_{11}(\Phi) = M_{11}(-\Phi) = \int \frac{d\omega}{2\pi} T_l(\omega, \Phi) + \int \frac{d\omega}{\pi} \mathcal{T}_{\text{P}}(\omega, \Phi) m_0(\omega, \Phi), \quad (4.102)$$

$$\begin{aligned} M_{12}(\Phi) = M_{21}(-\Phi) &= \int \frac{d\omega}{2\pi} (\omega - \mu_{\text{R}}) T_l(\omega, \Phi) + \int \frac{d\omega}{\pi} (\omega - \mu_{\text{R}}) \mathcal{T}_{\text{P}}(\omega, \Phi) m_0(\omega, \Phi) \\ &+ \frac{\omega_0}{2} \int \frac{d\omega}{\pi} \mathcal{T}_{\text{P}}(\omega, \Phi) [-m_2(\omega, -\Phi) - m_1(\omega) \sin \Phi], \end{aligned} \quad (4.103)$$

$$M_{13}(\Phi) = M_{31}(-\Phi) = \omega_0 \int \frac{d\omega}{\pi} \mathcal{T}_{\text{P}}(\omega, \Phi) m_2(\omega, \Phi), \quad (4.104)$$

$$\begin{aligned} M_{22}(\Phi) = M_{22}(-\Phi) &= \int \frac{d\omega}{2\pi} (\omega - \mu_{\text{R}})^2 T_l(\omega, \Phi) + \int \frac{d\omega}{\pi} (\omega - \mu_{\text{R}})^2 \mathcal{T}_{\text{P}}(\omega, \Phi) m_0(\omega, \Phi) \\ &+ \omega_0 \int \frac{d\omega}{\pi} (\omega - \mu_{\text{R}}) \mathcal{T}_{\text{P}}(\omega, \Phi) \cdot -\frac{m_2(\omega, \Phi) + m_2(\omega, -\Phi)}{2} \\ &+ \frac{\omega_0^2}{4} \int \frac{d\omega}{\pi} \{2 + [\overline{m}_2(\omega, \Phi) + \overline{m}_2(\omega, -\Phi)] + \overline{m}_0(\omega, \Phi)\}, \end{aligned} \quad (4.105)$$

$$M_{23}(\Phi) = M_{32}(-\Phi) = \omega_0 \int \frac{d\omega}{\pi} (\omega - \mu_{\text{R}}) \mathcal{T}_{\text{P}}(\omega, \Phi) m_2(\omega, \Phi) - \omega_0^2 \int \frac{d\omega}{2\pi} \mathcal{T}_{\text{P}}(\omega, \Phi) [2 + \overline{m}_2(\omega, \Phi)], \quad (4.106)$$

$$M_{33}(\Phi) = M_{33}(-\Phi) = 2\omega_0^2 \int \frac{d\omega}{\pi} \mathcal{T}_{\text{P}}(\omega, \Phi), \quad (4.107)$$

where

$$m_0(\omega, \Phi) = 1 - \overline{\alpha}(\omega_+) \overline{\alpha}(\omega_-) r_0(\omega_+) r_0(\omega_-) + \alpha(\omega_+) \alpha(\omega_-) t_0(\omega_+) t_0(\omega_-) \sin^2 \Phi, \quad (4.108)$$

$$m_1(\omega) = \alpha(\omega_+) t_0(\omega_+) \overline{\alpha}(\omega_-) r_0(\omega_-) - \alpha(\omega_-) t_0(\omega_-) \overline{\alpha}(\omega_+) r_0(\omega_+), \quad (4.109)$$

$$m_2(\omega, \Phi) = \overline{\alpha}(\omega_-) r_0(\omega_-) - \alpha(\omega_-) t_0(\omega_-) \sin \Phi - \overline{\alpha}(\omega_+) r_0(\omega_+) + \alpha(\omega_+) t_0(\omega_+) \sin \Phi, \quad (4.110)$$

$$\overline{m}_0(\omega, \Phi) = 1 + \overline{\alpha}(\omega_+) \overline{\alpha}(\omega_-) r_0(\omega_+) r_0(\omega_-) - \alpha(\omega_+) \alpha(\omega_-) t_0(\omega_+) t_0(\omega_-) \sin^2 \Phi, \quad (4.111)$$

$$\overline{m}_2(\omega, \Phi) = \overline{\alpha}(\omega_-) r_0(\omega_-) + \alpha(\omega_-) t_0(\omega_-) \sin \Phi + \overline{\alpha}(\omega_+) r_0(\omega_+) + \alpha(\omega_+) t_0(\omega_+) \sin \Phi. \quad (4.112)$$

Note that the terms containing \mathcal{T}_P are $\mathcal{O}(\gamma^2)$. The linear-response coefficients depend on the choice of the affinities; if we did not use the correct affinities, the Onsager-Casimir relation would not hold [62]. All off-diagonal elements of \mathbb{M} contain terms odd in the magnetic flux Φ (which obey the Onsager-Casimir reciprocity relations). Remarkably enough, *all* these odd terms arise from inelastic processes in which the charge carriers exchange energy (ω_0) with the vibrational modes. All elements of \mathbb{M} also contain terms even in the flux; these arise from elastic as well as inelastic processes of the transport electrons [155]. In the absence of the coupling of the electrons with the vibrational modes, the linear-response coefficients would be even in the flux and \mathbb{M} would be symmetric.

We make the following two assumptions in order to make the linear-response coefficients simpler: $\Gamma_L(\omega)$ and $\Gamma_R(\omega)$ are energy independent $\Gamma_L(\omega) = \Gamma_L, \Gamma_R(\omega) = \Gamma_R$, which is called the wide-band approximation, and the symmetric resonant widths $\Gamma_L = \Gamma_R$. The former makes $\alpha(\omega), \bar{\alpha}(\omega), t_0(\omega), r_0(\omega)$ independent of ω , while the latter makes $\bar{\alpha} = 0$, which results in $m_1 = m_2 = \bar{m}_2 = 0$. In this case, therefore, we obtain the linear-response coefficients under the assumptions above as

$$\begin{pmatrix} J_e \\ J_Q^L \\ J_Q^P \end{pmatrix} = \begin{pmatrix} G & G\mathcal{S} & 0 \\ G\mathcal{S} & \kappa_0 & -P(1+a) \\ 0 & -P(1-a) & 2P \end{pmatrix} \begin{pmatrix} V \\ \delta t_{\text{el}} \\ \delta t_{\text{e-p}} \end{pmatrix}, \quad (4.113)$$

where we used the notations as $M_{11} = G, M_{12} = G\mathcal{S}, M_{22} = \kappa_0$,

$$P = \omega_0^2 \int \frac{d\omega}{\pi} \mathcal{T}_P(\omega, \Phi), \quad (4.114)$$

and

$$a \equiv t_0 \sin \Phi. \quad (4.115)$$

We also used the fact $\alpha = 1$, which we find from $\bar{\alpha} = 0$ and Eq. (4.77). In Eq. (4.113), G is the electric conductance and \mathcal{S} is the Seebeck coefficient; κ_0 is the “bare” thermal conductance of the electrons, *i.e.*, for $\gamma = 0$, the heat conductance of the electrons is $\kappa_0 - G\mathcal{S}^2$. These three coefficients, for the ring geometry of Fig. 4.2, are functions of $\cos \Phi$ [155]. $2P \geq 0$ is the heat conductance of the phonons, which is proportional to γ^2 , the electron-phonon coupling squared [155]. Note that we will omit ω and Φ dependences of the linear-response coefficients hereafter if not necessary.

4.3.5 A constraint from the nonnegativity of the three-terminal entropy production

Inserting the explicit expressions for the currents [Eq. (4.113)] into Eq. (4.94), one finds that the entropy production of the three-terminal device is non-negative, $\dot{S} \geq 0$, for

$$\kappa_0 - G\mathcal{S}^2 - \frac{P}{2} \geq 0, \quad \text{i.e.} \quad 2\frac{\kappa_0}{P} \geq 1 + \zeta, \quad (4.116)$$

where $\zeta = G\mathcal{S}^2/(\kappa_0 - G\mathcal{S}^2)$ is the figure of merit of the conventional electronic two-terminal device; see *e.g.*, Ref. [109]. This condition is obtained by the following calculation:

$$T_R \dot{S} = J_e V + J_Q^L \delta t_{\text{el}} + J_Q^P \delta t_{\text{e-p}} \quad (4.117)$$

$$= GV^2 + 2\mathcal{S}G\delta_{\text{el}}V + \kappa_0\delta_{\text{el}}^2 - 2P\delta_{\text{el}}\delta_{\text{e-p}} + 2P\delta_{\text{e-p}}^2 \quad (4.118)$$

$$= G(V + \mathcal{S}\delta_{\text{el}})^2 + 2P(\delta_{\text{e-p}} - \delta_{\text{el}})^2 + (\kappa_0 - G\mathcal{S}^2 - 2P)\delta_{\text{el}}^2 \geq 0. \quad (4.119)$$

4.3.6 From the 3×3 to the effective 2×2 matrix with a probe condition

In order to check the consistency of Benenti *et al.*'s result [90] from our point of view, we should make an asymmetric 2×2 linear-response matrix. Moreover, as shown in Ref. [22], the upper bound of the efficiency may not reach the Carnot one when there are two heat currents. In this case, therefore, we should make the electronic or phononic heat currents vanish in order to obtain the Carnot efficiency. Here we take the probe condition [151], which is the same way as in Section 4.2. Let us take δt_{el} to make J_Q^L zero. The expression of J_Q^L is obtained from Eq. (4.113) as

$$J_Q^L = GSV + \kappa_0\delta t_{\text{el}} - P(1+a)\delta t_{\text{e-p}}. \quad (4.120)$$

Solving $J_Q^L = 0$ with respect to $\delta t_{\text{e-p}}$, we obtain

$$\delta t_{\text{e-p}} = -\frac{1}{\kappa_0}[GSV - P(1+a)\delta t_{\text{el}}]. \quad (4.121)$$

Note that we will discuss the case when we take $\delta t_{\text{e-p}}$ to make J_Q^P zero in Subsection 4.4.2. The setup then becomes an effective two-terminal one, in which electric power is produced at the expense of heat current from the Bosonic reservoirs. The effective 2×2 linear-response matrix is obtained with inserting Eq. (4.121) to the expressions of J_e and J_Q^P obtained from Eq. (4.113) as

$$\begin{pmatrix} J_e \\ J_Q^P \end{pmatrix} = \begin{pmatrix} \frac{G}{1+\zeta} & \frac{PG\mathcal{S}}{\kappa_0}(1+a) \\ \frac{PG\mathcal{S}}{\kappa_0}(1-a) & \frac{P^2}{\kappa_0}(\zeta_{\text{max}} + a^2) \end{pmatrix} \begin{pmatrix} V \\ \delta t_{\text{e-p}} \end{pmatrix}, \quad (4.122)$$

where $\zeta_{\text{max}} = -1 + 2\kappa_0/P$ is the upper bound on ζ imposed by the condition (4.116). We find that the matrix is asymmetric, that is, the off-diagonal elements are not even in the magnetic field.

We here remark that when we take $J_Q^P = 0$ as the probe condition, we obtain $\delta t_{\text{e-p}}$ to make $J_Q^P = 0$ as

$$\delta t_{\text{e-p}} = \frac{1-a}{2}\delta t_{\text{el}}, \quad (4.123)$$

which comes from the condition

$$J_Q^P = -P(1-a)\delta t_{\text{el}} + 2P\delta t_{\text{e-p}} = 0. \quad (4.124)$$

Note that the expression of J_Q^P comes from Eq. (4.113). Inserting Eq. (4.123) to the expressions

of J_e and J_Q^L found from Eq. (4.113), we obtain the following effective 2×2 matrix:

$$\begin{pmatrix} J_e \\ J_Q^L \end{pmatrix} = \begin{pmatrix} G & G\mathcal{S} \\ G\mathcal{S} & \kappa_0 - \frac{P}{2}(1 - a^2) \end{pmatrix} \begin{pmatrix} V \\ \delta t_{\text{el}} \end{pmatrix}, \quad (4.125)$$

which is an *symmetric* matrix. Therefore, we cannot achieve the Carnot efficiency with non-vanishing power with the probe condition $J_Q^P = 0$; see Section 2.3 for the conditions to achieve the Carnot efficiency with nonvanishing power. We will consider general cases for the probe condition $J_Q^P = 0$ without the assumptions in Subsection 4.4.2

4.3.7 A constraint from the nonnegativity of the entropy production of the effective two-terminal setup

The entropy production in the effective two-terminal setup described by Eq. (4.122), which is proportional to $J_e V + J_Q^P \delta t_{e-p}$, is non-negative for

$$2\frac{\kappa_0}{P} + a^2 \geq 1 + \zeta. \quad (4.126)$$

This condition comes from the calculation

$$T_R \dot{S}^{2 \times 2} = J_e V + J_Q^P \delta t_{e-p} \quad (4.127)$$

$$= \frac{G}{1 + \zeta} V^2 + \frac{2PG\mathcal{S}}{\kappa_0} V \delta t_{e-p} + \frac{P^2}{\kappa_0} (\zeta_{\text{max}} + a^2) \delta t_{e-p}^2 \quad (4.128)$$

$$= \frac{G}{1 + \zeta} \left[V + \frac{P\mathcal{S}(1 + \zeta)}{\kappa_0} \delta t_{e-p} \right]^2 + \frac{P^2}{\kappa_0} (\zeta_{\text{max}} + a^2 - \zeta) \geq 0 \quad (4.129)$$

with $\zeta_{\text{max}} = -1 + 2\kappa_0/P$, where we used $G\mathcal{S}^2/\kappa_0 = \zeta/(1 + \zeta)$. The equality in Eq. (4.126) is what Benenti *et al.* [90] used in discussing the possibility to achieve the Carnot efficiency with nonvanishing power; see also Chapter 2. However, taking account of the three-terminal setup, which is the background of the effective two-terminal setup, implies that the stricter inequality (4.116) must hold, and that the equality of Eq. (4.126) is not achievable for a nonzero value of $a = t_0 \sin \Phi$. This means that as long as the magnetic field is finite, the entropy production of the effective two-terminal setup (4.129) cannot vanish. Thus, the Carnot efficiency is not reached, although the symmetry of the 2×2 linear-response matrix (4.122) is broken. This is one of the main result of the present section. In other words, in our specific model, we cannot attain the condition $|x| > 1$ and $y = 4x/(x - 1)^2$, with which Benenti *et al.* argue that we can attain the Carnot efficiency with nonvanishing power. Here we repeat the definitions of x and y as

$$x \equiv \frac{L_{12}}{L_{21}}, \quad y \equiv \frac{L_{12}L_{21}}{L_{11}L_{22} - L_{12}L_{21}}, \quad (4.130)$$

where L_{ij} is a component of the effective 2×2 matrix.

4.3.8 The efficiency at the maximum power

Let us calculate the efficiency at the maximum power and the maximum efficiency with respect to a . Let us begin with the effective 2×2 matrix:

$$\begin{pmatrix} J_e \\ J_Q^P \end{pmatrix} = \begin{pmatrix} \frac{G}{1+\zeta} & \frac{PG\mathcal{S}}{\kappa_0}(1+a) \\ \frac{PG\mathcal{S}}{\kappa_0}(1-a) & \frac{P^2}{\kappa_0}(\zeta_{\max} + a^2) \end{pmatrix} \begin{pmatrix} V \\ \delta t_{e-p} \end{pmatrix}. \quad (4.131)$$

Since we have already calculated the voltage that gives the maximum power, the maximum power, the efficiency at the maximum power and so on for a general asymmetric 2×2 matrix in Section 2, we can easily obtain them in the present case by simply inserting each element of the 2×2 matrix (4.131) to the equations in Section 2.3.

Let us consider first the maximum power. From the expression,

$$J_e = \frac{G}{1+\zeta}V + \frac{PG\mathcal{S}}{\kappa_0}(1+a)\delta t_{e-p}, \quad (4.132)$$

we obtain the expression of the power in the form

$$\dot{W} = -J_e V = -\frac{G}{1+\zeta}V^2 - \frac{PG\mathcal{S}}{\kappa_0}(1+a)\delta t_{e-p}V. \quad (4.133)$$

Differentiating this with respect to V and setting it to be zero, we obtain the following condition:

$$-\frac{2G}{1+\zeta}V - \frac{PG\mathcal{S}}{\kappa_0}(1+a)\delta t_{e-p} = 0, \quad (4.134)$$

from which we find

$$V_{\max p} = -\frac{(1+\zeta)(1+a)P\mathcal{S}}{2\kappa_0}\delta t_{e-p}. \quad (4.135)$$

Inserting this to the expression of the power, we obtain

$$\dot{W}_{\max} = -\frac{G}{1+\zeta} \frac{P^2\mathcal{S}^2(1+\zeta)^2(1+a)^2}{4\kappa_0^2} \delta t_{e-p}^2 + \frac{PG\mathcal{S}}{\kappa_0}(1+a) \frac{(1+\zeta)(1+a)}{2\kappa_0} P\mathcal{S} \delta t_{e-p}^2 \quad (4.136)$$

$$= \kappa_0 \delta t_{e-p}^2 \frac{\zeta(1+a)^2}{(\zeta_{\max} + 1)^2} \leq 4\kappa_0 \delta t_{e-p}^2 \frac{\zeta_{\max}}{(\zeta_{\max} + 1)^2}, \quad (4.137)$$

where we used the equations

$$\frac{G\mathcal{S}^2}{\kappa_0} = \frac{\zeta}{\zeta + 1}, \quad \frac{P}{2\kappa_0} = \frac{1}{\zeta_{\max} + 1}, \quad (4.138)$$

and $a \leq 1, \zeta \leq \zeta_{\max}$.

Inserting each element of the effective 2×2 linear-response matrix (4.131) to Eq. (2.112), we obtain the efficiency at the maximum power as

$$\eta(V_{\max p}) = \frac{\eta_c}{4} \frac{(1+a)^2 \zeta}{\zeta_{\max} + a^2 - 2(1-a^2)\zeta}. \quad (4.139)$$

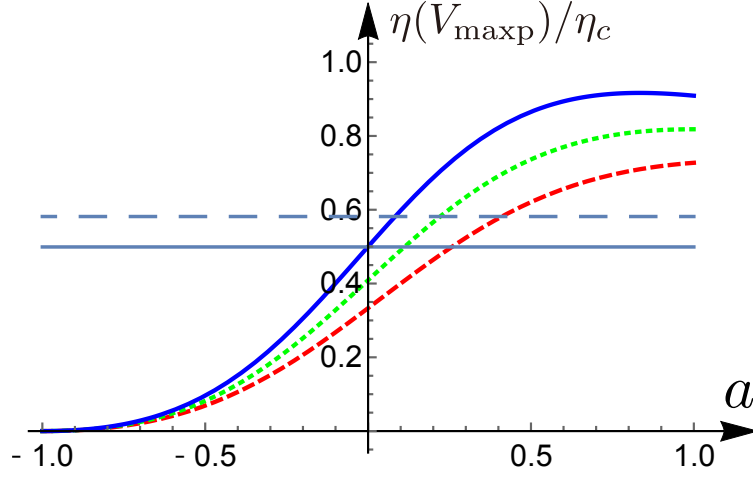


Figure 4.5: The efficiency at the maximum power of the effective two-terminal device (scaled by the Carnot efficiency η_c), Eq. (4.139), as a function of the asymmetry parameter a , for $\zeta_{\max} = 10$; $\zeta = 8$ [the dashed (red) curve], 9 [the dotted (green) curve], and 10 [the thick (blue) line]. The horizontal line is $\eta(V_{\max p}, \zeta = \zeta_{\max})/\eta_c$ of the two-terminal junction. The thick horizontal line in the middle shows the Curzon-Ahlborn bound $\eta_{CA}/\eta_c = 0.5$, while the dotted one shows $4\eta_c/7$, which is Brandner *et al.*'s upper limit in Eq. (4.53).

We plot the efficiency at the maximum power with respect to a in Fig. 4.5. We see that the efficiency at the maximum power may be larger than the CA bound $\eta_c/2$ in Eq. (2.22) (the thick horizontal line in the middle) and Brander *et al.*'s bound $4\eta_c/7$ in Eq. (4.53) (the dotted horizontal line). However, note that this is the result to the order of γ^2 without vertex corrections; see the discussion in Section 4.6. We also see that the efficiency at the maximum power has a maximum. Indeed we can obtain this maximum analytically as follows. Differentiating Eq. (4.139) with respect to a , we obtain the following:

$$\frac{\partial \eta(V_{\max p})}{\partial a} \propto (1+a) \left(-a + \frac{2\zeta_{\max} - \zeta}{2 + \zeta} \right). \quad (4.140)$$

Since $-1 \leq a \leq 1$, the parameter a that gives the maximum is as follows:

$$a = \begin{cases} 1 & \text{for } \frac{2\zeta_{\max} - \zeta}{2 + \zeta} > 1, \\ \frac{2\zeta_{\max} - \zeta}{2 + \zeta} & \text{for } \frac{2\zeta_{\max} - \zeta}{2 + \zeta} \leq 1. \end{cases} \quad (4.141)$$

By transforming Eq. (4.141), we obtain

$$a = \begin{cases} 1 & \text{for } \zeta < \zeta_{\max} - 1, \\ \frac{2\zeta_{\max} - \zeta}{2 + \zeta} & \text{for } \zeta \geq \zeta_{\max} - 1. \end{cases} \quad (4.142)$$

For $\zeta < \zeta_{\max} - 1$, inserting $a = 1$ into Eq. (4.139), we obtain the maximum value of the efficiency

at maximum power in the form

$$\max_a \eta(V_{\max}) = \eta_c \frac{\zeta}{\zeta_{\max} + 1}, \quad (4.143)$$

while for $\zeta \geq \zeta_{\max} - 1$, inserting $a = (2\zeta_{\max} - \zeta)/(2 + \zeta)$ into Eq. (4.139), we obtain

$$\max_a \eta(V_{\max}) = \eta_c \frac{\left(1 + \frac{2\zeta_{\max} - \zeta}{2 + \zeta}\right)^2 \frac{\zeta}{4}}{\zeta_{\max} + \left(\frac{2\zeta_{\max} - \zeta}{2 + \zeta}\right)^2 - \left[1 - \left(\frac{2\zeta_{\max} - \zeta}{2 + \zeta}\right)^2\right] \frac{\zeta}{2}} \quad (4.144)$$

$$= \eta_c \frac{\zeta(1 + \zeta_{\max})}{(2 + \zeta)(2\zeta_{\max} - \zeta)}. \quad (4.145)$$

The result is summarized as follows:

$$\max_a \eta(V_{\max}) = \begin{cases} \eta_c \frac{\zeta}{\zeta_{\max} + 1} & \text{for } \zeta < \zeta_{\max} - 1, \\ \eta_c \frac{\zeta(1 + \zeta_{\max})}{(2 + \zeta)(2\zeta_{\max} - \zeta)} & \text{for } \zeta \geq \zeta_{\max} - 1. \end{cases} \quad (4.146)$$

4.3.9 The maximum efficiency

Let us next consider the maximum efficiency. Inserting the effective 2×2 matrix (4.131) to Eqs. (2.49) and (2.60), at the voltage

$$V_{\max} = \frac{P(\zeta_{\max} + a^2)}{G\mathcal{S}(1 - a)} \left(\sqrt{1 - \frac{(1 - a^2)\zeta}{\zeta_{\max} + a^2}} - 1 \right) \delta t_{e-p}, \quad (4.147)$$

we obtain the maximum efficiency as

$$\eta(V_{\max}) = \eta_c \frac{1 + a}{1 - a} \frac{1 - \sqrt{1 - \frac{(1 - a^2)\zeta}{\zeta_{\max} + a^2}}}{1 + \sqrt{1 - \frac{(1 - a^2)\zeta}{\zeta_{\max} + a^2}}} \quad (4.148)$$

$$= \eta_c \frac{\sqrt{1 + \tilde{\zeta}} - 1}{\sqrt{1 + \tilde{\zeta}} + 1}, \quad (4.149)$$

with the new figure of merit of the effective two-terminal device:

$$\tilde{\zeta} = \zeta \frac{(1 - a^2)^2 / (\zeta_{\max} + a^2)}{\left(\sqrt{1 - (1 - a^2)\zeta / (\zeta_{\max} + a^2)} - a \right)^2}. \quad (4.150)$$

Note that the maximum efficiency of the two-terminal electronic device is

$$\eta(V_{\max}) = \eta_c \frac{\sqrt{1 + \tilde{\zeta}} - 1}{\sqrt{1 + \tilde{\zeta}} + 1} \quad (4.151)$$

if the electron-phonon coupling γ is zero: Since ζ has a term of $\mathcal{O}(\gamma^2)$, ζ with a finite strength

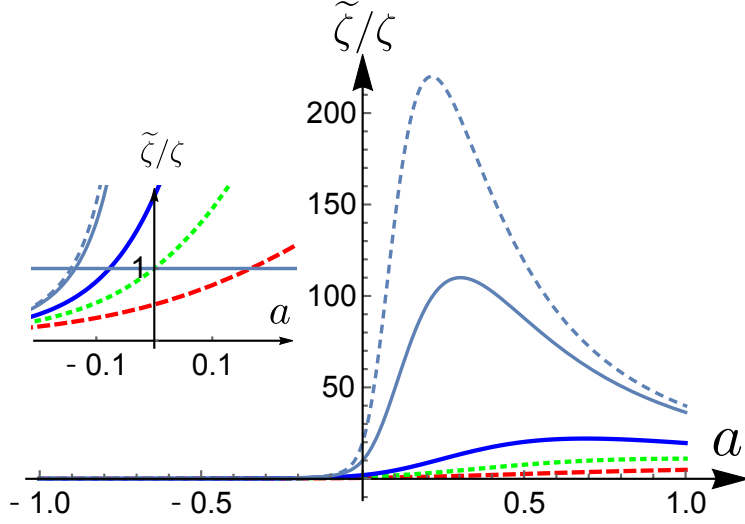


Figure 4.6: The effective two-terminal figure of merit $\tilde{\zeta}$, Eq. (4.150) (scaled by ζ), as a function of a , for $\zeta_{\max} = 10$; $\zeta = 8$ [the dashed (red) curve], 9 [the dotted (green) curve], 9.5 [the thick (blue) line], 9.9 [the thin (black) curve], and 9.95 [the thin dashed (black) curve]. Inset: The range where $\tilde{\zeta}/\zeta$ crosses 1.

of the electron-phonon coupling γ is not the same as the figure of merit of the two-terminal electronic device. We plot $\tilde{\zeta}/\zeta$ as a function of a in Fig. 4.6, which shows that $\tilde{\zeta}$ can significantly exceed ζ . As for $\eta(V_{\max})$, $\tilde{\zeta}$ has a maximum at a certain positive a , which grows and moves to smaller values of a as ζ increases. However, we cannot show analytically the value of a that gives the maximum and the maximum value of the new figure of merit. The inset displays the region around $\zeta = \tilde{\zeta}$. As seen, $\tilde{\zeta}$ increasingly exceeds ζ , making the effective two-terminal device better than the electronic two-terminal one. However, note again that ζ with a finite γ is not the same as the figure of merit of the two-terminal electronic device in the strict sense.

4.3.10 Asymmetry of the efficiency with respect to $a = t_0 \sin \Phi$

We find from Figs. 4.5 and 4.6 that both the efficiency at the maximum power and the maximum efficiency are asymmetric with respect to $a = t_0 \sin \Phi$, which is the effect of the inelastic scattering because the currents without the electron-phonon interaction are symmetric with respect to $a = t_0 \sin \Phi$. This asymmetry comes from the inelastic part of the current,

$$J_V^L(\omega, \Phi) = -i \frac{\Gamma}{2} |\mathcal{G}_{dd}^a|^2 \{a_+ [\Sigma_V^<(1 - f_L) + \Sigma_V^>f_L] + b \sin \Phi [\Sigma_V^<(1 - f_R) + \Sigma_V^>f_R]\}, \quad (4.152)$$

as shown in Eq. (B.129), where we omit the ω and Φ dependences of the right-hand side for brevity; see Subsection 4.3.3 for the definitions of each parameter appearing in the expression above. Note that we assume the symmetric resonant widths, so that $\bar{\alpha} = 0$.

Let us explain the asymmetry intuitively. We find that the effect of the magnetic field vanishes at $t_0 = 0$, which makes $a = 0$. Since t_0 is the transmission amplitude for the lower arm of the ring, the circular current is important for the asymmetry. As the asymmetry comes

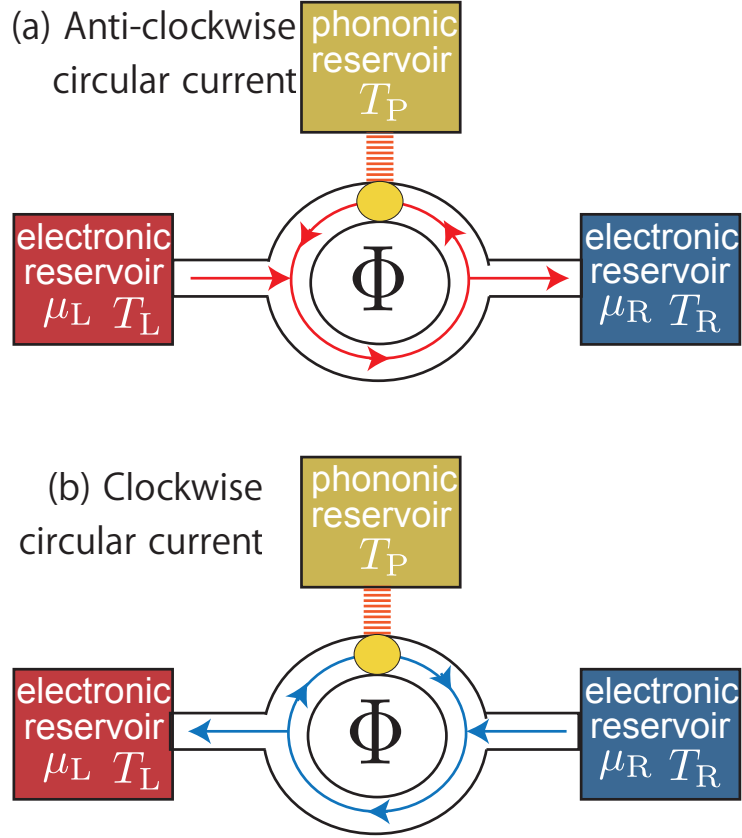


Figure 4.7: Schematic pictures of the flow of *inelastic* electric current for (a) anti-clockwise and (b) clockwise direction. In the case of (a), more electric current goes from left to right, while more goes from right to left in the case of (b).

from the inelastic part of the current, we consider the current that goes through the dot, on which there is an electron-phonon interaction. For simplicity, let us consider only the inelastic circular electric current with $t_0 = 1$. We assume that a positive magnetic flux tries to pull the current in the anti-clockwise direction while a negative one in the clockwise direction. As shown in Fig. 4.7, the current tends to run from the left reservoir, go around the ring in the anti-clockwise direction, then run to the right reservoir for a positive flux, while to the left reservoir for a negative one. Since an electric current from the left to the right produces an electric power while one from the right to the left does not, the asymmetry of the efficiency with respect to a happens.

4.3.11 Calculation with experimental values

Let us calculate the efficiency at the maximum power and the maximum efficiency using experimental parameters under the assumptions of energy-independent symmetric resonant widths. We need the following parameters: the energy of phonons $\hbar\omega_0$; the strength of the electron-phonon coupling γ ; the temperature of the right reservoir T_R and the temperature difference $T_P - T_R$; the resonance widths from the coupling between the dot and the reservoir $\Gamma_L = \Gamma_R$

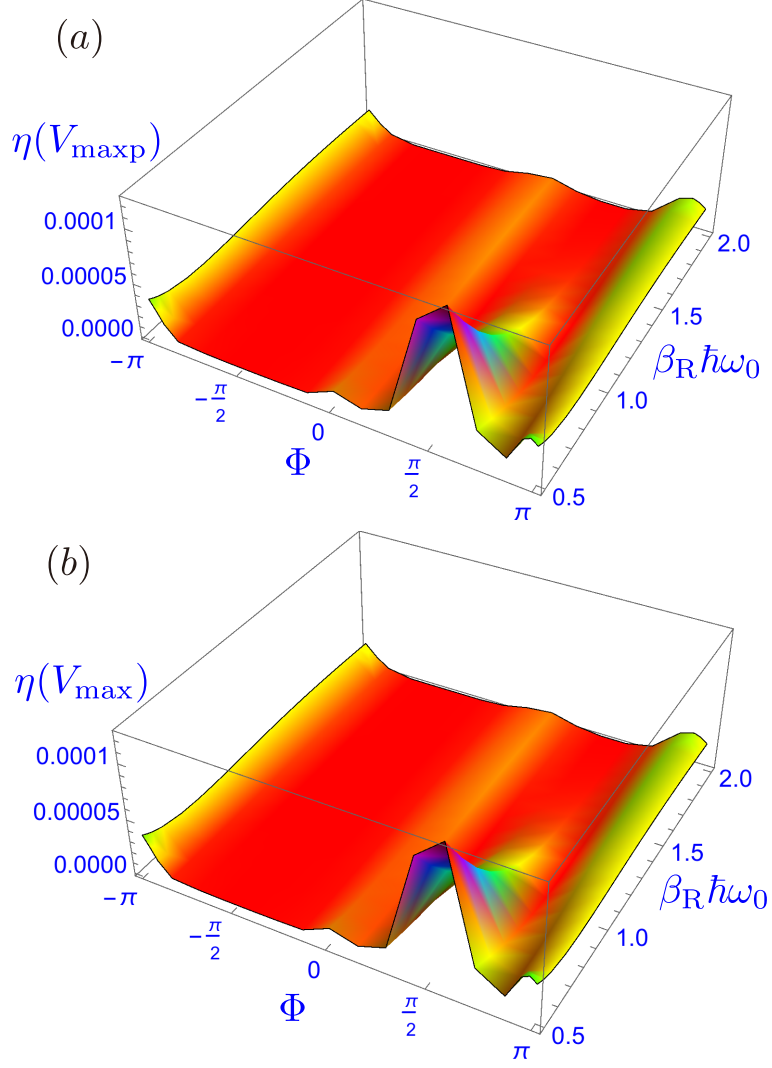


Figure 4.8: Numerical plots of (a) the efficiency at the maximum power and (b) the maximum efficiency with respect to the magnetic flux ϕ and $\beta_R \hbar \omega_0$. We set $\Gamma_L = \Gamma_R = \beta_R^{-1} \lambda = 1$ meV (see Subsection 4.3.3 for their definitions), $\gamma = 0.3\Gamma_L = 0.3$ meV, $\mu_R/e = 0$ V, $\epsilon_d = 1$ meV, and $T_P - T_R = 1$ K.

as well as that between the electronic reservoirs λ ; the chemical potential of the right reservoir μ_R ; the energy level of the dot (including the porolon shift $\Delta\epsilon_V$ in Eq. (B.84) and the real part of the self energy) ϵ_d . For experimental estimates, we refer to the experiment using suspended carbon nanotube quantum dots [158], according to which the parameters are of the order of meV. We thereby set $\Gamma_L = \Gamma_R = \beta_R^{-1}\lambda = 1$ meV (see Subsection 4.3.3 for their definitions), $\gamma = 0.3\Gamma_L = 0.3$ meV, $\mu_R/e = 0$ V, $\epsilon_d = 1$ meV, and $T_P - T_R = 1$ K. With these values, we numerically calculate the linear-response coefficients (4.102)-(4.107), from which we obtain the efficiency at the maximum power and the maximum efficiency. Figs. 4.8(a) and (b) show the plot of the efficiency at the maximum power and the maximum efficiency, respectively, with respect to the magnetic flux ϕ and $\beta_R\hbar\omega_0$. Note that the two plots look almost the same.

Let us calculate the value of the efficiency at the maximum power and the maximum efficiency. We set $\Phi = \pi/2$, around which we can obtain a high maximum efficiency and the efficiency at the maximum power as observed from Figs. 4.8(a) and (b). We also set $\hbar\omega_0 = 1$ meV, $T_R = 10$ K according to Ref. [158], which makes $\beta_R\hbar\omega_0 \approx 0.93$. Note that $k_B = 8.6 \times 10^{-5}$ eV/K. With them, we obtain the efficiency at the maximum power $\eta(V = V_{\max}) = 4 \times 10^{-5}\eta_c$ from Eq. (2.112) at the voltage difference $|V_{\max}| = 2 \times 10^{-3}$ V = 2 mV from Eq. (2.106), while the maximum efficiency $\eta(V = V_{\max}) = 4 \times 10^{-5}\eta_c$ from Eq. (2.60) at the voltage difference $|V_{\max}| = 3 \times 10^{-6}$ eV = 3 μ V from Eq. (2.49).

4.4 Further considerations

4.4.1 For an asymmetric resonant widths $\Gamma_L \neq \Gamma_R$

We have considered so far the case of symmetric resonant widths $\Gamma_L = \Gamma_R$. In the present section, we consider whether the results change for asymmetric resonant widths $\Gamma_L \neq \Gamma_R$.

When we assume the wide-band approximation but asymmetric resonant widths $\Gamma_L \neq \Gamma_R$, the parameters $m_0, \bar{m}_0, \bar{m}_2$ are modified as

$$m_0(\Phi) = 1 - \bar{\alpha}^2 r_0^2 + \alpha^2 t_0^2 \sin^2 \Phi, \quad (4.153)$$

$$\bar{m}_0(\Phi) = 1 + \bar{\alpha}^2 r_0^2 - \alpha^2 t_0^2 \sin^2 \Phi, \quad (4.154)$$

$$\bar{m}_2(\Phi) = 2(\bar{\alpha}r_0 - \alpha t_0 \sin \Phi), \quad (4.155)$$

while $m_1 = m_2 = 0$; see the definitions Eqs. (4.108)-(4.112). Note that we recover the case of symmetric resonant widths for $\alpha = 1, \bar{\alpha} = 0$. This change modifies G, \mathcal{S}, κ_0 , and a . In particular, a is modified as

$$a = t_0 \sin \Phi \rightarrow \alpha t_0 \sin \Phi - \bar{\alpha} r_0. \quad (4.156)$$

Since this change modifies G, \mathcal{S}, κ_0 , and a , the result may change quantitatively. In particular, as shown in Eq. (4.157), a is modified as

$$a = t_0 \sin \Phi \rightarrow \alpha t_0 \sin \Phi - \bar{\alpha} r_0, \quad (4.157)$$

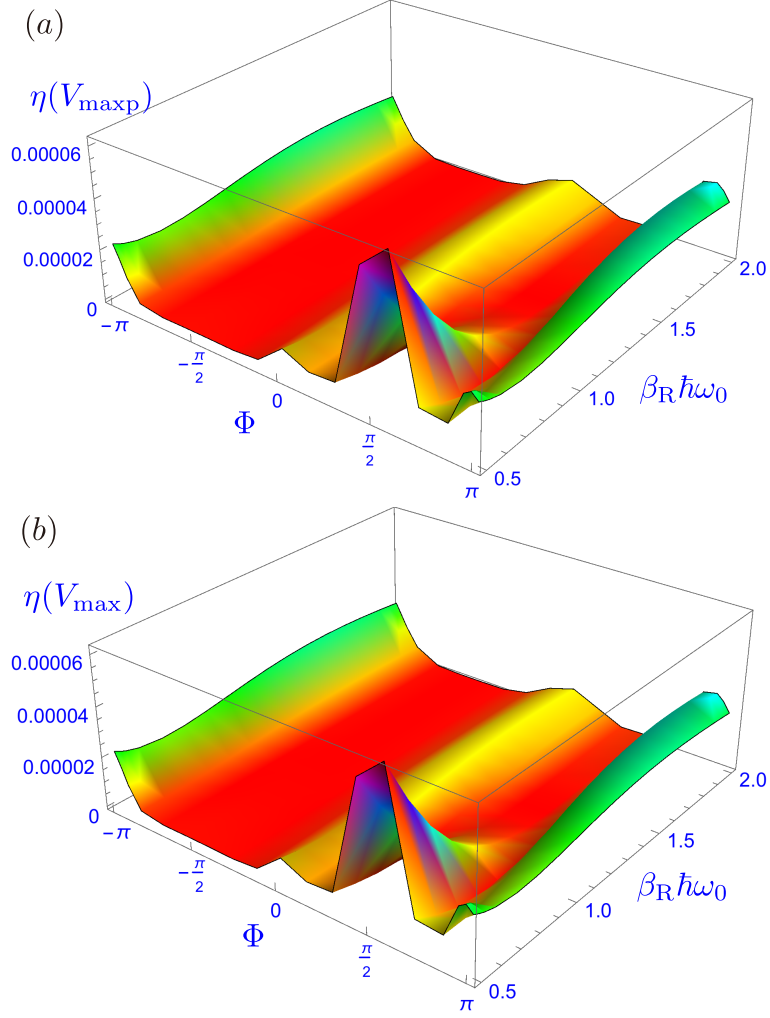


Figure 4.9: Numerical plots of (a) the efficiency at the maximum power and (b) the maximum efficiency with respect to the magnetic flux ϕ and $\beta_R \hbar \omega_0$. We set $\Gamma_L = 0.5$ meV, $\Gamma_R = 1.5$ meV, $\beta_R^{-1} \lambda = 1$ meV and we make the other parameters the same as those used in Figs. 4.8(a) and (b).

where $r_0^2 = 1 - t_0^2$ and

$$\alpha = \frac{2\sqrt{\Gamma_L \Gamma_R}}{\Gamma_L + \Gamma_R}, \quad \bar{\alpha} = \frac{\Gamma_L - \Gamma_R}{\Gamma_L + \Gamma_R}. \quad (4.158)$$

Note that $\alpha^2 + \bar{\alpha}^2 = 1$. The modification (4.157) therefore increases or decreases the value of a depending mainly on the sign of $\bar{\alpha}$. We believe that, however, the result does not change qualitatively. Indeed, with comparing the plots of the efficiency at the maximum power and the maximum efficiency with an asymmetric resonance widths in Figs. 4.9 (a) and (b) with those in Figs. 4.8(a) and (b), we see that the behavior of both plots looks the same qualitatively although the values of them are different.

We here remark on the probe condition $J_Q^P = 0$. For the asymmetric resonant widths, the parameters G, \mathcal{S}, κ_0 and a change. However, the effective 2×2 matrix remains symmetric. Therefore, we cannot achieve the Carnot efficiency with nonvanishing power for the probe condition $J_Q^P = 0$ even for an asymmetric resonant width in the wide-band limit.

4.4.2 The probe condition $J_Q^P = 0$ for general cases

In the present subsection, we consider the case with the probe condition $J_Q^P = 0$ for a general case. For a general case without the assumptions of symmetric energy-independent couplings and even with vertex corrections,

$$\begin{pmatrix} J_e \\ J_Q^L \\ J_Q^P \end{pmatrix} = \begin{pmatrix} M_{11} & M_{12} & M_{13} \\ M_{21} & M_{22} & M_{23} \\ M_{31} & M_{32} & M_{33} \end{pmatrix} \begin{pmatrix} V \\ \delta t_{\text{el}} \\ \delta t_{\text{e-p}} \end{pmatrix}, \quad (4.159)$$

the effective 2×2 matrix under the probe condition

$$J_Q^P = M_{31}V + M_{32}\delta t_{\text{el}} + M_{33}\delta t_{\text{e-p}} = 0 \quad (4.160)$$

is calculated as

$$\begin{pmatrix} J_e \\ J_Q^L \end{pmatrix} = \begin{pmatrix} M_{11} - \frac{M_{13}M_{31}}{M_{33}} & M_{12} - \frac{M_{13}M_{32}}{M_{33}} \\ M_{21} - \frac{M_{23}M_{31}}{M_{33}} & M_{22} - \frac{M_{23}M_{32}}{M_{33}} \end{pmatrix} \begin{pmatrix} V \\ \delta t_{\text{el}} \end{pmatrix} \quad (4.161)$$

by inserting the condition

$$\delta t_{\text{e-p}} = -\frac{M_{31}}{M_{33}}V - \frac{M_{32}}{M_{33}}\delta t_{\text{el}} \quad (4.162)$$

obtained from Eq. (4.160) to the matrix (4.159). We obtain the ratio of the off-diagonal elements of the effective 2×2 matrix (4.161), x as

$$x = \frac{M_{12} - M_{13}M_{32}/M_{33}}{M_{21} - M_{23}M_{31}/M_{33}} = \frac{\mathcal{O}(1) + \mathcal{O}(\gamma^2)}{\mathcal{O}(1) + \mathcal{O}(\gamma^2)} \approx \mathcal{O}(1) + \mathcal{O}(\gamma^2), \quad (4.163)$$

where we used the fact that the asymmetry of the matrix comes from the effect of phonons, that is, the terms causing the asymmetry are $\mathcal{O}(\gamma^2)$; when $\gamma = 0$, we have $M_{12} = M_{21}$. We can confirm the fact above from the expressions of the linear-response coefficients (4.102)-(4.107).

As shown in Eq. (4.163), only the terms of order γ^2 makes x different from unity. Therefore

it is possible to achieve the Carnot efficiency with nonvanishing power if the conditions in Eq. (2.88) are satisfied. The efficiency at the maximum power can also exceed the CA bound $\eta_c/2$, but not much because the difference of x from unity is small, $\mathcal{O}(\gamma^2)$.

4.5 Restriction for the effective 2×2 matrix from the nonnegativity from the general 3×3 matrix

In the previous section, we assume that the coupling is symmetric and independent of energy as well as the weak electron-phonon coupling. In the present section, we consider the general case of the asymmetric 3×3 matrix

$$\mathbb{L} = \begin{pmatrix} L_{11} & L_{12} & L_{13} \\ L_{21} & L_{22} & L_{23} \\ L_{31} & L_{32} & L_{33} \end{pmatrix} \quad (4.164)$$

and obtain the condition for the Carnot efficiency with nonvanishing power, which is not satisfied for our specific model in Section 4.3.

The matrix (4.164) can be divided into the symmetric part and the asymmetric part as

$$\mathbb{L}(B) = \frac{\mathbb{L}(B) + \mathbb{L}(-B)}{2} + \frac{\mathbb{L}(B) - \mathbb{L}(-B)}{2} \quad (4.165)$$

$$\equiv \mathbb{L}^{\text{sym}} + \mathbb{L}^{\text{asym}} \quad (4.166)$$

$$= \begin{pmatrix} S_{11} & S_{12} & S_{13} \\ S_{12} & S_{22} & S_{23} \\ S_{13} & S_{23} & S_{33} \end{pmatrix} + \begin{pmatrix} 0 & A_{12} & A_{13} \\ -A_{12} & 0 & A_{23} \\ -A_{13} & -A_{23} & 0 \end{pmatrix}, \quad (4.167)$$

where B is a magnetic field. The linear-response expansion with S_{ij} and A_{ij} is

$$\begin{pmatrix} j_1 \\ j_2 \\ j_3 \end{pmatrix} = \begin{pmatrix} S_{11} & S_{12} + A_{12} & S_{13} + A_{13} \\ S_{12} - A_{12} & S_{22} & S_{23} + A_{23} \\ S_{13} - A_{13} & S_{23} - A_{23} & S_{33} \end{pmatrix} \begin{pmatrix} f_1 \\ f_2 \\ f_3 \end{pmatrix}, \quad (4.168)$$

where j_1, j_2, j_3 are independent currents and f_1, f_2, f_3 are conjugate affinities. Note that we can apply this analysis to other systems with the 3×3 linear-response matrix. We can easily confirm that the asymmetric part does not contribute to the entropy production:

$$(f_1 \ f_2 \ f_3) \mathbb{L}^{\text{asym}} \begin{pmatrix} f_1 \\ f_2 \\ f_3 \end{pmatrix} = 0. \quad (4.169)$$

Therefore, the condition for nonnegativity of the entropy production is

$$\dot{S}^{3 \times 3} = (f_1 \ f_2 \ f_3) \mathbb{L}^{\text{sym}} \begin{pmatrix} f_1 \\ f_2 \\ f_3 \end{pmatrix} \geq 0. \quad (4.170)$$

Since the matrix \mathbb{L}^{sym} is symmetric, we know from the theorem of quadratic forms that the necessary and sufficient condition for Eq. (4.170) to hold is that the determinants of all the principal minors are nonnegative:

$$S_{11} \geq 0, \quad S_{22} \geq 0, \quad S_{33} \geq 0, \quad (4.171)$$

$$s_{11} \equiv S_{22}S_{33} - S_{23}^2 \geq 0, \quad (4.172)$$

$$s_{22} \equiv S_{11}S_{33} - S_{13}^2 \geq 0, \quad (4.173)$$

$$s_{33} \equiv S_{11}S_{22} - S_{12}^2 \geq 0, \quad (4.174)$$

$$\det \mathbb{L}^{\text{sym}} \geq 0, \quad (4.175)$$

where s_{11}, s_{22}, s_{33} are the principal minors of \mathbb{L}^{sym} . For later use, we also define the determinant s_{12} as

$$s_{12} \equiv S_{12}S_{33} - S_{13}S_{23}, \quad (4.176)$$

with which we write the condition Eq. (4.175) as

$$\det \mathbb{L}^{\text{sym}} = \frac{s_{11}s_{12} - s_{12}^2}{S_{33}} \geq 0. \quad (4.177)$$

Let us take f_3 as the probe condition to make $j_3 = 0$, which yields

$$f_3 = -\frac{S_{13} - A_{13}}{S_{33}}f_1 - \frac{S_{23} - A_{23}}{S_{33}}f_2. \quad (4.178)$$

With this f_3 , we obtain the effective 2×2 matrix as

$$\begin{pmatrix} j_1 \\ j_2 \end{pmatrix} = \begin{pmatrix} S_{11} - \frac{S_{13}^2 - A_{13}^2}{S_{33}} & S_{12} + A_{12} - \frac{(S_{13} + A_{13})(S_{23} - A_{23})}{S_{33}} \\ S_{12} - A_{12} - \frac{(S_{23} + A_{23})(S_{13} - A_{13})}{S_{33}} & S_{22} - \frac{S_{23}^2 - A_{23}^2}{S_{33}} \end{pmatrix} \begin{pmatrix} f_1 \\ f_2 \end{pmatrix} \quad (4.179)$$

$$\begin{aligned} &= \left[\frac{1}{S_{33}} \begin{pmatrix} s_{22} + A_{13}^2 & s_{12} + A_{13}A_{23} \\ s_{12} + A_{13}A_{23} & s_{11} + A_{23}^2 \end{pmatrix} \right. \\ &\quad \left. + \frac{1}{S_{33}} \begin{pmatrix} 0 & S_{13}A_{23} - S_{23}A_{13} + S_{33}A_{12} \\ -S_{13}A_{23} + S_{23}A_{13} - S_{33}A_{12} & 0 \end{pmatrix} \right] \begin{pmatrix} f_1 \\ f_2 \end{pmatrix} \end{aligned} \quad (4.180)$$

$$\equiv (\mathbb{L}_{2 \times 2}^{\text{sym}} + \mathbb{L}_{2 \times 2}^{\text{asym}}) \begin{pmatrix} f_1 \\ f_2 \end{pmatrix}. \quad (4.181)$$

Let us investigate whether the entropy production of the effective 2×2 matrix

$$\dot{S}^{2 \times 2} = \begin{pmatrix} f_1 & f_2 \end{pmatrix} \mathbb{L}_{2 \times 2}^{\text{sym}} \begin{pmatrix} f_1 \\ f_2 \end{pmatrix} \quad (4.182)$$

can be zero or not, that is, whether we can achieve the Carnot efficiency or not. Note that we used the fact that

$$\begin{pmatrix} f_1 & f_2 \end{pmatrix} \mathbb{L}_{2 \times 2}^{\text{asym}} \begin{pmatrix} f_1 \\ f_2 \end{pmatrix} = 0. \quad (4.183)$$

Owing to the theorem of quadratic forms, the entropy production $\dot{S}^{2 \times 2}$ is zero if and only if

the determinant $\det \mathbb{L}_{2 \times 2}^{\text{sym}}$ is zero.

We obtain $\det \mathbb{L}_{2 \times 2}^{\text{sym}}$ multiplied by S_{33}^2 in the form

$$S_{33}^2 \det \mathbb{L}_{2 \times 2}^{\text{sym}} = (s_{11} + A_{23}^2)(s_{22} + A_{13}^2) - (s_{12} + A_{13}A_{23})^2 \quad (4.184)$$

$$= s_{11}s_{22} - s_{12}^2 + s_{11}A_{13}^2 + s_{22}A_{23}^2 - 2s_{12}A_{13}A_{23} \quad (4.185)$$

$$= \left(1 + \frac{A_{23}^2}{s_{11}}\right) (s_{11}s_{22} - s_{12}^2) + s_{11} \left(A_{13} - \frac{s_{12}}{s_{11}}A_{23}\right)^2 \quad (4.186)$$

$$= \left(1 + \frac{A_{13}^2}{s_{22}}\right) (s_{11}s_{22} - s_{12}^2) + s_{22} \left(A_{23} - \frac{s_{12}}{s_{22}}A_{13}\right)^2. \quad (4.187)$$

Both of the two terms in Eq. (4.186) and those in Eq. (4.187) are nonnegative because of $s_{11} \geq 0$, $s_{22} \geq 0$ and $s_{11}s_{22} - s_{12}^2 \geq 0$ from the nonnegativity of the original 3×3 entropy production (4.172), (4.173) and (4.177). We thus find that $\det \mathbb{L}_{2 \times 2}^{\text{sym}}$ is zero if and only if the two terms in Eq. (4.186) are zero and the two terms in Eq. (4.187) are zero. From these observations, we know that $s_{11}s_{22} - s_{12}^2 = 0$ is necessary for $\det \mathbb{L}_{2 \times 2}^{\text{sym}} = 0$. Under the condition $s_{11}s_{22} - s_{12}^2 = 0$, the entropy production of the effective 2×2 matrix, Eq. (4.182), is zero if and only if ‘ $s_{11} = 0$ or $s_{11}A_{13} = s_{12}A_{23}$ ’ and ‘ $s_{22} = 0$ or $s_{22}A_{23} = s_{12}A_{13}$ ’, which means that there are four ways to make the entropy production zero. Let us check if we can obtain nonvanishing power in each case.

1. For $s_{11} = 0$ and $s_{22} = 0$, we find $s_{12} = 0$ from $s_{11}s_{22} - s_{12}^2 = 0$, in which there is a possibility to achieve nonvanishing power. The effective 2×2 linear-response matrix becomes

$$\mathbb{L}_{2 \times 2} = \frac{1}{S_{33}} \begin{pmatrix} A_{13}^2 & A_{13}A_{23} + S_{13}A_{23} - S_{23}A_{13} + S_{33}A_{12} \\ A_{13}A_{23} - S_{13}A_{23} + S_{23}A_{13} - S_{33}A_{12} & A_{23}^2 \end{pmatrix}. \quad (4.188)$$

2. For $s_{11} = 0$ and $s_{22}A_{23} = s_{12}A_{13}$, we find $s_{22}A_{23} = 0$ because we find $s_{12} = 0$ from $s_{11}s_{22} - s_{12}^2 = 0$ and $s_{11} = 0$. Since $s_{22} = 0$ gives the same case as the case 1 above, we set $A_{23} = 0$, which makes $\{2, 2\}$ element zero. The effective 2×2 linear-response matrix becomes

$$\mathbb{L}_{2 \times 2} = \frac{1}{S_{33}} \begin{pmatrix} s_{22} + A_{13}^2 & -S_{23}A_{13} + S_{33}A_{12} \\ S_{23}A_{13} - S_{33}A_{12} & 0 \end{pmatrix}. \quad (4.189)$$

This means that the power at the maximum efficiency (2.55) becomes zero. Thus we cannot achieve the Carnot efficiency with nonvanishing power in this case.

3. For $s_{11}A_{13} = s_{12}A_{23}$ and $s_{22} = 0$, we find $s_{12} = 0$ from $s_{11}s_{22} - s_{12}^2 = 0$ and $s_{22} = 0$, which gives $s_{11}A_{13} = 0$. Since $s_{11} = 0$ gives the same case as the case 1 above, we set $A_{13} = 0$. This makes the $\{1, 2\}$ element of the effective 2×2 matrix zero, which makes the ratio of the off-diagonal element $x = -1$: The effective 2×2 linear-response matrix becomes

$$\mathbb{L}_{2 \times 2} = \frac{1}{S_{33}} \begin{pmatrix} 0 & S_{13}A_{23} + S_{33}A_{12} \\ -S_{13}A_{23} - S_{33}A_{12} & s_{11} + A_{23}^2 \end{pmatrix}. \quad (4.190)$$

Thus we cannot achieve the Carnot efficiency with nonvanishing power.

4. For $s_{11}A_{13} = s_{12}A_{23}$ and $s_{22}A_{23} = s_{12}A_{13}$, we do not find any conditions that prevent us from obtaining the Carnot efficiency with nonvanishing power.

We thus clarified from the nonnegativity of the entropy production of the 3×3 matrix the conditions for the Carnot efficiency with nonvanishing power.

We should note here why our specific case prevents the Carnot efficiency with nonvanishing power. Our specific setup in Eq. (4.113) makes the (1,3) and (3,1) elements zero, that is, $S_{13} = A_{13} = 0$, as well as the asymmetric elements of the (1,2) and (2,1) elements zero, that is, $A_{12} = 0$. For the case 1, the effective linear-response matrix (4.191) becomes

$$\mathbb{L}_{2 \times 2} = \frac{1}{S_{33}} \begin{pmatrix} 0 & 0 \\ 0 & A_{23}^2 \end{pmatrix}, \quad (4.191)$$

with which we find that the ratio of the off-diagonal elements $x = 1$. We thus find that we cannot satisfy the condition $|x| > 1$, and thus we cannot attain the Carnot efficiency with nonvanishing power in the case 1. For the case 4, the linear-response matrix (4.181) becomes

$$\mathbb{L}_{2 \times 2} = \frac{1}{S_{33}} \begin{pmatrix} s_{22} & s_{12} \\ s_{12} & s_{11} \end{pmatrix}, \quad (4.192)$$

with which we again find that the ratio of the off-diagonal elements $x = 1$ and thus we cannot attain the Carnot efficiency with nonvanishing power in the case 4. With these observations, we find that we cannot attain the Carnot efficiency with nonvanishing power for our specific setup in Eq. (4.113) owing to $S_{13} = A_{13} = A_{12} = 0$.

4.6 Summary and Conclusion

In the present chapter, we have investigated for quantum thermoelectricity whether there is a possibility to achieve the Carnot efficiency with nonvanishing power, as Benenti *et al.* claimed [90]. In Section 4.1, we have reviewed several attempts and have explained that no one has succeeded in achieving the Carnot efficiency with nonvanishing power. In Section 4.2, we have focused the attempts for mesoscopic thermoelectricity in the framework of the Landauer-Büttiker formula. In this case, Brandner and his colleagues finally proved for any number of (all-electronic) reservoirs [10, 14, 107, 152] that we cannot achieve the Carnot efficiency owing to the strong bound for the linear-response coefficients from the unitarity of the scattering matrix. In Section 4.3, we have included electron-phonon scatterings in the Hamiltonian, to which we cannot apply the Landauer-Büttiker formula, and therefore we cannot apply Brandner *et al.*'s result. We have considered the model with three reservoirs, the Aharonov-Bohm ring, and electron-phonon interactions; see Fig. 4.2. By assuming the symmetric and energy independent resonant widths, neglecting vertex corrections, and taking the electron-phonon coupling into account only up to the second order, we have first proved that we cannot achieve the Carnot efficiency with nonvanishing power because of the nonnegativity of the entropy production of the original three terminals, which means that it is not sufficient to consider only the effective 2×2

linear-response matrix. We have shown that we can achieve a high efficiency at the maximum power and the maximum efficiency with a magnetic field and phonons. Within our framework, the efficiency of our device can exceed that in the three-terminal all-electronic device [10].

We here remark that the calculation in Section 4.3 has been done to the second order of the coupling between electrons and phonons *without* vertex corrections. In general, vertex corrections can affect the result in mesoscopic transport systems [159]. It is an important future work to incorporate the corrections and investigate how it affects our results, particularly the result that the efficiency of our device exceed that in the three-terminal all-electronic device [10] within our framework.

In Section 4.4, we have considered the effect of the asymmetric resonant widths $\Gamma_L \neq \Gamma_R$, which we believe does not affect the result qualitatively. We have also considered the result with the other probe condition $J_Q^P = 0$. In this case, we have found that it is possible to achieve the Carnot efficiency with nonvanishing power if the conditions in Eq. (2.88) are satisfied and that the efficiency at the maximum power can also exceed the CA bound $\eta_c/2$, but not much because the difference of x from unity is small, $\mathcal{O}(\gamma^2)$.

In Section 4.5, we have investigated the restriction for the original 3×3 linear-response matrix in fully general cases. We have found that although there appears a restriction from the original matrix, the Carnot efficiency with nonvanishing power is not prohibited in two cases. Note that the mesoscopic thermoelectric devices using the Landauer-Büttiker formula in Section 4.2 do not satisfy these two cases owing to the strong bound from the unitarity of the scattering matrix.

Quantum thermoelectricity with inelastic scatterings under a magnetic field has not yet been investigated very much. Although our calculation neglected the vertex corrections [159], was done to the second order of the electron-phonon coupling, and assume the symmetric energy-independent couplings, we have demonstrated the possibility to achieve a high maximum efficiency and the efficiency at the maximum power within the framework of our setup above. The possibility of a high efficiency should attract much interest and be actively researched in the future. We believe that our result is a starting point to investigate how inelastic scattering and a magnetic field affect the efficiency.

One possible future work is to find the restriction that prohibits the Carnot efficiency with nonvanishing power with the properties of phonons or the Keldysh Green's functions. An experimental realization of our model may test the predictions concerning the advantages of phonon heat source over an electronic one for producing electricity, in particular under the effect of a magnetic field. Another possible case including inelastic scattering is a model with electron-electron interactions, which is another interesting future work.

Chapter 5

Summary and future work

5.1 Summary

In the present thesis, we have investigated thermoelectricity with high efficiency and power.

In Chapter 1, we have explained the relation among quantum thermoelectricity and other fields: stochastic thermodynamics, quantum thermodynamics, and nonequilibrium physics. We have also explained how thermoelectricity can be seen as a steady-state heat engine, whose high efficiency and high power we have considered in the present thesis. We will give related future works in the next section.

In Chapter 2, we have constructed the linear irreversible thermodynamics, which describes thermoelectricity in the linear-response regime. The important restrictions in the linear irreversible thermodynamics are Onsager’s reciprocal relation [91] (or the Onsager-Casimir relations [92] under a magnetic field) and the second law of thermodynamics, that is, the nonnegativity of the entropy production. We have first shown that we can achieve the Carnot efficiency with zero power for a symmetric linear-response matrix. We have next shown that there is a possibility to achieve the Carnot efficiency with nonvanishing power for an asymmetric linear-response matrix if and only if the linear-response coefficients satisfy the specific conditions, which we have shown in Chapter 4 that several specific models cannot satisfy these conditions. We have also given the example in the framework of the Landauer-Büttiker formula with two reservoirs. We have found that the linear-response matrix is symmetric even though there is a magnetic field in this case.

In Chapter 3, we have investigated efficient thermoelectricity for a symmetric linear-response matrix. We have represented the conventional thermoelectric coefficients, such as the electric conductivity, the Seebeck coefficient, and the thermal conductivity, in terms of the linear-response coefficient. Since the Seebeck coefficient is one of the main parameters to describe the thermoelectric efficiency, we have considered thermoelectricity near Anderson localization transitions [160], which is expected to give a high Seebeck coefficient. For a single mobility edge, we have corrected and extended previous studies and found universal approximations that allow us to deduce the critical exponent for the zero-temperature conductivity from thermoelectric measurements. In particular, we have found that at nonzero low temperatures the Seebeck coefficient and the thermoelectric efficiency can be very large on the “insulating” side, that is, for chemical potentials below the (zero-temperature) localization threshold. Corrections to

the leading power-law singularity in the zero-temperature conductivity have been shown to introduce nonuniversal temperature-dependent corrections to the otherwise universal functions which describe the Seebeck coefficient, the figure of merit and the Wiedemann-Franz ratio. Next, we have shown that the thermoelectric coefficients to have interesting dependences on the system size. While the Seebeck coefficient decreases with decreasing size, the figure of merit, first decreases but then increases, while the Wiedemann-Franz ratio first increases but then decreases as the size decreases. Small (but finite) samples may thus have larger thermoelectric efficiencies. In the last part we have studied thermoelectricity in systems with a pair of localization edges, the ubiquitous situation in random systems near the centers of electronic energy bands. As the disorder increases, the two thresholds approach each other, and then the Seebeck coefficient and the figure of merit increase significantly, as expected from the general arguments of Mahan and Sofo for a narrow energy range of the zero-temperature metallic behavior.

We have next investigated the possibility to achieve the Carnot efficiency with nonvanishing power for an asymmetric linear-response matrix in Chapter 4. We have mainly focused the attempts with thermoelectricity in mesoscopic transport systems. Brandner *et al.* have proved [10, 14, 107, 152] that we cannot achieve the Carnot efficiency with nonvanishing power in the framework of the Landauer-Büttiker formula using the unitarity of the scattering matrix. However, little is known for the case to which we cannot apply the Landauer-Büttiker formula, which we have investigated with a mesoscopic thermoelectric device made of an Aharonov-Bohm ring threaded by a magnetic flux, incorporating an electron-phonon scattering. We have found the following two results [36]: First, we have found for a specific setup of energy-independent and symmetric resonant widths and without vertex corrections that, contrary to Benenti *et al.*'s claim [90], our model cannot reach the Carnot efficiency under a magnetic field because of the nonnegativity condition on the entropy production of the original model with three reservoirs. Second, within the approximations that the vertex corrections are neglected and the electron-phonon coupling is taken into account only up to the second order, we have demonstrated that including the electron-phonon interaction under a magnetic field can enhance the thermoelectric efficiency significantly. We have finally considered the case with a general 3×3 asymmetric matrix, in which we have found the condition for the Carnot efficiency with nonvanishing power. We have shown that this condition is not satisfied in our specific setup of energy-independent and symmetric resonant widths.

5.2 Future work

Quantum thermoelectricity, particularly thermoelectricity in mesoscopic systems, has a lot of future prospects of research work. We list them below from the viewpoints that we introduced in Chapter 1.

From the viewpoint of stochastic thermodynamics given in Subsection 1.1.2, fluctuation is crucial in small systems. It may be interesting to verify the fluctuation theorem for our device used in Chapter 4. For an application, it is also interesting to investigate a magnetic-field dependence of the fluctuation of the currents. We might be able to control the fluctuations with a magnetic field. Recently, the inequality between the entropy production and the fluctuation of currents called the thermodynamic uncertainty relation has attracted much interest [161–168].

The uncertainty relation can be investigated with our model.

From the viewpoint of information thermodynamics given in Subsection 1.1.3, a possible future work is to incorporate a magnetic field into the autonomous Maxwell demon [48, 49, 73], which includes an electron-electron scattering with three reservoirs. The restriction from the nonnegativity of the 3×3 matrix works in the setup. It is interesting to check whether or not we have an asymmetric linear-response matrix and obtain the Carnot efficiency with nonvanishing power.

In Subsection 1.1.4 from the viewpoint of quantum thermodynamics, we explained that we can define work and heat even in the case of strong coupling for quantum thermoelectricity [15, 78]. However, it is not obvious how to define them for quantum thermoelectricity under periodic driving [169, 170]. For weak coupling between the reservoir and the system under adiabatic driving, we can construct thermodynamics [169–171]; we can derive the heat current and prove the laws of thermodynamics. In this case, an asymmetric 3×3 linear-response matrix was obtained [169, 170, 172]. Therefore, we may be able to use our bound from the nonnegativity of the 3×3 matrix discussed in Chapter 4. For strong coupling on the other hand, however, we do not even know the expression of the heat current. Esposito *et al.* [171] have tried to define the heat current, which satisfied the laws of thermodynamics. A possible future work is to investigate its validity and calculate the efficiency, with which we may find an efficient thermoelectricity.

From the viewpoint of nonequilibrium thermodynamics and statistical physics explained in Subsection 1.1.5, it is interesting to investigate nonlinear effects of our device in Chapter 4. In particular, one of the recent interests is a heat diode that utilizes phonons [82, 87]. Since it is not known how a magnetic field affects a heat rectification, our device, which includes a magnetic field, may be a good candidate to investigate.

We believe that a breakthrough of thermoelectricity will come from the quantum world. The idea from fundamental physics may produce a good and an interesting thermoelectricity, which may attract many attentions. Seeking quantum thermoelectricity may contribute not only to the applied physics, but also to our interest of what quantum is and how it affects the real world.

Appendix A

Approximations in Chapter 3

In this Appendix we derive approximate analytic expressions for the integrals $K_n(x, z)$ defined in Eq. (3.24) and for the Onsager coefficients. The results are used in Sec. 3.2 to obtain analytic approximations for the Seebeck coefficient, the figure of merit, and the Wiedemann-Franz ratio.

A.1 Low temperatures and $\mu - E_c \gg k_B T$

When $k_B T \ll E - \mu$, *i.e.*, $\epsilon \gg 1$, the symmetric function $1/\cosh^2(\epsilon)$ decays exponentially for $|\epsilon| > 3$, and the main contributions to integrals of the form $\int_{-z}^{\infty} d\epsilon G(\epsilon)/[4\cosh^2(\epsilon)]$, for an arbitrary function $G(\epsilon)$ which does not change rapidly around $\epsilon = 0$, come from small ϵ . On the other hand, the lower limit of the integral is large and negative, because $z = (\mu - E_c)/(k_B T) \gg 1$. Therefore we can replace the lower limit of the integrals by $-\infty$ and expand $G(\epsilon)$ in powers of ϵ . This procedure is equivalent to the Sommerfeld expansion [110]. The result is

$$\int_{-z}^{\infty} d\epsilon \frac{G(\epsilon)}{4\cosh^2(\epsilon/2)} = G(0) + \frac{\pi^2}{6} G''(0) + \frac{7\pi^4}{360} G''''(0) + \dots \quad (\text{A.1})$$

For $G(\epsilon) = \epsilon^n(\epsilon + z)^n$ one finds

$$\begin{aligned} K_n(x, z) = & z^x \left(\delta_{n,0} + \frac{\pi^2}{6} [2\delta_{n,2} + 2\delta_{n,1}xz^{-1} + x(x-1)\delta_{n,0}z^{-2}] \right. \\ & + \frac{7\pi^4}{360} [24\delta_{n,4} + 24\delta_{n,3}xz^{-1} + 12\delta_{n,2}x(x-1)z^{-2} \\ & \left. + 4\delta_{n,1}x(x-1)(x-2)z^{-3} + \delta_{n,0}x(x-1)(x-2)(x-3)z^{-4}] \right) + \dots \quad (\text{A.2}) \end{aligned}$$

The linear-response coefficients introduced in Eqs. (3.1), (3.2), and (3.8) become series in $1/z^2$ as in

$$\begin{aligned} L_{11} = & A(tz)^x \left[1 + at^y + \frac{\pi^2}{6} x(x-1) \frac{1}{z^2} + \mathcal{O}[z^{-4}, (at^y)^2] \right], \\ L_{12} = & A \frac{k_B T}{|e|} \frac{\pi^2}{3} t^x z^{x-1} \left[x + a(x+y)t^y + \frac{7\pi^2}{30} x(x-1)(x-2) \frac{1}{z^2} + \mathcal{O}[z^{-4}, (at^y)^2] \right], \end{aligned}$$

$$L_{22} = A \left(\frac{k_B T}{e} \right)^2 \frac{\pi^2}{3} (tz)^x \left[1 + at^y + \frac{7\pi^2}{10} x(x-1) \frac{1}{z^2} + \mathcal{O}[z^{-4}, (at^y)^2] \right], \quad (\text{A.3})$$

where $t = k_B T / |E_c|$, A is the coefficient of the leading term, and a is the coefficient of the next term in the zero-temperature conductivity, Eq. (3.17). The Seebeck coefficient, the figure of merit, and the Wiedemann-Franz ratio are then given by

$$S = \frac{L_{12}}{T L_{11}} = \frac{k_B}{|e|} \frac{\pi^2}{3} \frac{1}{z} \left[x + \frac{\pi^2}{15} x(x-1)(x-7) \frac{1}{z^2} + ayt^y + \mathcal{O}[z^{-4}, (at^y)^2] \right], \quad (\text{A.4})$$

$$ZT = \frac{L_{12}^2}{L_{11} L_{22} - L_{12}^2} = \frac{\pi^2 x^2}{3z^2} \left[1 - \frac{\pi^2}{15} (x^2 + 8x - 14) \frac{1}{z^2} + 2 \frac{y}{x} at^y + \mathcal{O}[z^{-4}, (at^y)^2] \right], \quad (\text{A.5})$$

and

$$\mathcal{L} = \frac{k_B^2}{e^2} \frac{\pi^2}{3} \left[1 + \frac{\pi^2}{15} x(3x-8) \frac{1}{z^2} + \mathcal{O}[z^{-4}, (at^y)^2] \right]. \quad (\text{A.6})$$

A.2 At the mobility edge: $|z| = 0$

At $\mu = E_c$, *i.e.*, $z = 0$, the integrals in Eqs. (3.24) can be calculated analytically. Expanding the integrand, we find

$$\begin{aligned} K_n(x, 0) &= \int_0^\infty d\epsilon \epsilon^{x+n} \sum_{m=1}^\infty (-1)^m m e^{-m\epsilon} = \sum_{m=1}^\infty (-1)^m m^{-(x+n)} \Gamma(x+n+1) \\ &= \eta(x+n)(x+n) \Gamma(x+n) = (x+n) I_{x+n} \end{aligned} \quad (\text{A.7})$$

for all $n+x > -1$, where $\Gamma(u)$ is the Gamma function, $\eta(u) = (1 - 2^{1-u})\zeta(u)$ is the Dirichlet eta function,

$$I_u \equiv (1 - 2^{1-u})\zeta(u)\Gamma(u), \quad (\text{A.8})$$

and $\zeta(u)$ is the Riemann zeta function. At $u = 1$ the zeta function diverges, but the expression for I_u is continuous, with $I_1 = \ln 2$. At times (*e.g.*, Ref. [126]), the form $I_u = \int_0^\infty dx x^{u-1} / (1+e^x)$ is used; however, this equality is valid only for $u > 0$, while Eq. (A.8) is valid for all $u > -1$.

A.3 High temperatures: $|z| \ll 1$

For $|z| \ll 1$ we expand $K_n(x, z)$ in powers of z . The leading-order term comes from

$$\left. \frac{\partial K_n(x, z)}{\partial z} \right|_{z=0} = x K_{n-1}(x, 0) = x(n+x-1) I_{n+x-1}. \quad (\text{A.9})$$

Thus,

$$K_n(x, z) = K_n(x, 0) + xK_{n-1}(x, 0)z + \mathcal{O}(z^2) = (n+x)I_{n+x} + x(n+x-1)I_{n+x-1}z + \mathcal{O}(z^2), \quad (\text{A.10})$$

and the Onsager coefficients [see Eqs. (3.1) and (3.8)] become

$$\begin{aligned} L_{11} &= At^x \left\{ xI_x + x(x-1)I_{x-1}z + at^y [(x+y)I_{x+y} + (x+y)(x+y-1)I_{x+y-1}z] + \mathcal{O}[z^2, (at^y)^2] \right\}, \\ L_{12} &= A \frac{k_B T}{|e|} t^x \left\{ (x+1)I_{x+1} + x^2 I_x z + at^y [(x+y+1)I_{x+y+1} + (x+y)^2 I_{x+y}z] + \mathcal{O}[z^2, (at^y)^2] \right\}, \\ L_{22} &= A \left(\frac{k_B T}{e} \right)^2 t^x \left\{ (x+2)I_{x+2} + x(x+1)I_{x+1}z \right. \\ &\quad \left. + at^y [(x+y+2)I_{x+y+2} + (x+y)(x+y+1)I_{x+y+1}z] \right. \\ &\quad \left. + \mathcal{O}[z^2, (at^y)^2] \right\}. \end{aligned} \quad (\text{A.11})$$

In this regime, the leading corrections to the Seebeck coefficient S are

$$S \approx \frac{k_B}{|e|} \frac{(x+1)I_{x+1} + x^2 I_x z + at^y (x+y+1)I_{x+y+1}}{xI_x + x(x-1)I_{x-1}z + at^y (x+y)I_{x+y}} = S_0 - S_1 z + S_2 at^y, \quad (\text{A.12})$$

where

$$\begin{aligned} S_0 &= \frac{k_B}{|e|} \frac{(x+1)I_{x+1}}{xI_x}, \quad S_1 = -\frac{k_B}{|e|} \left[x - \frac{(x^2-1)I_{x-1}I_{x+1}}{xI_x^2} \right], \\ S_2 &= \frac{k_B}{|e|} \left[\frac{(x+y+1)I_{x+y+1}}{xI_x} - \frac{(x+y)(x+1)I_{x+y}I_{x+1}}{x^2 I_x^2} \right], \end{aligned} \quad (\text{A.13})$$

with further corrections of order z^2 , zat^y , and $(at^y)^2$, and those to the figure of merit ZT are

$$ZT \approx Z_0 + Z_1 z + Z_2 at^y, \quad (\text{A.14})$$

where

$$\begin{aligned} Z_1 &= Z_0 \left[\frac{2x^2 I_x}{(x+1)I_{x+1}} - \frac{x(x-1)(x+2)I_{x-1}I_{x+2} - x^2(x+1)I_x I_{x+1}}{x(x+2)I_x I_{x+2} - (x+1)^2 I_{x+1}^2} \right], \\ Z_2 &= Z_0 \left\{ \frac{[(x+2)xI_{x+2}I_x - (x+1)^2 I_{x+1}^2][2(x+y+1)(x+1)I_{x+y+1}I_{x+1}]}{[(x+2)xI_{x+2}I_x - (x+1)^2 I_{x+1}^2](x+1)^2 I_{x+1}^2} \right. \\ &\quad \left. - \frac{[(x+y)(x+2)I_{x+y}I_{x+2} + (x+y+2)xI_{x+y+2}I_x - 2(x+y+1)(x+1)I_{x+y+1}I_{x+1}]}{[(x+2)xI_{x+2}I_x - (x+1)^2 I_{x+1}^2]} \right\}, \end{aligned} \quad (\text{A.15})$$

with Z_0 given in Eq. (3.38). The Wiedemann-franz ratio is expanded as

$$\mathcal{L} \approx \mathcal{L}_{00}(x) - \mathcal{L}_1(x)z + \mathcal{L}_2 at^y, \quad (\text{A.16})$$

where [114]

$$\mathcal{L}_{00}(x) = \left(\frac{k_B}{e}\right)^2 \left[\frac{(x+2)I_{x+2}}{xI_x} - \frac{(x+1)^2 I_{x+1}^2}{(xI_x)^2} \right], \quad (\text{A.17})$$

while

$$\mathcal{L}_1(x) = 2\frac{S_0 S_1}{Z_0} + (S_0/Z_0)^2 Z_1, \quad \mathcal{L}_2(x) = 2\frac{S_0 S_2}{Z_0} - (S_0/Z_0)^2 Z_2. \quad (\text{A.18})$$

Surprisingly, in the range $0 < x < 2$, $\mathcal{L}_{00}(x)$ is very close to the linear approximant $(k_B/e)^2(1.38 + 0.81x)$.

A.4 Low temperatures and $\mu - E_c \ll -k_B T$

When $z = (\mu - E_c)/(k_B T)$ is large and negative, the lower bound of K_n in Eq. (3.24) is large and positive, and therefore the integration variable ϵ is always very large, $\epsilon \gg 1$. We can then use the expansion

$$\frac{1}{4 \cosh(\epsilon/2)} = e^{-\epsilon} - 2e^{-2\epsilon} + \mathcal{O}(e^{-3\epsilon}). \quad (\text{A.19})$$

Writing

$$K_n(x, z) = \int_0^\infty du (u - z)^n u^x (e^{z-u} - 2e^{2z-2u} + \dots), \quad (\text{A.20})$$

and using $\int_0^\infty du u^x e^{-mu} = \Gamma(1+x)/m^{1+x}$, we find

$$\begin{aligned} K_0(x, z) &= e^z \Gamma(1+x) \left[1 - \frac{e^z}{2^x} + \mathcal{O}(e^{2z}) \right], \\ K_1(x, z) &= e^z \Gamma(1+x) \left[1 + x - z - e^z \frac{1+x-2z}{2^{1+x}} + \mathcal{O}(e^{2z}) \right], \\ K_2(x, z) &= e^z \Gamma(1+x) \left\{ (x+1)(x+2) - 2(x+1)z + z^2 \right. \\ &\quad \left. - e^z \frac{(x+1)(x+2) - 4(x+1)z + 4z^2}{2^{x+2}} + \mathcal{O}(e^{2z}) \right\}. \end{aligned} \quad (\text{A.21})$$

With these approximations, we arrive at

$$\begin{aligned} L_{11} &= A t^x e^z \left[\Gamma(1+x) \left(1 - \frac{e^z}{2^x} \right) + a t^y \Gamma(1+x+y) \left(1 - \frac{e^z}{2^{x+y}} \right) + \mathcal{O}(e^{2z}, a^2 t^{2y}) \right], \\ L_{12} &= A \frac{k_B T}{|e|} t^x e^z \left[\Gamma(1+x) \left(1 + x - z - e^z \frac{1+x-2z}{2^{1+x}} \right) \right. \\ &\quad \left. + a t^y \Gamma(1+x+y) \left(1 + x + y - z - e^z \frac{1+x+y-2z}{2^{1+x+y}} + \mathcal{O}(e^{2z}, a^2 t^{2y}) \right) \right], \\ L_{22} &= A \left(\frac{k_B T}{e} \right)^2 t^x e^z \left\{ \Gamma(1+x) [(1+x)(2+x) - 2(x+1)z + z^2] \right. \end{aligned}$$

$$\begin{aligned}
& -e^z \frac{(x+1)(x+2) - 4(x+1)z + 4z^2}{2^{x+2}} + at^y \Gamma(1+x+y) [(1+x+y)(2+x+y) \\
& - 2(1+x+y)z + z^2 - e^z \frac{(1+x+y)(2+x+y) - 4(1+x+y)z + 4z^2}{2^{x+y+2}} + \mathcal{O}(e^{2z}, a^2 t^{2y}) \Big\}, \\
& \tag{A.22}
\end{aligned}$$

and thus

$$S = \frac{k_B}{|e|} \left[(1+x-z) + \frac{1+x}{2^{x+1}} e^z + ayt^y \frac{\Gamma(1+x+y)}{\Gamma(1+x)} + \mathcal{O}(e^{2z}, a^2 t^{2y}) \right] \tag{A.23}$$

and

$$\begin{aligned}
ZT &= \frac{(1+x-z)^2}{1+x} + \frac{(1+x-z)[x(3+x-z) + 2(1+z)]}{2^{2+x}(1+x)} e^z \\
&+ at^y \frac{(1+x-z)\Gamma(1+x+y)}{(1+x)^2\Gamma(1+x)} \left[4 + 4x^2 + x(8+3y+y^2-4z) - y(-3+z) - y^2(-1+z) - 4z \right] \\
&+ \mathcal{O}(e^{2z}, a^2 t^{2y}). \\
& \tag{A.24}
\end{aligned}$$

The expression for \mathcal{L} is given in Eq. (3.39).

Appendix B

Calculation of the currents with phonon with the Keldysh Green's function

In this Appendix, we explain the derivation of the expressions of the currents (4.81) (4.82) and (4.85) in details, which are used in Section 4.3. The calculation is the review of Ref. [155]. Throughout the Appendix, we set $\hbar = 1$.

B.1 The expression of the current with Green's functions

We first repeat the Hamiltonian in Eq. (B.1),

$$\begin{aligned} \mathcal{H} = & [\epsilon_d + \gamma(b^\dagger + b)]c_d^\dagger c_d + \omega_0 \left(b^\dagger b + \frac{1}{2}\right) + \sum_{k_L} \epsilon_{k_L} c_{k_L}^\dagger c_{k_L} + \sum_{k_R} \epsilon_{k_R} c_{k_R}^\dagger c_{k_R} \\ & + \sum_{k_L} (V_{k_L} c_{k_L}^\dagger c_d + \text{H.c.}) + \sum_{k_R} (V_{k_R} c_{k_R}^\dagger c_d + \text{H.c.}) + \sum_{k_L, k_R} (V_{k_L k_R} e^{i\Phi} c_{k_L}^\dagger c_{k_R} + \text{H.c.}). \end{aligned} \quad (\text{B.1})$$

The electric current from the left reservoir is given by

$$J_e(t) \equiv -e \langle \dot{N}_L \rangle = -ie \langle [H, N_L] \rangle \quad (\text{B.2})$$

$$= -e \left[\sum_{k_L} (G_{k_L d}^<(t, t) - G_{d k_L}^<(t, t)) + \sum_{k_L k_R} V_{k_L k_R} (e^{-i\Phi} G_{k_L k_R}^<(t, t) - e^{i\Phi} G_{k_R k_L}^<(t, t)) \right], \quad (\text{B.3})$$

where $N_L = \sum_{k_L} c_{k_L}^\dagger c_{k_L}$ and we define the following (lesser) Green's function:

$$G_{ab}^<(t, t') = i \langle c_{k_L}^\dagger(t') c_d(t) \rangle, \quad (a, b = d, k_L, k_R) \quad (\text{B.4})$$

The Fourier transformation of $J_e(t)$ gives

$$J_e(t) = -e \int \frac{d\omega}{2\pi} J_L(\omega, \Phi), \quad (\text{B.5})$$

where

$$J_L(\omega, \Phi) = \sum_{k_L} V_{k_L} [G_{k_L d}^<(\omega) - G_{d k_L}^<(\omega)] + \sum_{k_L k_R} V_{k_L k_R} [e^{-i\Phi} G_{k_L k_R}^<(\omega) - e^{i\Phi} G_{k_R k_L}^<(\omega)]. \quad (\text{B.6})$$

This expression tells us that we need to calculate the lesser components of the (contour-ordered) Green's functions appearing in Eq. (B.6) in order to calculate the current.

B.2 The Dyson equations of various (contour-ordered) Green's functions

In order to calculate the lesser components of the (contour-ordered) Green's functions appearing in Eq. (B.6), it is convenient to obtain the contour-ordered Green's function and then calculate its lesser component with the Langreth theorem, which we will introduce in Section B.3. The contour-ordered Green's function is obtained by solving its Dyson equation, which is the main purpose of the present section. We use the method of the equation of motion [79] to obtain the Dyson equation.

B.2.1 The Dyson equations of $G_{k_L d}$, $G_{k_R k_L}$, $G_{k_R d}$, and so on

Let us first consider the equation of motion of the following contour-ordered Green's function:

$$G_{k_L d}(\tau, \tau') \equiv -i \langle T_C c_{k_L}(\tau) c_d^\dagger(\tau') \rangle, \quad (\text{B.7})$$

where τ, τ' are the times on the Keldysh contour. With differentiating $G_{k_L d}(\tau, \tau')$ with respect to τ , we obtain the following equation of motion as

$$i \frac{dG_{k_L d}(\tau, \tau')}{d\tau} = \left\langle T_C \frac{dc_{k_L}(\tau)}{d\tau} c_d^\dagger(\tau') \right\rangle \quad (\text{B.8})$$

$$= \epsilon_{k_L} G_{k_L d}(\tau, \tau') + V_{k_L} G_{dd}(\tau, \tau') + \sum_{k_R} V_{k_L k_R} e^{i\Phi} G_{k_R d}(\tau, \tau'). \quad (\text{B.9})$$

Let us here introduce the free Green's function $g_{k_L}(\tau, \tau')$ defined as

$$g_{k_L}(\tau, \tau') = -i \left\langle T_C c_{k_L}(\tau) c_{k_L}^\dagger(\tau') \right\rangle_{\text{free}}, \quad (\text{B.10})$$

where $\langle \cdot \rangle_{\text{free}}$ means that the expectation value is taken with respect to the decoupling Hamiltonian with $V_{k_L d} = V_{k_R d} = V_{k_L k_L} = \gamma = 0$. We will use it hereafter. We find that this free Green's

function obeys the following equation:

$$\left(i \frac{d}{d\tau} - \epsilon_{k_L}\right) g_{k_L}(\tau, \tau') = \delta(\tau - \tau'). \quad (\text{B.11})$$

Using the free Green's function (B.38), we solve the equation of motion (B.9) as

$$G_{k_L d}(\tau, \tau') = \int d\tau_1 g_{k_L}(\tau, \tau_1) \left[V_{k_L} G_{dd}(\tau_1, \tau') + \sum_{k_R} V_{k_L k_R} e^{i\Phi} G_{k_R d}(\tau_1, \tau') \right]. \quad (\text{B.12})$$

Since we treat the steady-state, we assume that a function of τ, τ' has a time-translational invariant, $f(\tau, \tau') = f(\tau - \tau')$. We assume this fact throughout the present Appendix. With this assumption, Eq. (B.12) becomes

$$G_{k_L d}(\tau - \tau') = \int d\tau_1 g_{k_L}(\tau - \tau_1) \left[V_{k_L} G_{dd}(\tau_1 - \tau') + \sum_{k_R} V_{k_L k_R} e^{i\Phi} G_{k_R d}(\tau_1 - \tau') \right], \quad (\text{B.13})$$

whose Fourier transformation is

$$G_{k_L d}(\omega) = g_{k_L}(\omega) [V_{k_L} G_{dd}(\omega) + \sum_{k_R} V_{k_L k_R} e^{i\Phi} G_{k_R d}(\omega)]. \quad (\text{B.14})$$

This is the Dyson equation of $G_{k_L d}(\omega)$. In the same way, we obtain the following Dyson equations:

$$G_{dk_L} = \left[V_{k_L} G_{dd} + \sum_{k_R} V_{k_R k_L} e^{-i\Phi} G_{dk_R} \right] g_{k_L}, \quad (\text{B.15})$$

$$G_{k_R d} = g_{k_R} \left[V_{k_R} G_{dd} + \sum_{k_L'} V_{k_R k_L'} e^{-i\Phi} G_{k_L' d} \right], \quad (\text{B.16})$$

$$G_{dk_R} = \left[V_{k_R} G_{dd} + \sum_{k_L'} V_{k_L' k_R} e^{i\Phi} G_{dk_L'} \right] g_{k_R}, \quad (\text{B.17})$$

where we omit the ω dependence for brevity. Note that we differentiated with respect to not τ but τ' when we obtained the equation of motion of G_{dk_L} and G_{dk_R} . With assuming $V_{k_L k_R} = \Lambda V_{k_L} V_{k_R}$, we obtain the following equations from these Dyson equations:

$$\sum_{k_L} V_{k_L} G_{k_L d} = (1 - \Lambda^2 \hat{\Gamma}_L \hat{\Gamma}_R)^{-1} (\hat{\Gamma}_L + \Lambda e^{i\Phi} \hat{\Gamma}_L \hat{\Gamma}_R) G_{dd} \equiv \Sigma_L G_{dd}, \quad (\text{B.18})$$

$$\sum_{k_L} V_{k_L} G_{dk_L} = G_{dd} (\hat{\Gamma}_L + \Lambda e^{-i\Phi} \hat{\Gamma}_R \hat{\Gamma}_L) (1 - \Lambda^2 \hat{\Gamma}_R \hat{\Gamma}_L)^{-1} \equiv G_{dd} \tilde{\Sigma}_L, \quad (\text{B.19})$$

$$\sum_{k_R} V_{k_R} G_{k_R d} = (1 - \Lambda^2 \hat{\Gamma}_R \hat{\Gamma}_L)^{-1} (\hat{\Gamma}_R + \Lambda e^{-i\Phi} \hat{\Gamma}_R \hat{\Gamma}_L) G_{dd} \equiv \Sigma_R G_{dd}, \quad (\text{B.20})$$

$$\sum_{k_R} V_{k_R} G_{dk_R} = G_{dd} (\hat{\Gamma}_R + \Lambda e^{i\Phi} \hat{\Gamma}_L \hat{\Gamma}_R) (1 - \Lambda^2 \hat{\Gamma}_L \hat{\Gamma}_R)^{-1} \equiv G_{dd} \tilde{\Sigma}_R, \quad (\text{B.21})$$

where we introduced the new (contour-ordered) Green's function as

$$\hat{\Gamma}_{L(R)}(\omega) \equiv \sum_{k_L(k_R)} V_{k_L(k_R)} g_{k_L(k_R)}(\omega) V_{k_L(k_R)}, \quad (\text{B.22})$$

and defined the self-energies as follows:

$$\Sigma_L \equiv (1 - \Lambda^2 \hat{\Gamma}_L \hat{\Gamma}_R)^{-1} (\hat{\Gamma}_L + \Lambda e^{i\Phi} \hat{\Gamma}_L \hat{\Gamma}_R), \quad (\text{B.23})$$

$$\tilde{\Sigma}_L \equiv (\hat{\Gamma}_L + \Lambda e^{-i\Phi} \hat{\Gamma}_R \hat{\Gamma}_L) (1 - \Lambda^2 \hat{\Gamma}_R \hat{\Gamma}_L)^{-1}, \quad (\text{B.24})$$

$$\Sigma_R \equiv (1 - \Lambda^2 \hat{\Gamma}_R \hat{\Gamma}_L)^{-1} (\hat{\Gamma}_R + \Lambda e^{-i\Phi} \hat{\Gamma}_R \hat{\Gamma}_L), \quad (\text{B.25})$$

$$\tilde{\Sigma}_R \equiv (\hat{\Gamma}_R + \Lambda e^{i\Phi} \hat{\Gamma}_L \hat{\Gamma}_R) (1 - \Lambda^2 \hat{\Gamma}_L \hat{\Gamma}_R)^{-1}. \quad (\text{B.26})$$

Let us note the Dyson equations of other (contour-ordered) Green's functions in the forms

$$G_{k_L k_R} = g_{k_L} \left(V_{k_L} G_{dk_R} + e^{i\Phi} \sum_{k_R'} V_{k_L k_R'} G_{k_R' k_R} \right), \quad (\text{B.27})$$

$$G_{k_R' k_R} = g_{k_R'} \left(\delta_{k_R k_R'} + V_{k_R'} G_{dk_R} + \sum_{k_L'} V_{k_R' k_L'} e^{-i\Phi} G_{k_L' k_R} \right), \quad (\text{B.28})$$

which leads to

$$e^{-i\Phi} \sum_{k_L, k_R} V_{k_L k_R} G_{k_L k_R} = -1 + (1 - \Lambda^2 \hat{\Gamma}_L \hat{\Gamma}_R)^{-1} + \Lambda e^{-i\Phi} \Sigma_L G_{dd} \tilde{\Sigma}_R. \quad (\text{B.29})$$

In the same way, starting from the Dyson equations

$$G_{k_R k_L} = g_{k_R} \left(V_{k_R} G_{dk_L} + e^{-i\Phi} \sum_{k_L'} V_{k_R k_L'} G_{k_L' k_L} \right), \quad (\text{B.30})$$

$$G_{k_L' k_L} = g_{k_L'} \left(\delta_{k_L k_L'} + V_{k_L'} G_{dk_L} + \sum_{k_R'} V_{k_L' k_R'} e^{i\Phi} G_{k_R' k_L} \right), \quad (\text{B.31})$$

we obtain the following equation:

$$e^{i\Phi} \sum_{k_L, k_R} V_{k_L k_R} G_{k_R k_L} = -1 + (1 - \Lambda^2 \hat{\Gamma}_R \hat{\Gamma}_L)^{-1} + \Lambda e^{i\Phi} \Sigma_R G_{dd} \tilde{\Sigma}_L. \quad (\text{B.32})$$

Inserting Eqs. (B.18), (B.19), (B.29) and (B.32) into (B.6), we obtain the integrand of the current as

$$J_L = \left[\Sigma_L G_{dd} - G_{dd} \tilde{\Sigma}_L + (1 - \Lambda^2 \hat{\Gamma}_L \hat{\Gamma}_R)^{-1} - (1 - \Lambda^2 \hat{\Gamma}_R \hat{\Gamma}_L)^{-1} \right. \\ \left. + \Lambda e^{-i\Phi} \Sigma_L G_{dd} \tilde{\Sigma}_R - \Lambda e^{i\Phi} \Sigma_R G_{dd} \tilde{\Sigma}_L \right]^<, \quad (\text{B.33})$$

which is expressed by the Green's function of the dot G_{dd} . Note that we omit the dependence on ω and Φ in the last expression for brevity. From the expression (B.33), we first find that we need G_{dd} to obtain the expression of the current, whose Dyson equation we obtain in the next section. We next find that we need the way to calculate the lesser component of the product of the contour-ordered Green's function. Such a lesser component is calculated by the Langreth theorem [79], which we will show in Section B.3.

B.2.2 The Dyson equation of the Green's function of the dot G_{dd}

Let us obtain the Dyson equation of the contour-ordered Green's function of the dot $G_{dd}(\tau, \tau') = -i \langle T_C c_d(\tau) c_d^\dagger(\tau') \rangle$. As in the same way to obtain the Dyson equation (B.14) with the method of the equation of motion [79], we obtain the following Dyson equation:

$$G_{dd}(\omega) = g_d(\omega) \left(1 + \sum_{k, \alpha \in L, R} V_{k\alpha} G_{k\alpha d}(\omega) + \gamma G_{dQd}(\omega) \right) \quad (\text{B.34})$$

$$= g_d(\omega) [1 + \Sigma_l G_{dd}(\omega) + \gamma G_{dQd}(\omega)], \quad (\text{B.35})$$

where $g_d(\omega)$ is the Fourier transformation of

$$g_d(\tau - \tau') = -i \left\langle T_C c_d(\tau) c_d^\dagger(\tau') \right\rangle_{\text{free}}, \quad (\text{B.36})$$

$G_{dQd}(\omega)$ is the Fourier transformation of

$$G_{dQd}(\tau - \tau') \equiv -i \left\langle T_C c_d(\tau) [b(\tau) + b^\dagger(\tau)] c_d^\dagger(\tau') \right\rangle, \quad (\text{B.37})$$

Let us here consider the free Green's function $g_d(\tau, \tau')$ defined as

$$g_d(\tau, \tau') = -i \left\langle T_C c_d(\tau) c_d^\dagger(\tau') \right\rangle_{\text{free}}, \quad (\text{B.38})$$

Here we used Eqs. (B.18) and (B.20) in the second equality and we defined $\Sigma_l \equiv \Sigma_L + \Sigma_R$ in the last equality. The equation (B.35) is the Dyson equation of the contour-ordered Green's function of the dot, from which we find that we need the Dyson equation of $G_{dQd}(\omega)$.

Let us then obtain the Dyson equation of $G_{dQd}(\omega)$. Differentiating (B.37) with respect to τ' and carrying out the Fourier transformation, we obtain the Dyson equation in the energy space as

$$G_{dQd}(\omega) = \left[\langle b(\omega) + b^\dagger(\omega) \rangle + \sum_{k, \alpha \in L, R} V_{k\alpha} G_{dQk\alpha}(\omega) + \gamma G_{dQdQ}(\omega) \right] g_d(\omega), \quad (\text{B.39})$$

where $G_{dQk\alpha}(\omega)$ and $G_{dQdQ}(\omega)$ is the Fourier transformation of

$$G_{dQk\alpha}(\tau - \tau') \equiv -i \left\langle T_C c_d(\tau) [b(\tau) + b^\dagger(\tau)] c_{k\alpha}^\dagger(\tau') \right\rangle, \quad (\text{B.40})$$

$$G_{dQdQ}(\tau - \tau') \equiv -i \left\langle T_C c_d(\tau) [b(\tau) + b^\dagger(\tau)] [b(\tau') + b^\dagger(\tau')] c_d^\dagger(\tau') \right\rangle, \quad (\text{B.41})$$

respectively.

The Dyson equation of $G_{dQk\alpha}(\omega)$ is obtained in the same way as

$$G_{dQk_L} = \left[V_{k_L} G_{dQd} + \sum_{k_R} V_{k_R k_L} e^{-i\Phi} G_{dQk_R} \right] g_{k_L}, \quad (\text{B.42})$$

$$G_{dQk_R} = \left[V_{k_R} G_{dQd} + \sum_{k_L} V_{k_L k_R} e^{i\Phi} G_{dQk_L} \right] g_{k_R}, \quad (\text{B.43})$$

which are similar forms to Eqs. (B.15) and (B.17). We here omitted the dependence on ω and Φ for brevity. In the same way as to obtain Eqs. (B.19) and (B.21), we obtain the following equations:

$$\sum_{k_L} V_{k_L} G_{dQk_L} = G_{dQd} \tilde{\Sigma}_L, \quad \sum_{k_R} V_{k_R} G_{dQk_R} = G_{dQd} \tilde{\Sigma}_R, \quad (\text{B.44})$$

where the self-energies $\tilde{\Sigma}_L$ and $\tilde{\Sigma}_R$ are defined in Eqs. (B.24) and (B.26), respectively. Inserting Eq. (B.44) to (B.39), we express the Dyson equation of $G_{dQd}(\omega)$ as

$$G_{dQd} = \left[\langle b + b^\dagger \rangle + G_{dQd} \tilde{\Sigma}_l + \gamma G_{dQdQ} \right] g_d, \quad (\text{B.45})$$

where we define $\tilde{\Sigma}_l \equiv \tilde{\Sigma}_L + \tilde{\Sigma}_R$.

Inserting the Dyson equation of G_{dQd} (B.45) to that of G_{dd} (B.35), we finally obtain the following Dyson equation of G_{dd} :

$$G_{dd} = g_d [1 + \Sigma_l G_{dd} + \gamma G_{dQd}] \quad (\text{B.46})$$

$$= g_d \left\{ 1 + \Sigma_l G_{dd} + \gamma \left[\langle b + b^\dagger \rangle + G_{dQd} \tilde{\Sigma}_l + \gamma G_{dQdQ} \right] g_d \right\}, \quad (\text{B.47})$$

We will calculate the retarded, advanced and the lesser components of each (contour-ordered) Green's function from the Dyson equations in Section B.4 after we introduce the Langreth theorem in the next Section, which enables us to calculate the lesser component of the product of contour-ordered Green's functions.

B.3 Langreth theorem

The expression of the current (B.6) and the Dyson equation of the dot (B.47) contain the products of contour-ordered Green's functions. In order to obtain the lesser component of such a product, Langreth theorem [79] is very convenient.

Let us consider the following contour-ordered Green's functions for some quantities A, B, C, D :

$$G_{AB}(\tau_1, \tau_2) = -i \langle T_C A(\tau_1) B(\tau_2) \rangle, \quad (\text{B.48})$$

$$G_{CD}(\tau_1, \tau_2) = -i \langle T_C C(\tau_1) D(\tau_2) \rangle. \quad (\text{B.49})$$

In the calculation of a Green's function, we often encounter the time-convolution of the operator

written on the Keldysh contour such as

$$I(\tau_1, \tau_2) = \int_{C_K} d\tau G_{AB}(\tau_1, \tau) G_{CD}(\tau, \tau_2), \quad (\text{B.50})$$

where \int_{C_K} means the integral on the Keldysh contour C_K . The Langreth theorem describes a projection of the convolution $I(\tau_1, \tau_2)$ from the Keldysh contour to the real-time one [79].

Since the proof of the Langreth theorem is given in the textbook [79], we list the results below. Each component of the time-convolution $I(\tau_1, \tau_2)$ is given as follows:

$$I^<(t_1, t_2) = \int_{-\infty}^{\infty} dt [G_{AB}^r(t_1, t) G_{CD}^<(t, t_2) + G_{AB}^<(t_1, t) G_{CD}^a(t, t_2)], \quad (\text{B.51})$$

$$I^>(t_1, t_2) = \int_{-\infty}^{\infty} dt [G_{AB}^r(t_1, t) G_{CD}^>(t, t_2) + G_{AB}^>(t_1, t) G_{CD}^a(t, t_2)], \quad (\text{B.52})$$

$$I^r(t_1, t_2) = \int_{t_2}^{t_1} dt G_{AB}^r(t_1, t) G_{CD}^r(t, t_2), \quad (\text{B.53})$$

and

$$I^a(t_1, t_2) = \int_{t_2}^{t_1} dt G_{AB}^a(t_1, t) G_{CD}^a(t, t_2). \quad (\text{B.54})$$

For steady state, we assume the time-translational symmetry $f(t_1, t_2) = f(t_1 - t_2)$, in which the above Langreth theorems are expressed in the energy space with the Fourier transformation as

$$I^<(\omega) = G_{AB}^r(\omega) G_{CD}^<(\omega) + G_{AB}^<(\omega) G_{CD}^a(\omega), \quad (\text{B.55})$$

$$I^r(\omega) = G_{AB}^r(\omega) G_{CD}^r(\omega), \quad (\text{B.56})$$

$$I^a(\omega) = G_{AB}^a(\omega) G_{CD}^a(\omega), \quad (\text{B.57})$$

which we often use in calculations below.

B.4 Calculation of the retarded, advanced and the lesser components of the Green's functions

Since we have the Dyson equations of the contour-ordered Green's functions, let us obtain the retarded, the advanced, and the lesser components of the Green's functions. Note that the definitions of them are given in Eqs. (4.59), (4.60), (4.61) and (4.62). We only repeat them here as follows:

$$G_{AB}^r(t_1, t_2) \equiv -i\theta(t_1 - t_2) \langle \{A(t_1), B(t_2)\} \rangle, \quad (\text{B.58})$$

$$G_{AB}^a(t_1, t_2) \equiv i\theta(t_2 - t_1) \langle \{A(t_1), B(t_2)\} \rangle, \quad (\text{B.59})$$

$$G_{AB}^<(t_1, t_2) \equiv i \langle B(t_2) A(t_1) \rangle, \quad (\text{B.60})$$

$$G_{AB}^>(t_1, t_2) \equiv -i \langle A(t_2) B(t_1) \rangle. \quad (\text{B.61})$$

For preparation, let us calculate each component of the contour-ordered Green's functions that have appeared so far. Let us first calculate the components of the free Green's function of a reservoir $g_{k\alpha} = -i \langle T_C c_{k_L}(\tau) c_{k_L}^\dagger(\tau') \rangle_{\text{free}}$ in Eq. (B.38). Using the definitions of the retarded, the advanced, and the lesser components of the Green's functions (B.58) and (B.60) as well as the Fourier transformation, we obtain the following:

$$g_{k\alpha}^r(\omega) = \frac{1}{\omega - \epsilon_{k\alpha} + i\eta}, \quad g_{k\alpha}^a(\omega) = \frac{1}{\omega - \epsilon_{k\alpha} - i\eta} = [g_{k\alpha}^r(\omega)]^*, \quad (\text{B.62})$$

$$g_{k\alpha}^<(\omega) = 2\pi i \delta(\epsilon_{k\alpha} - \omega) f_\alpha(\omega), \quad (\text{B.63})$$

where η is a infinitesimal parameter, $f_\alpha(\omega) = [1 + e^{\beta_\alpha(\omega - \mu_\alpha)}]^{-1}$ and $\beta = (k_B T_\alpha)^{-1}$. Here T_α and μ_α are the temperature, and the chemical potential of the reservoir, respectively, with k_B denoting the Boltzmann constant.

In the same way, we obtain the components of the free Green's function of the dot $g_d = -i \langle T_C c_d(\tau) c_d^\dagger(\tau') \rangle_{\text{free}}$ in Eq. (B.36):

$$g_d^r(\omega) = \frac{1}{\omega - \epsilon_d + i\eta}, \quad g_d^a(\omega) = [g_d^r(\omega)]^*, \quad g_d^<(\omega) = 0. \quad (\text{B.64})$$

where we assume that there is no electrons in the dot initially.

With these calculations, we obtain each component of the Green's function $\hat{\Gamma}_L(\omega)$ and $\hat{\Gamma}_R(\omega)$ in Eq. (B.22) as

$$\hat{\Gamma}_{L(R)}^r(\omega) = \sum_{k_L(k_R)} \frac{|V_{k_L(k_R)}|^2}{\omega - \epsilon_{k\alpha} + i\eta} = \pi i \sum_{k_L(k_R)} |V_{k_L(k_R)}|^2 \delta(\epsilon_{k\alpha} - \omega), \quad \hat{\Gamma}_{L(R)}^a(\omega) = [\hat{\Gamma}_{L(R)}^r(\omega)]^*, \quad (\text{B.65})$$

$$\hat{\Gamma}_{L(R)}^<(\omega) = 2\pi i \sum_{k_L(k_R)} |V_{k_L(k_R)}|^2 \delta(\epsilon_{k\alpha} - \omega) f_\alpha(\omega). \quad (\text{B.66})$$

Then let us calculate the retarded, the advanced, and the lesser components of the self-energies in Eqs. (B.23)-(B.26). For the self-energies Σ_L and Σ_R in Eqs. (B.23) and (B.25), we calculate their retarded and advanced components with the Langreth theorem (B.56) and (B.57) as

$$\Sigma_L^r = \tilde{\Sigma}_L^r = -i \frac{\Gamma_L(\omega) - ie^{i\Phi} \sqrt{\lambda(\omega) \Gamma_L(\omega) \Gamma_R(\omega)}}{1 + \lambda(\omega)}, \quad \Sigma_L^a = \tilde{\Sigma}_L^a = [\Sigma_L^r]^* \quad (\text{B.67})$$

and

$$\Sigma_R^r = \tilde{\Sigma}_R^r = -i \frac{\Gamma_R(\omega) - ie^{-i\Phi} \sqrt{\lambda \Gamma_L(\omega) \Gamma_R(\omega)}}{1 + \lambda(\omega)}, \quad \Sigma_R^a = \tilde{\Sigma}_R^a = [\Sigma_R^r]^*, \quad (\text{B.68})$$

where we defined the resonant width from the coupling of the left (right) reservoir,

$$\Gamma_{L(R)}(\omega) = \frac{\pi}{2} \sum_{k_L(k_R)} |V_{k_L(k_R)}|^2 \delta(\omega - \epsilon_{k_L(k_R)}), \quad (\text{B.69})$$

and that between the reservoirs

$$\lambda(\omega) = \pi^2 \sum_{k_L, k_R} |V_{k_L k_R}|^2 \delta(\omega - \epsilon_{k_L}) \delta(\omega - \epsilon_{k_R}). \quad (\text{B.70})$$

Similarly, we obtain the lesser components of the self-energies as in

$$\Sigma_L^< = \frac{2}{1+\lambda} \left[-i\Gamma_L f_L - e^{i\Phi} (f_R - f_L) \sqrt{\lambda\Gamma_L\Gamma_R} \right] + 2\lambda(f_R - f_L)(-i\Gamma_L - e^{i\Phi} \sqrt{\lambda\Gamma_L\Gamma_R}), \quad (\text{B.71})$$

$$\Sigma_R^< = \frac{2}{1+\lambda} \left[-i\Gamma_R f_R + e^{-i\Phi} (f_R - f_L) \sqrt{\lambda\Gamma_L\Gamma_R} \right] + 2\lambda(f_R - f_L)(i\Gamma_R + e^{-i\Phi} \sqrt{\lambda\Gamma_L\Gamma_R}), \quad (\text{B.72})$$

$$\tilde{\Sigma}_L^< = 2\lambda(f_R - f_L)(-i\Gamma_L + e^{-i\Phi} \sqrt{\lambda\Gamma_L\Gamma_R}) + \frac{2}{1+\lambda} \left[-i\Gamma_L f_L - e^{-i\Phi} (f_R - f_L) \sqrt{\lambda\Gamma_L\Gamma_R} \right], \quad (\text{B.73})$$

$$\tilde{\Sigma}_R^< = -2\lambda(f_R - f_L)(-i\Gamma_R + e^{i\Phi} \sqrt{\lambda\Gamma_L\Gamma_R}) + \frac{2}{1+\lambda} \left[-i\Gamma_R f_R - e^{i\Phi} (f_R - f_L) \sqrt{\lambda\Gamma_L\Gamma_R} \right], \quad (\text{B.74})$$

where we omit the dependence on ω for brevity. We find the following relation from the four lesser components above:

$$\Sigma_l^{r,<} = (\Sigma_L + \Sigma_R)^{r,<} = \tilde{\Sigma}_l^{r,<} = (\tilde{\Sigma}_L + \tilde{\Sigma}_R)^{r,<}. \quad (\text{B.75})$$

Each component of the self-energy $\Sigma_l(\omega)$ is finally obtained from Eqs. (B.71) and (B.72) as

$$\Sigma_l^r(\omega, \Phi) \equiv \frac{-i}{2[1+\lambda(\omega)]} [\Gamma_L(\omega) + \Gamma_R(\omega) - 2i\sqrt{\lambda(\omega)\Gamma_L(\omega)\Gamma_R(\omega)} \cos \Phi], \quad \Sigma_l^a(\omega, \Phi) = [\Sigma_l^r(\omega, \Phi)]^* \quad (\text{B.76})$$

$$\begin{aligned} \Sigma_l^<(\omega, \Phi) \equiv & \frac{i}{[1+\lambda(\omega)]^2} \{ f_L(\omega) [\Gamma_L(\omega) + \lambda(\omega)\Gamma_R(\omega)] + f_R(\omega) [\Gamma_R(\omega) + \lambda(\omega)\Gamma_L(\omega)] \\ & + 2\sqrt{\lambda(\omega)\Gamma_L(\omega)\Gamma_R(\omega)} [f_R(\omega) - f_L(\omega)] \sin \Phi \}. \end{aligned} \quad (\text{B.77})$$

Note that in the calculation, we used the fact that unity in energy space is $\delta(\tau_1 - \tau_2)$ in time space on the Keldysh contour and the lesser component of this in energy space, $1^<$, is always zero because τ_1 and τ_2 are on a different path for a lesser component: see the definition of a lesser component (4.59). For later use, we calculate the grater component of Σ_l from the relation $\Sigma_l^> = \Sigma_l^r - \Sigma_l^a + \Sigma_l^<$ in Eq. (4.63), which results in

$$\begin{aligned} \Sigma_l^>(\omega, \Phi) \equiv & \frac{i}{[1+\lambda(\omega)]^2} \{ [f_L(\omega) - 1] [\Gamma_L(\omega) + \lambda(\omega)\Gamma_R(\omega)] + [f_R(\omega) - 1] [\Gamma_R(\omega) + \lambda(\omega)\Gamma_L(\omega)] \\ & + 2\sqrt{\lambda(\omega)\Gamma_L(\omega)\Gamma_R(\omega)} [f_R(\omega) - f_L(\omega)] \sin \Phi \}. \end{aligned} \quad (\text{B.78})$$

With applying the Langreth theorems Eq. (B.55), (B.56) and (B.57), we obtain each component of the contour-ordered Green's function of the dot with $\gamma = 0$, defined as $\mathcal{G}_{dd} \equiv G_{dd}|_{\gamma=0}$,

as follows:

$$\mathcal{G}_{dd}^r(\omega, \Phi) = \frac{1}{\omega - \epsilon_d - \Sigma_l^r(\omega, \Phi)}, \quad \mathcal{G}_{dd}^a(\omega, \Phi) = [\mathcal{G}_{dd}^r(\omega, \Phi)]^*, \quad (\text{B.79})$$

$$\mathcal{G}_{dd}^<(\omega, \Phi) = \mathcal{G}_{dd}^r(\omega, \Phi) \Sigma_l^<(\omega, \Phi) \mathcal{G}_{dd}^a(\omega, \Phi). \quad (\text{B.80})$$

Let us calculate each component of G_{dd} in Eq. (B.47). let us first treat $\gamma \langle b + b^\dagger \rangle$. We can show

$$\gamma \langle b + b^\dagger \rangle \equiv \Delta\epsilon_V = -\frac{2\gamma^2}{\omega_0} \langle c_d^\dagger c_d \rangle = \frac{2i\gamma^2}{\omega_d} \int \frac{d\omega}{2\pi} \mathcal{G}_{dd}^<(\omega), \quad (\text{B.81})$$

which we interpret as the porolon shift [157], in the following way. We take the expectation value of $b + b^\dagger$ with respect to $|N, n'\rangle$, where N is the number of electrons on the dot and n' is the number of the phonons. Using the perturbation theory, we expand $|N, n'\rangle$ to the first order of γ as follows:

$$|N, n'\rangle = |N\rangle \otimes |n'\rangle + \gamma (c_d c_d^\dagger) |N\rangle \otimes \left(\sum_{n(\neq n')} \frac{\langle n|b + b^\dagger|n'\rangle}{\omega_0(n - n')} \right) |n\rangle + \mathcal{O}(\gamma^2), \quad (\text{B.82})$$

with which we calculate the term $\langle b + b^\dagger \rangle$ as

$$\langle N, n'|b + b^\dagger|N, n'\rangle = -\frac{2\gamma}{\omega_0} \langle N|c_d c_d^\dagger|N\rangle + \mathcal{O}(\gamma^2). \quad (\text{B.83})$$

We thus obtain

$$\Delta\epsilon_V(\omega, \Phi) \equiv -\frac{2\gamma^2}{\omega_0} \langle c_d^\dagger c_d \rangle = \frac{2i\gamma^2}{\omega_d} \int \frac{d\omega}{2\pi} \mathcal{G}_{dd}^<(\omega, \Phi), \quad (\text{B.84})$$

which we call the porolon shift.

Let us next consider each component of $G_{dQk\alpha}$. From Eq. (B.44) with the Langreth theorem (B.56), we find its retarded component as

$$\sum_{k, \alpha \in \text{L, R}} V_{k\alpha} G_{dQk\alpha}^r = G_{dQd}^r \Sigma_l^r, \quad (\text{B.85})$$

while the lesser component from the theorem (B.55) as

$$\sum_{k, \alpha \in \text{L, R}} V_{k\alpha} G_{dQk\alpha}^< = \tilde{\Sigma}_l^< G_{dQd}^r + \tilde{\Sigma}_l^a G_{dQd}^<. \quad (\text{B.86})$$

Let us obtain the retarded component of G_{dQd} . Applying the Langreth theorem (B.56) to Eq. (B.39) and using (B.85). we obtain the retarded component of G_{dQd} as

$$\gamma G_{dQd}^r = \frac{\gamma \langle b + b^\dagger \rangle + \Sigma_V^r}{\omega - \epsilon_d - \Sigma_l^r}, \quad (\text{B.87})$$

where we define

$$\Sigma_V^r = \gamma^2 G_{dQdQ}^r. \quad (\text{B.88})$$

The lesser component of G_{dQd} is calculated as

$$\begin{aligned}\gamma G_{dQd}^{\leq} &= (\mathcal{G}_{dd}^r [\gamma \langle b + b^\dagger \rangle + \gamma^2 G_{dQdQ}^r] \Sigma_l^{\leq} + \gamma^2 G_{dQdQ}^{\leq}) \mathcal{G}_{dd}^a \\ &= (\mathcal{G}_{dd}^r [\gamma \langle b + b^\dagger \rangle + \Sigma_V^r] \Sigma_l^{\leq} + \Sigma_V^{\leq}) \mathcal{G}_{dd}^a,\end{aligned}\quad (\text{B.89})$$

where we define

$$\Sigma_V^{\leq} = \gamma^2 G_{dQdQ}^{\leq}. \quad (\text{B.90})$$

Let us calculate the advanced and the lesser component of the contour-ordered Green's function G_{dQdQ} to obtain the expressions of Σ_V^r and Σ_V^{\leq} . Since this Green's function appears in the form $\gamma^2 G_{dQdQ}$, we calculate the zeroth order of γ in the calculation, that is, we can see that the electrons and phonons are decoupled in the calculation. Let us calculate the retarded component of G_{dQdQ} as

$$G_{dQdQ}^r = -i \int_0^\infty dt e^{i\omega t} \langle \{c_d(t)(b(t) + b^\dagger(t)), (b + b^\dagger)c_d\} \rangle \quad (\text{B.91})$$

$$\begin{aligned}&= i \int \frac{d\omega'}{2\pi} \left[\mathcal{G}_{dd}^>(\omega', \Phi) \left(\frac{1+N}{\omega - \omega' - \omega_0 + i0^+} + \frac{N}{\omega - \omega' + \omega_0 + i0^+} \right) \right. \\ &\quad \left. - \mathcal{G}_{dd}^{\leq}(\omega', \Phi) \left(\frac{1+N}{\omega - \omega' + \omega_0 + i0^+} + \frac{N}{\omega - \omega' - \omega_0 + i0^+} \right) \right],\end{aligned}\quad (\text{B.92})$$

where the time evolution of the operators of phonons are given by $b^\dagger(t) = e^{i\omega_0 t}$ and $b(t) = e^{-i\omega_0 t}$ since we can see that the electrons and phonons are decoupled in the calculation. With these observations, we obtain the expression of $\Sigma_V^r \equiv \gamma^2 G_{dQdQ}^r$ as

$$\begin{aligned}\Sigma_V^r(\omega, \Phi) &= i\gamma^2 \int \frac{d\omega'}{2\pi} \left[\mathcal{G}_{dd}^>(\omega', \Phi) \left(\frac{1+N}{\omega - \omega' - \omega_0 + i0^+} + \frac{N}{\omega - \omega' + \omega_0 + i0^+} \right) \right. \\ &\quad \left. - \mathcal{G}_{dd}^{\leq}(\omega', \Phi) \left(\frac{1+N}{\omega - \omega' + \omega_0 + i0^+} + \frac{N}{\omega - \omega' - \omega_0 + i0^+} \right) \right].\end{aligned}\quad (\text{B.93})$$

Similarly, we obtain the lesser component as

$$G_{dQdQ}^{\leq}(\omega, \Phi) = i \int dt e^{i\omega t} \langle (b + b^\dagger) c_0^\dagger [b(t) + b^\dagger(t)] c_d(t) \rangle \quad (\text{B.94})$$

$$= N \mathcal{G}_{dd}^{\leq}(\omega - \omega_0, \Phi) + (1+N) \mathcal{G}_{dd}^{\leq}(\omega + \omega_0, \Phi), \quad (\text{B.95})$$

where N is the Bose-Einstein distribution of the third, Bosonic reservoir defined as

$$N \equiv \frac{1}{e^{\beta_P \omega_0} - 1}. \quad (\text{B.96})$$

Therefore we obtain

$$\Sigma_V^{\leq}(\omega, \Phi) = \gamma^2 G_{dQdQ}^{\leq}(\omega, \Phi) = \gamma^2 [N \mathcal{G}_{dd}^{\leq}(\omega - \omega_0, \Phi) + (1+N) \mathcal{G}_{dd}^{\leq}(\omega + \omega_0, \Phi)] \quad (\text{B.97})$$

$$= \gamma^2 [|\mathcal{G}_{dd}^a(\omega - \omega_0, \Phi)|^2 N \Sigma_l^{\leq}(\omega - \omega_0, \Phi) + |\mathcal{G}_{dd}^a(\omega + \omega_0, \Phi)|^2 (1+N) \Sigma_l^{\leq}(\omega + \omega_0, \Phi)], \quad (\text{B.98})$$

where we used in the second line $\mathcal{G}_{dd}^{<, >} = \mathcal{G}_{dd}^a \Sigma_l^{<, >} \mathcal{G}_{dd}^r = |\mathcal{G}_{dd}^a|^2 \Sigma_l^{<, >}$ found from Eqs. (B.101)-(B.103). Moreover, for later use, we calculate the greater component of Σ_V with the relation $\Sigma_V^r - \Sigma_V^a = \Sigma_V^> - \Sigma_V^<$ to obtain $\Sigma_V^>(\omega)$ coming from the fact that the self-energy also satisfies the relation Eq. (4.63) [79]:

$$\Sigma_V^>(\omega, \Phi) = \gamma^2 \left[|\mathcal{G}_{dd}^a(\omega + \omega_0, \Phi)|^2 N \Sigma_l^>(\omega + \omega_0, \Phi) + |\mathcal{G}_{dd}^a(\omega - \omega_0, \Phi)|^2 (1 + N) \Sigma_l^>(\omega - \omega_0, \Phi) \right], \quad (\text{B.99})$$

Let us finally calculate the retarded and the lesser components of G_{dd} . Applying the Langreth theorem (B.57) to the Dyson equation of the dot (B.47) and inserting Eq. (B.87), we obtain the retarded component as

$$(\omega - \epsilon_d - \Sigma_l^r) G_{dd}^r = 1 + \gamma \frac{\langle b + b^\dagger \rangle + \gamma G_{dQdQ}^r}{\omega - \epsilon_d - \Sigma_l^r}, \quad (\text{B.100})$$

which leads to

$$G_{dd}^r(\omega, \Phi) = \frac{1}{[\mathcal{G}_{dd}^r(\omega, \Phi)]^{-1} - \Delta \epsilon_V(\omega, \Phi) - \Sigma_V^r(\omega, \Phi)}, \quad (\text{B.101})$$

where we used the fact that we are working up to second order in γ . Note that we obtain the advanced component as $G_{dd}^a(\omega, \Phi) = [G_{dd}^r(\omega, \Phi)]^*$.

We obtain the lesser component by applying the Langreth theorem (B.55) to the Dyson equation of the dot Eq. (B.47) and using Eq. (B.89) as

$$\begin{aligned} G_{dd}^< &= \mathcal{G}_{dd}^r (\Sigma_l^< G_{dd}^a + \gamma G_{dQd}^<) \\ &= \mathcal{G}_{dd}^r \{ \Sigma_l^< + G_{dd}^a + (\mathcal{G}_{dd}^r [\gamma \langle b + b^\dagger \rangle + \Sigma_V^r] \Sigma_l^< + \Sigma_V^<) \mathcal{G}_{dd}^a \}, \end{aligned} \quad (\text{B.102})$$

which leads to

$$G_{dd}^<(\omega, \Phi) = G_{dd}^r(\omega, \Phi) [\Sigma_l^<(\omega, \Phi) + \Sigma_V^<(\omega, \Phi)] G_{dd}^a(\omega, \Phi). \quad (\text{B.103})$$

Here we used the fact that we are working up to second order in γ ; for example,

$$\mathcal{G}_{dd}^r \Sigma_V^< \mathcal{G}_{dd}^a = G_{dd}^r \Sigma_V^< G_{dd}^a \quad (\text{B.104})$$

holds since we are working up to second order in γ .

B.4.1 The expression of the integrand of the current

Since now we have all the expressions of the retarded, the advanced, and the lesser components of all the Green's functions and the self-energies, we can obtain the expression of the integrand of the current with applying the Langreth theorem for lesser components (B.55) to the expression of the integrand of the current (B.33). Inserting the components of the Green's functions Eqs. (B.67), (B.68), (B.71), (B.72), (B.73), (B.74), (B.101), and (B.103) to Eq. (B.33) and carrying out the calculation, we finally obtain the following integrand of the current ($-\langle \dot{N}_L \rangle \equiv$

$\int d\omega/2\pi \times J_L(\omega, \Phi)$ with $\langle \dot{N}_L \rangle$ denoting the particle current *into* the reservoir) as follows:

$$J_L(\omega, \Phi) = [f_R(\omega) - f_L(\omega)] \{t_0(\omega)^2 [1 - \Gamma(\omega) \text{Im} G_{dd}^a(\omega, \Phi)] + t_0(\omega) r_0(\omega) \Gamma(\omega) \alpha(\omega) \cos \Phi \text{Re} G_{dd}^a(\omega, \Phi)\} \\ - i \frac{\Gamma(\omega)}{2} \{[1 + r_0(\omega) \bar{\alpha}(\omega)] [G_{dd}^<(\omega, \Phi) - f_L(\omega) (G_{dd}^a(\omega, \Phi) - G_{dd}^r(\omega, \Phi))] \\ + \alpha(\omega) t_0(\omega) \sin \Phi [G_{dd}^<(\omega, \Phi) - f_R(\omega) (G_{dd}^a(\omega, \Phi) - G_{dd}^r(\omega, \Phi))]\}, \quad (\text{B.105})$$

where

$$\Gamma(\omega) = \frac{\Gamma_L(\omega) + \Gamma_R(\omega)}{1 + \lambda(\omega)} \quad (\text{B.106})$$

is the total width of the resonance level of the dot,

$$t_0^2(\omega) = \frac{4\lambda(\omega)}{[1 + \lambda(\omega)]^2}, \quad r_0^2(\omega) = 1 - t_0^2(\omega), \quad (\text{B.107})$$

are, respectively, the transmission and reflection probabilities of the lower arm of the Aharonov-Bohm ring and

$$\alpha(\omega) = \frac{2\sqrt{\Gamma_L(\omega)\Gamma_R(\omega)}}{\Gamma_L(\omega) + \Gamma_R(\omega)}, \quad \bar{\alpha}(\omega) = \frac{\Gamma_L(\omega) - \Gamma_R(\omega)}{\Gamma_L(\omega) + \Gamma_R(\omega)}, \quad (\text{B.108})$$

characterize the asymmetry of $\Gamma_L(\omega)$ and $\Gamma_R(\omega)$. Note that

$$\alpha^2(\omega) + \bar{\alpha}^2(\omega) = 1. \quad (\text{B.109})$$

Similarly, we obtain the integrand of the current J_R ($-\langle \dot{N}_R \rangle \equiv \int d\omega/2\pi \times J_R(\omega, \Phi)$) by changing $L \leftrightarrow R$ and $\phi \leftrightarrow -\phi$ in Eq. (B.105) as

$$J_R = (f_L - f_R) (t_0^2 [1 - \Gamma \text{Im} G_{dd}^a] + t_0 r_0 \Gamma \alpha \cos \Phi \text{Re} G_{dd}^a) \\ - i \frac{\Gamma}{2} \{[1 + r_0 \bar{\alpha}] [G_{dd}^< - f_R (G_{dd}^a - G_{dd}^r)] - \alpha t_0 \sin \Phi [G_{dd}^< - f_L (G_{dd}^a - G_{dd}^r)]\}, \quad (\text{B.110})$$

where we omitted the dependence on ω and Φ for brevity.

B.4.2 The heat current from the Bosonic reservoir from the conservation of energy

Let us confirm the conservation of particle and obtain the heat current of phonons from considering the conservation of energy. For simplicity, we omit the dependence on ω and Φ if not necessary. Since

$$-\langle \dot{N}_L \rangle - \langle \dot{N}_R \rangle = \int \frac{d\omega}{2\pi} (J_L + J_R), \quad -\langle \dot{E}_L \rangle - \langle \dot{E}_R \rangle = \int \frac{d\omega}{2\pi} \omega (J_L + J_R), \quad (\text{B.111})$$

we calculate the following quantity to check the conservation law by inserting the expression of J_L (B.105) and that of J_R (B.110):

$$\begin{aligned} & \int \frac{d\omega}{2\pi} \omega^s [J_L(\omega) + J_R(\omega)] \\ &= \int \frac{d\omega}{2\pi} \omega^s [(\Sigma_l^r - \Sigma_l^a) G_{dd}^< + \Sigma_l^< (G_{dd}^a - G_{dd}^r)] \end{aligned} \quad (\text{B.112})$$

$$= \int \frac{d\omega}{2\pi} \omega^s |G_{dd}^a|^2 [\Sigma_l^> \Sigma_V^< - \Sigma_l^< \Sigma_V^>] \quad (\text{B.113})$$

$$= \gamma^2 \int \frac{d\omega}{2\pi} |\mathcal{G}_{dd}^a(\omega_+)|^2 |\mathcal{G}_{dd}^a(\omega_-)|^2 (\omega_+^s - \omega_-^s) [N \Sigma_l^>(\omega_+) \Sigma_l^<(\omega_-) - (1+N) \Sigma_l^<(\omega_+) \Sigma_l^>(\omega_-)], \quad (\text{B.114})$$

where $s = 0$ for the particle current and $s = 1$ for the energy current,

$$\omega_{\pm} \equiv \omega \pm \frac{\omega_0}{2}, \quad (\text{B.115})$$

and we switch from $|G_{dd}^a|^2$ to $|\mathcal{G}_{dd}^a|^2$ because we are working to the order of γ^2 . We also used

$$G_{dd}^a - G_{dd}^r = G_{dd}^< - G_{dd}^> = |G_{dd}^a|^2 (\Sigma_l^< + \Sigma_V^< - \Sigma_l^> - \Sigma_V^>), \quad (\text{B.116})$$

$$G_{dd}^< = |G_{dd}^a|^2 (\Sigma_l^< + \Sigma_V^<), \quad (\text{B.117})$$

$$\Sigma_l^r - \Sigma_l^a = \Sigma_l^> - \Sigma_l^<, \quad (\text{B.118})$$

as well as Eqs. (B.98) and (B.99), where the first two relations come from Eqs. (B.101)-(B.103) while the third one comes from the fact that the self-energy also satisfies the relation Eq. (4.63) [79]. Since the right-hand side of Eq. (B.114) is zero for $s = 0$, we find that the particle current is conserved.

For $s = 1$, the energy current is not conserved because of the heat current from the Bosonic reservoir as

$$J_Q^P = -\langle \dot{E}_L \rangle - \langle \dot{E}_R \rangle = \int \frac{d\omega}{2\pi} \omega (J_L + J_R) \quad (\text{B.119})$$

where $\langle \dot{E}_\alpha \rangle$ ($\alpha = L, R$) is the energy current *into* the α reservoir and J_Q^P is the heat current *from* the Bosonic reservoir. Inserting the lesser and greater components of the self-energies Σ_L (B.77) and (B.78) as well as those of Σ_V (B.98) and (B.99), we obtain the expression of the heat current of phonons with $s = 1$ in Eq. (B.114) as

$$\begin{aligned} J_Q^P &= \omega_0 \int \frac{d\omega}{2\pi} c(\omega, \Phi) \{ F_{LL}(\omega) [g_{+-}(\omega_+, \Phi) g_{+-}(\omega_-, \Phi)] + F_{RR}(\omega) [g_{-+}(\omega_+, \Phi) g_{-+}(\omega_-, \Phi)] \\ &\quad + F_{LR}(\omega) [g_{+-}(\omega_+, \Phi) g_{-+}(\omega_-, \Phi)] + F_{RL}(\omega) [g_{-+}(\omega_+, \Phi) g_{+-}(\omega_-, \Phi)] \}, \end{aligned} \quad (\text{B.120})$$

where we defined

$$c(\omega, \Phi) \equiv \gamma^2 \frac{\Gamma(\omega_+) \Gamma(\omega_-)}{4} |\mathcal{G}_{dd}^a(\omega_+, \Phi) \mathcal{G}_{dd}^a(\omega_-, \Phi)|^2, \quad (\text{B.121})$$

$$g_{\pm\pm}(\omega, \Phi) \equiv a_{\pm}(\omega) \pm b(\omega) \sin \Phi, \quad g_{\pm\mp}(\omega, \Phi) \equiv a_{\pm}(\omega) \mp b(\omega) \sin \Phi. \quad (\text{B.122})$$

and

$$F_{\alpha\beta}(\omega) \equiv N[1 - f_{\alpha}(\omega_+)]f_{\beta}(\omega_-) - (1 + N)[1 - f_{\beta}(\omega_-)]f_{\alpha}(\omega_+). \quad (\text{B.123})$$

Here we also defined

$$a_{\pm}(\omega) = 1 \pm \bar{\alpha}(\omega)r_0(\omega), \quad b(\omega) = \alpha(\omega)t_0(\omega). \quad (\text{B.124})$$

B.4.3 Dividing the current into an elastic and inelastic parts

Since we would like to expand the currents with thermodynamic affinities, it is convenient to write the current explicitly in terms of the distributions of each reservoir. It is also convenient to divided the currents into the terms including only the Fermi distributions f_L, f_R , which we call the elastic part, and those including the Bose distribution N , which we call the inelastic part, so that we can see the inelastic effect clearer. Since the Bose distribution is included in the lesser and greater components of the self-energy $\Sigma_V^<, \Sigma_V^>$, let us divide the current (B.105) into the terms without them and those with them using the following relations:

$$G_{dd}^< = |G_{dd}^a|^2(\Sigma_l^< + \Sigma_V^<), \quad (\text{B.125})$$

$$\begin{aligned} G_{dd}^a - G_{dd}^r &= |G_{dd}^a|^2(\Sigma_l^a + \Sigma_V^a - \Sigma_l^r - \Sigma_V^r) \\ &= |G_{dd}^a|^2(2i \text{Im} \Sigma_l^a + \Sigma_V^< - \Sigma_V^>), \end{aligned} \quad (\text{B.126})$$

which we find from Eqs. (B.101) and (B.103). The result is the following:

$$J_L(\omega, \Phi) = [f_R(\omega) - f_L(\omega)]J_l(\omega, \Phi) + J_V^L(\omega, \Phi), \quad (\text{B.127})$$

where

$$J_l(\omega, \Phi) = t_0^2 \left(1 - \Gamma \text{Im} G_{dd}^a + \frac{\Gamma^2}{4} [1 - \alpha^2 \cos^2 \Phi] |G_{dd}^a|^2 \right) + t_0 r_0 \Gamma \alpha \cos \Phi \text{Re} G_{dd}^a + \frac{\Gamma^2 \alpha^2}{4} |G_{dd}^a|^2 \quad (\text{B.128})$$

is the elastic part and

$$J_V^L(\omega, \Phi) = -i \frac{\Gamma}{2} |\mathcal{G}_{dd}^a|^2 \{ a_+ [\Sigma_V^< (1 - f_L) + \Sigma_V^> f_L] + b \sin \Phi [\Sigma_V^< (1 - f_R) + \Sigma_V^> f_R] \} \quad (\text{B.129})$$

is the elastic part, where the definitions of a_{\pm} and b are given in Eq. (B.124). Note that we omit the dependence on ω and Φ of the right-hand sides in Eqs. (B.128) and Eqs. (B.129).

Let us express the inelastic part with respect to the distributions of each reservoir explicitly. Inserting Eqs. (B.98) and (B.99) into Eq. (B.129), we obtain the inelastic part as

$$\begin{aligned} J_V^L &= c(\omega_-, \Phi) a_+(\omega) \{ a_+(\omega - \omega_0) F_{LL}(\omega_-) + a_-(\omega - \omega_0) F_{LR}(\omega_-) \\ &\quad + b(\omega - \omega_0) \sin \Phi [F_{LR}(\omega_-) - F_{LL}(\omega_-)] \} \\ &\quad - c(\omega_+, \Phi) a_+(\omega) \{ a_+(\omega + \omega_0) F_{LL}(\omega_+) + a_-(\omega + \omega_0) F_{RL}(\omega_+) \\ &\quad + b(\omega + \omega_0) \sin \Phi [F_{RL}(\omega_+) - F_{LL}(\omega_+)] \} \end{aligned}$$

$$\begin{aligned}
& + c(\omega_-, \Phi) b(\omega) \sin \Phi \{a_+(\omega - \omega_0) F_{\text{RL}}(\omega_-) + a_-(\omega - \omega_0) F_{\text{RR}}(\omega_-) \\
& + b(\omega - \omega_0) \sin \Phi [F_{\text{RR}}(\omega_-) - F_{\text{RL}}(\omega_-)]\} \\
& - c(\omega_+, \Phi) b(\omega) \sin \Phi \{a_+(\omega + \omega_0) F_{\text{LR}}(\omega_+) + a_-(\omega + \omega_0) F_{\text{RR}}(\omega_+) \\
& + b(\omega + \omega_0) \sin \Phi [F_{\text{RR}}(\omega_+) - F_{\text{LR}}(\omega_+)]\}, \tag{B.130}
\end{aligned}$$

where $F_{\alpha\beta}$ was defined in Eq. (B.123).

With these calculations, we obtain the electric current as

$$J_e = -e \langle \dot{N}_L \rangle = -e \int \frac{d\omega}{2\pi} J_L(\omega, \Phi) \tag{B.131}$$

$$= e \int \frac{d\omega}{2\pi} [f_L(\omega) - f_R(\omega)] J_l(\omega, \Phi) + e \int \frac{d\omega}{2\pi} c(\omega, \Phi) J_{V0}^L(\omega, \Phi), \tag{B.132}$$

and the heat current from the left electronic reservoir

$$J_Q^L = - \int \frac{d\omega}{2\pi} (\omega - \mu_L) J_L(\omega, \Phi) \tag{B.133}$$

$$= \int \frac{d\omega}{2\pi} (\omega - \mu_L) [f_L(\omega) - f_R(\omega)] J_l(\omega, \Phi) + \int \frac{d\omega}{2\pi} c(\omega, \Phi) [J_{V1}^L(\omega, \Phi) - \mu_L J_{V0}^L(\omega, \Phi)], \tag{B.134}$$

where

$$\begin{aligned}
J_{Vs}^L(\omega, \Phi) = & F_{\text{LL}}(\omega) \{ -\omega_+^s a_+(\omega_+) g_{+-}(\omega_-, \Phi) + \omega_-^s a_+(\omega_-) g_{+-}(\omega_+, \Phi) \} \\
& + F_{\text{RR}}(\omega) \{ -\omega_+^s b(\omega_+) \sin \Phi g_{-+}(\omega_-, \Phi) + \omega_-^s b(\omega_-) \sin \Phi g_{-+}(\omega_+, \Phi) \} \\
& + F_{\text{LR}}(\omega) \{ -\omega_+^s a_+(\omega_+) g_{-+}(\omega_-, \Phi) + \omega_-^s b(\omega_-) \sin \Phi g_{-+}(\omega_+, \Phi) \} \\
& + F_{\text{RL}}(\omega) \{ -\omega_+^s b(\omega_+) \sin \Phi g_{+-}(\omega_-, \Phi) + \omega_-^s a_+(\omega_-) g_{+-}(\omega_+, \Phi) \}, \tag{B.135}
\end{aligned}$$

Note that when we calculated $\int d\omega/2\pi \omega^s J_V^L(\omega)$, we shifted the integral variable $\omega \rightarrow \omega_+$ for the terms multiplied with $c(\omega_-, \Phi)$ and with shifting $\omega \rightarrow \omega_-$ for the terms multiplied with $c(\omega_+, \Phi)$.

Bibliography

- [1] A. F. Ioffe, L. Stil'bans, E. Iordanishvili, T. Stavitskaya, A. Gelbtuch, and G. Vineyard, *Phys. Today* **12**, 42 (1959).
- [2] A. F. Ioffe and L. S. Stil'bans, *Rep. Prog. Phys.* **22**, 167 (1959).
- [3] L. D. Hicks and M. S. Dresselhaus, *Phys. Rev. B* **47**, 16631 (1993).
- [4] L. D. Hicks and M. S. Dresselhaus, *Phys. Rev. B* **47**, 12727 (1993).
- [5] M. Dresselhaus, G. Chen, M. Tang, R. Yang, H. Lee, D. Wang, Z. Ren, J.-P. Fleurial, and P. Gogna, *Adv. Mater.* **19**, 1043 (2007).
- [6] R. Sánchez and M. Büttiker, *Phys. Rev. B* **83**, 085428 (2011).
- [7] B. Sothmann, R. Sánchez, A. N. Jordan, and M. Büttiker, *Phys. Rev. B* **85**, 205301 (2012).
- [8] B. Sothmann and M. Büttiker, *Europhys. Lett.* **99**, 27001 (2012).
- [9] D. M. Kennes, D. Schuricht, and V. Meden, *Europhys. Lett.* **102**, 57003 (2013).
- [10] K. Brandner, K. Saito, and U. Seifert, *Phys. Rev. Lett.* **110**, 070603 (2013).
- [11] B. Sothmann, R. Sánchez, A. N. Jordan, and M. Büttiker, *New J. Phys.* **15**, 095021 (2013).
- [12] M. Mintchev, L. Santoni, and P. Sorba, *arXiv:1310.2392* (2013).
- [13] S. Hershfield, K. A. Muttalib, and B. J. Nartowt, *Phys. Rev. B* **88**, 085426 (2013).
- [14] K. Brandner and U. Seifert, *New J. Phys.* **15**, 105003 (2013).
- [15] R. S. Whitney, *Phys. Rev. B* **87**, 115404 (2013).
- [16] J. Meair and P. Jacquod, *J. Phys.: Condens. Matter* **25**, 082201 (2013).
- [17] D. Sánchez and R. López, *Phys. Rev. Lett.* **110**, 026804 (2013).
- [18] R. López and D. Sánchez, *Phys. Rev. B* **88**, 045129 (2013).
- [19] A. N. Jordan, B. Sothmann, R. Sánchez, and M. Büttiker, *Phys. Rev. B* **87**, 075312 (2013).
- [20] R. S. Whitney, *Phys. Rev. B* **88**, 064302 (2013).
- [21] S.-Y. Hwang, D. Sánchez, M. Lee, and R. López, *New J. Phys.* **15**, 105012 (2013).
- [22] F. Mazza, R. Bosisio, G. Benenti, V. Giovannetti, R. Fazio, and F. Taddei, *New J. Phys.* **16**, 085001 (2014).

- [23] R. S. Whitney, Phys. Rev. Lett. **112**, 130601 (2014).
- [24] O. Entin-Wohlman, Y. Imry, and A. Aharony, Phys. Rev. B **91**, 054302 (2015).
- [25] C. Bergenfeldt, P. Samuelsson, B. Sothmann, C. Flindt, and M. Büttiker, Phys. Rev. Lett. **112**, 076803 (2014).
- [26] B. Sothmann, R. Sánchez, and A. N. Jordan, Europhys. Lett. **107**, 47003 (2014).
- [27] D. Sánchez and H. Linke, New J. Phys. **16**, 110201 (2014).
- [28] A. Crépieux and F. Michelini, J. Phys.: Condens. Matter **27**, 015302 (2015).
- [29] R. S. Whitney, Phys. Rev. B **91**, 115425 (2015).
- [30] P. P. Hofer and B. Sothmann, Phys. Rev. B **91**, 195406 (2015).
- [31] B. Sothmann, R. Sánchez, and A. N. Jordan, Nanotechnology **26**, 032001 (2015).
- [32] M. Mintchev, L. Santoni, and P. Sorba, J. Phys. A: Math. Theor. **48**, 055003 (2015).
- [33] R. Sánchez, B. Sothmann, and A. N. Jordan, Phys. Rev. Lett. **114**, 146801 (2015).
- [34] J.-H. Jiang, B. K. Agarwalla, and D. Segal, Phys. Rev. Lett. **115**, 040601 (2015).
- [35] M. Esposito, M. A. Ochoa, and M. Galperin, Phys. Rev. B **91**, 115417 (2015).
- [36] K. Yamamoto, O. Entin-Wohlman, A. Aharony, and N. Hatano, Phys. Rev. B **94**, 121402 (2016).
- [37] J.-T. Lü, J.-S. Wang, P. Hedegard, and M. Brandbyge, Phys. Rev. B **93**, 205404 (2016).
- [38] H. Thierschmann, R. Sánchez, B. Sothmann, H. Buhmann, and L. W. Molenkamp, C. R. Physique **17**, 1109 (2016).
- [39] R. S. Whitney, R. Sánchez, F. Haupt, and J. Splettstoesser, Physica E **75**, 257 (2016).
- [40] D. Sánchez and R. López, C. R. Physique **17**, 1060 (2016).
- [41] S.-Y. Hwang, R. López, and D. Sánchez, Phys. Rev. B **94**, 054506 (2016).
- [42] B. Szukiewicz, U. Eckern, and K. I. Wysokiński, New J. Phys. **18**, 023050 (2016).
- [43] H. Okada and Y. Utsumi, J. Phys. Soc. Jpn. **86**, 024007 (2017).
- [44] P. A. Erdman, F. Mazza, R. Bosisio, G. Benenti, R. Fazio, and F. Taddei, Phys. Rev. B **95**, 245432 (2017).
- [45] I. Iyyappan and M. Ponmurugan, J. Stat. Mech. Theor. Exp., 093207 (2017).
- [46] G. Benenti, G. Casati, K. Saito, and R. Whitney, Phys. Rep. **694**, 1 (2017).
- [47] H. Thierschmann, R. Sánchez, B. Sothmann, F. Arnold, C. Heyn, W. Hansen, H. Buhmann, and L. W. Molenkamp, Nat. Nanotech. **10**, 854 (2015).
- [48] J. V. Koski, A. Kutvonen, I. M. Khaymovich, T. Ala-Nissila, and J. P. Pekola, Phys. Rev. Lett. **115**, 260602 (2015).
- [49] J. V. Koski and J. P. Pekola, C. R. Physique **17**, 1130 (2016).
- [50] K. Chida, S. Desai, K. Nishiguchi, and A. Fujiwara, Nat. Commun. **8**, 15310 (2017).

- [51] J.-P. Brantut, C. Grenier, J. Meineke, D. Stadler, S. Krinner, C. Kollath, T. Esslinger, and A. Georges, *Science* **342**, 713 (2013).
- [52] E. Sevick, R. Prabhakar, S. R. Williams, and D. J. Searles, *Ann. Rev. Phys. Chem.* **59**, 603 (2008).
- [53] M. Esposito, U. Harbola, and S. Mukamel, *Rev. Mod. Phys.* **81**, 1665 (2009).
- [54] M. Campisi, P. Hänggi, and P. Talkner, *Rev. Mod. Phys.* **83**, 771 (2011).
- [55] C. Jarzynski, *Ann. Rev. Condens. Matter Phys.* **2**, 329 (2011).
- [56] U. Seifert, *Rep. Prog. Phys.* **75**, 126001 (2012).
- [57] C. V. den Broeck and M. Esposito, *Physica A* **418**, 6 (2015).
- [58] K. Saito and Y. Utsumi, *Phys. Rev. B* **78**, 115429 (2008).
- [59] S. Nakamura, Y. Yamauchi, M. Hashisaka, K. Chida, K. Kobayashi, T. Ono, R. Leturcq, K. Ensslin, K. Saito, Y. Utsumi, and A. C. Gossard, *Phys. Rev. Lett.* **104**, 080602 (2010).
- [60] S. Nakamura, Y. Yamauchi, M. Hashisaka, K. Chida, K. Kobayashi, T. Ono, R. Leturcq, K. Ensslin, K. Saito, Y. Utsumi, and A. C. Gossard, *Phys. Rev. B* **83**, 155431 (2011).
- [61] E. Iyoda, Y. Utsumi, and T. Kato, *J. Phys. Soc. Jpn.* **79**, 045003 (2010).
- [62] K. Yamamoto, arXiv:1504.05493 (2015).
- [63] G. Verley, M. Esposito, T. Willaert, and C. Van den Broeck, *Nat. Commun.* **5**, 4721 (2014).
- [64] S. Rana, P. S. Pal, A. Saha, and A. M. Jayannavar, *Phys. Rev. E* **90**, 042146 (2014).
- [65] K. Proesmans, B. Cleuren, and C. V. den Broeck, *Europhys. Lett.* **109**, 20004 (2015).
- [66] T. R. Gingrich, G. M. Rotskoff, S. Vaikuntanathan, and P. L. Geissler, *New J. Phys.* **16**, 102003 (2014).
- [67] G. Verley, T. Willaert, C. Van den Broeck, and M. Esposito, *Phys. Rev. E* **90**, 052145 (2014).
- [68] M. Polettini, G. Verley, and M. Esposito, *Phys. Rev. Lett.* **114**, 050601 (2015).
- [69] S. Datta, *Electronic Transport in Mesoscopic Systems* (Cambridge University Press, Cambridge, UK, 1997).
- [70] H. S. Leff and A. F. Rex, *Maxwell's demon 2: entropy, classical and quantum information, computing* (Institute of Physics, Bristol, 2003).
- [71] T. Sagawa and M. Ueda, *Phys. Rev. Lett.* **100**, 080403 (2008).
- [72] S. Toyabe, T. Sagawa, M. Ueda, E. Muneyuki, and M. Sano, *Nat. Phys.* **6**, 988 (2010).
- [73] P. Strasberg, G. Schaller, T. Brandes, and M. Esposito, *Phys. Rev. Lett.* **110**, 040601 (2013).
- [74] P. Strasberg, G. Schaller, N. Lambert, and T. Brandes, *New J. Phys.* **18**, 073007 (2016).
- [75] R. Kosloff, *Entropy* **15**, 2100 (2013).
- [76] J. Millen and A. Xuereb, *New J. Phys.* **18**, 011002 (2016).

- [77] H.-P. Breuer and F. Petruccione, *The theory of open quantum systems* (Oxford University Press Inc., New York, 2002).
- [78] K. Yamamoto and N. Hatano, Phys. Rev. E **92**, 042165 (2015).
- [79] H. Haug and A.-P. Jauho, *Quantum kinetics in transport and optics of semiconductors*, Vol. 2 (Springer, Berlin, Heidelberg, 2008).
- [80] J. Matthews, F. Battista, D. Sánchez, P. Samuelsson, and H. Linke, Phys. Rev. B **90**, 165428 (2014).
- [81] M. A. Sierra and D. Sánchez, Phys. Rev. B **90**, 115313 (2014).
- [82] J.-H. Jiang and Y. Imry, C. R. Physique **17**, 1047 (2016).
- [83] J.-H. Jiang and Y. Imry, Phys. Rev. Applied **7**, 064001 (2017).
- [84] D. Segal, Phys. Rev. Lett. **100**, 105901 (2008).
- [85] T. Ruokola and T. Ojanen, Phys. Rev. B **83**, 241404 (2011).
- [86] R. Sánchez, B. Sothmann, and A. N. Jordan, New J. Phys. **17**, 075006 (2015).
- [87] J.-H. Jiang, M. Kulkarni, D. Segal, and Y. Imry, Phys. Rev. B **92**, 045309 (2015).
- [88] R. Sánchez, H. Thierschmann, and L. W. Molenkamp, Phys. Rev. B **95**, 241401 (2017).
- [89] F. L. Curzon and B. Ahlborn, Am. J. Phys. **43**, 22 (1975).
- [90] G. Benenti, K. Saito, and G. Casati, Phys. Rev. Lett. **106**, 230602 (2011).
- [91] L. Onsager, Phys. Rev. **37**, 405 (1931).
- [92] H. B. G. Casimir, Rev. Mod. Phys. **17**, 343 (1945).
- [93] A. Vaudrey, F. Lanzetta, and M. Feidt, J. Non-Equilib. Thermodyn. **39**, 199 (2014).
- [94] C. Van den Broeck, Phys. Rev. Lett. **95**, 190602 (2005).
- [95] T. Schmiedl and U. Seifert, Europhys. Lett. **81**, 20003 (2008).
- [96] Y. Izumida and K. Okuda, Phys. Rev. E **80**, 021121 (2009).
- [97] M. Esposito, K. Lindenberg, and C. Van den Broeck, Europhys. Lett. **85**, 60010 (2009).
- [98] M. Esposito, K. Lindenberg, and C. Van den Broeck, Phys. Rev. Lett. **102**, 130602 (2009).
- [99] B. Gaveau, M. Moreau, and L. S. Schulman, Phys. Rev. Lett. **105**, 060601 (2010).
- [100] Y. Izumida and K. Okuda, Europhys. Lett. **97**, 10004 (2012).
- [101] Y. Izumida and K. Okuda, Phys. Rev. Lett. **112**, 180603 (2014).
- [102] S. Sheng and Z. C. Tu, Phys. Rev. E **89**, 012129 (2014).
- [103] S. Sheng and Z. C. Tu, Phys. Rev. E **91**, 022136 (2015).
- [104] Y. Izumida and K. Okuda, New J. Phys. **17**, 085011 (2015).
- [105] T. G. Sano and H. Hayakawa, Prog. Theor. Exp. Phys. **2016**, 083A03 (2016).
- [106] L. Cerino, A. Puglisi, and A. Vulpiani, Phys. Rev. E **93**, 042116 (2016).
- [107] K. Brandner, Doctoral thesis (University of Stuttgart, 2015).

- [108] M. Jonson and G. D. Mahan, Phys. Rev. B **42**, 9350 (1990).
- [109] G. Mahan and J. Sofo, Proc. Natl. Acad. Sci. USA **93**, 7436 (1996).
- [110] N. W. Ashcroft and N. D. Mermin, *Solid State Physics* (Holt, Rinehart and Winston, New York, 1976).
- [111] R. Kubo, J. Phys. Soc. Jpn. **12**, 570 (1957).
- [112] D. A. Greenwood, Proc. Phys. Soc. **71**, 585 (1958).
- [113] G. V. Chester and A. Thellung, Proc. Phys. Soc. **77**, 1005 (1961).
- [114] C. Villagonzalo, R. Römer, and M. Schreiber, Euro. Phys. J. B **12**, 179 (1999).
- [115] L. D. Hicks and M. S. Dresselhaus, Phys. Rev. B **47**, 12727 (1993).
- [116] P. A. Lee and T. V. Ramakrishnan, Rev. Mod. Phys. **57**, 287 (1985).
- [117] J. E. Enderby and A. C. Barnes, Rep. Prog. Phys. **53**, 85 (1990).
- [118] B. Kramer and A. MacKinnon, Rep. Prog. Phys. **56**, 1469 (1993).
- [119] K. Slevin and T. Ohtsuki, Phys. Rev. Lett. **82**, 382 (1999).
- [120] K. Slevin and T. Ohtsuki, New J. Phys. **16**, 015012 (2014).
- [121] M. Cutler and N. F. Mott, Phys. Rev. **181**, 1336 (1969).
- [122] U. Sivan and Y. Imry, Phys. Rev. B **33**, 551 (1986).
- [123] M. J. Kearney and P. N. Butcher, J. Phys. C: Solid State Phys. **21**, L265 (1988).
- [124] C. Castellani, C. Di Castro, M. Grilli, and G. Strinati, Phys. Rev. B **37**, 6663 (1988).
- [125] A. Kapitulnik, Appl. Phys. Lett. **60**, 180 (1992).
- [126] J. E. Enderby and A. C. Barnes, Phys. Rev. B **49**, 5062 (1994).
- [127] G. D. Guttman, E. Ben-Jacob, and D. J. Bergman, Phys. Rev. B **51**, 17758 (1995).
- [128] K. Durczewski and A. Krzywicki, Phys. Rev. B **58**, 10302 (1998).
- [129] Y. Imry and A. Amir, Int. J. Mod. Phys. B **24**, 1789 (2010).
- [130] G. Benenti, H. Ouerdane, and C. Goupil, C. R. Physique **17**, 1072 (2016).
- [131] A. Aharony and M. E. Fisher, Phys. Rev. B **27**, 4394 (1983).
- [132] E. Abrahams, P. W. Anderson, D. C. Licciardello, and T. V. Ramakrishnan, Phys. Rev. Lett. **42**, 673 (1979).
- [133] J. M. Ziman, J. Phys. C: Solid State Phys. **2**, 1230 (1969).
- [134] E. N. Economou and M. H. Cohen, Phys. Rev. Lett. **25**, 1445 (1970).
- [135] E. N. Economou and M. H. Cohen, Phys. Rev. B **5**, 2931 (1972).
- [136] J. Zhou, R. Yang, G. Chen, and M. S. Dresselhaus, Phys. Rev. Lett. **107**, 226601 (2011).
- [137] C. Jeong, R. Kim, and M. S. Lundstrom, J. Appl. Phys. **111**, 113707 (2012).
- [138] O. Entin-Wohlman, Y. Imry, and A. Aharony, Phys. Rev. B **91**, 054302 (2015).
- [139] J.-H. Jiang, O. Entin-Wohlman, and Y. Imry, Phys. Rev. B **87**, 205420 (2013).

- [140] T. Ying, Y. Gu, X. Chen, X. Wang, S. Jin, L. Zhao, W. Zhang, and X. Chen, *Sci. Adv.* **2**, e1501283 (2016).
- [141] D. Suri and R. S. Patel, *Appl. Phys. Lett.* **110**, 233108 (2017).
- [142] R. Bosisio, C. Gorini, G. Fleury, and J.-L. Pichard, *New J. Phys.* **16**, 095005 (2014).
- [143] V. Narayan, M. Pepper, and D. A. Ritchie, *C. R. Physique* **17**, 1123 (2016).
- [144] K. Saito, G. Benenti, G. Casati, and T. Prosen, *Phys. Rev. B* **84**, 201306(R) (2011).
- [145] V. Balachandran, G. Benenti, and G. Casati, *Phys. Rev. B* **87**, 165419 (2013).
- [146] K. Brandner, K. Saito, and U. Seifert, *Phys. Rev. X* **5**, 031019 (2015).
- [147] K. Proesmans and C. Van den Broeck, *Phys. Rev. Lett.* **115**, 090601 (2015).
- [148] K. Proesmans, B. Cleuren, and C. V. den Broeck, *J. Stat. Mech. Theor. Exp.* **2016**, 023202 (2016).
- [149] N. Shiraishi, K. Saito, and H. Tasaki, *Phys. Rev. Lett.* **117**, 190601 (2016).
- [150] N. Shiraishi and H. Tajima, *Phys. Rev. E* **96**, 022138 (2017).
- [151] M. Büttiker, *IBM J. Res. Dev.* **32**, 317 (1988).
- [152] K. Brandner and U. Seifert, *Phys. Rev. E* **91**, 012121 (2015).
- [153] U. Sivan and Y. Imry, *Phys. Rev. B* **33**, 551 (1986).
- [154] P. N. Butcher, *J. Phys.: Condens. Matter* **2**, 4869 (1990).
- [155] O. Entin-Wohlman and A. Aharony, *Phys. Rev. B* **85**, 085401 (2012).
- [156] O. Entin-Wohlman, Y. Imry, and A. Aharony, *Phys. Rev. B* **81**, 113408 (2010).
- [157] O. Entin-Wohlman, Y. Imry, and A. Aharony, *Phys. Rev. B* **80**, 035417 (2009).
- [158] R. Leturcq, C. Stampfer, K. Inderbitzin, L. Durrer, C. Hierold, E. Mariani, M. G. Schultz, F. von Oppen, and K. Ensslin, *Nat. Phys.* **5**, 327 (2009).
- [159] F. Haupt, T. Novotný, and W. Belzig, *Phys. Rev. B* **82**, 165441 (2010).
- [160] K. Yamamoto, A. Aharony, O. Entin-Wohlman, and N. Hatano, *Phys. Rev. B* **96**, 155201 (2017).
- [161] A. C. Barato and U. Seifert, *Phys. Rev. Lett.* **114**, 158101 (2015).
- [162] T. R. Gingrich, J. M. Horowitz, N. Perunov, and J. L. England, *Phys. Rev. Lett.* **116**, 120601 (2016).
- [163] A. C. Barato and U. Seifert, *Phys. Rev. X* **6**, 041053 (2016).
- [164] T. R. Gingrich, G. M. Rotskoff, and J. M. Horowitz, *J. Phys. A: Math. Theor.* **50**, 184004 (2017).
- [165] K. Proesmans and C. V. den Broeck, *Europhys. Lett.* **119**, 20001 (2017).
- [166] P. Pietzonka, F. Ritort, and U. Seifert, *Phys. Rev. E* **96**, 012101 (2017).
- [167] C. Hyeon and W. Hwang, *Phys. Rev. E* **96**, 012156 (2017).
- [168] K. Brandner, T. Hanazato, and K. Saito, *arXiv preprint arXiv:1710.04928* (2017).

- [169] M. F. Ludovico, M. Moskalets, D. Sánchez, and L. Arrachea, Phys. Rev. B **94**, 035436 (2016).
- [170] M. F. Ludovico, L. Arrachea, M. Moskalets, and D. Sánchez, Entropy **18**, 419 (2016).
- [171] M. Esposito, M. A. Ochoa, and M. Galperin, Phys. Rev. Lett. **114**, 080602 (2015).
- [172] M. Hasegawa and T. Kato, J. Phys. Soc. Jpn. **86**, 024710 (2017).